DOT/FAA/AR-04/41

Office of Aviation Research
Washington, D.C. 20591

Evaluation of Fuel Tank Flammability and the FAA Inerting System on the NASA 747 SCA

Michael Burns
William M. Cavage
Robert Morrison
Steven Summer

December 2004

Final Report

U.S. Department of Transportation
Federal Aviation Administration

NOTICE

Technical Report Documentation Page

1. Report No.	2. Government Accession No.	3. Recipient's Catalog No.
DOT/FAA/AR-04/41		

4. Title and Subtitle	5. Report Date
EVALUATION OF FUEL TANK FLAMMABILITY AND THE FAA INERTING SYSTEM ON THE NASA 747 SCA	December 2004
	6. Performing Organization Code

7. Author(s)	8. Performing Organization Report No.
Michael Burns, William M. Cavage, Robert Morrison, and Steven Summer	DOT/FAA/AR-04/41

9. Performing Organization Name and Address	10. Work Unit No. (TRAIS)
Federal Aviation Administration William J. Hughes Technical Center Airport and Aircraft Safety Research and Development Division Fire Safety Branch Atlantic City International Airport, NJ 08405	11. Contract or Grant No.

12. Sponsoring Agency Name and Address	13. Type of Report and Period Covered
U.S. Department of Transportation Federal Aviation Administration Office of Aviation Research Washington, DC 20591	Final Report
	14. Sponsoring Agency Code ANM-112

15. Supplementary Notes

16. Abstract

Extensive development and analysis has illustrated that fuel tank inerting could, potentially, be cost-effective if air separation modules, based on hollow-fiber membrane technology, could be packaged and used in an efficient way. To illustrate this, the Federal Aviation Administration (FAA) has developed a prototype onboard inert gas generation system that uses aircraft bleed air to generate nitrogen-enriched air (NEA) at varying flows and purities during a commercial airplane flight cycle. A series of ground and flight tests were performed, in conjunction with National Aeronautics and Space Administration (NASA) aircraft operations personnel, designed to evaluate the FAA inerting system used in conjunction with a compartmentalized center wing tank (CWT). Additionally, the flammability of both the CWT and one inboard wing fuel tank was measured. The system was mounted on a Boeing 747, operated by NASA, and used to inert the aircraft CWT during testing. The inerting system, CWT, and the number 2 main wing tanks were instrumented to analyze the system performance, fuel tank inerting, and flammability.

The results of the testing indicated that the FAA prototype inerting system operated as expected. Using a variable-flow methodology allowed a greater amount of NEA to be generated on descent when compared to the simple dual-flow methodology, but it had no measurable effect on the resulting average ullage oxygen concentration after each test, while improving inert gas distribution by decreasing the worst bay oxygen concentration when three similar tests were compared. The highest average ullage oxygen concentration observed on any flight test correlates directly with the worst bay oxygen concentration, illustrating the importance of maintaining a low average ullage oxygen concentration in good inert gas distribution. Oxygen diffusion between the bays of the tank was relatively rapid, and overnight dispersion of the ullage oxygen concentration was measured to be very small. Flammability measurements showed trends very similar to what was expected based on both experimental and computer model data. The equilibrium data agreed favorably with data from both the Fuel Air Ratio Calculator and the Condensation Model, while transient data trends matched closely with the Condensation Model with some discrepancies in total hydrocarbon concentration magnitude at altitude.

17. Key Words	18. Distribution Statement
Nitrogen-enriched air, OBIGGS, Hollow-fiber membrane, Air separation module, Total hydrocarbon concentration, Oxygen concentration, Thermocouple, Pressure transducer	This Document is available to the public through the National Technical Information Service (NTIS), Springfield, Virginia 22161

19. Security Classif. (of this report)	20. Security Classif. (of this page)	21. No. of Pages	22. Price
Unclassified	Unclassified	75	

Form DOT F 1700.7 (8-72) Reproduction of completed page authorized

ACKNOWLEDGMENT

The Federal Aviation Administration (FAA) and the Airport and Aircraft Safety Research and Development Division, Fire Safety Branch would like to acknowledge the contributions of NASA Johnson Space Center in supporting the extensive installation of equipment and instrumentation to accomplish the very difficult task of studying in-flight flammability and fuel tank inerting during flight tests on the NASA 747 SCA. Additionally, acknowledgement goes to the excellent test pilots and crew that supported the lengthy and time-consuming flight test plan provided by the FAA. The dedication and professionalism of the entire test and support personnel at Ellington Field, particularly the zero-g team, which allowed the FAA to achieve the project goals and objectives was significant, and their technical know-how and professionalism are the primary reasons for the success of the test program.

Further acknowledgement is extended to NASA Glen Research Center Fire Safety Research Program for lending financial and moral support to the project when it was needed most.

TABLE OF CONTENTS

LIST OF FIGURES

LIST OF TABLES

Table Page

LIST OF ACRONYMS

ACM	Air cycle machines
ASM	Air separation modules
CWT	Center wing tank
DAS	Data acquisition system
FAA	Federal Aviation Administration
FAR	Fuel air ratio
FAS	Flammability analysis system
ID	Inner diameter
LOC	Limiting oxygen concentration
NASA	National Aeronautics and Space Administration
NEA	Nitrogen-enriched air
OBIGGS	Onboard inert gas generation system
OBOAS	Onboard oxygen analysis system
OEA	Oxygen-enriched air
SCA	Space Shuttle Orbiter Carrier Aircraft
SCFM	Standard cubic feet per minute
SOV	System shutoff valve
STA	Station
THC	Total hydrocarbon concentration
WS	Wing station

EXECUTIVE SUMMARY

Significant emphasis has been placed on fuel tank safety since the TWA Flight 800 accident in July 1996. This has prompted the Federal Aviation Administration (FAA) to study methods that could limit the flammability exposure of the commercial transport fleet. The effort was focused on high-flammability exposure fuel tanks, which are center wing and body-style fuel tanks. Extensive development and analysis has illustrated that fuel tank inerting during aircraft operation could, potentially, be cost-effective if air separation modules (ASM) could be integrated into a system and used in an efficient manner. These ASMs are made of thousands of tiny, hair-sized, hollow-fiber membranes, which are fabricated into a vessel. When supplied with pressurized air, these modules will ventilate a waste stream of gas from a permeate vent that is rich in oxygen, carbon dioxide, and water vapor. This allows the product gas passing through the ASM to be rich in nitrogen.

To demonstrate using hollow-fiber membrane ASMs for inerting commercial transport airplane fuel tanks, the FAA, with the assistance of several aviation-oriented companies, has developed a prototype onboard inert gas generation system with ASMs that uses aircraft bleed air to generate nitrogen-enriched air (NEA) at varying flows and purities (NEA oxygen concentration) during a commercial airplane flight cycle. This system was designed to maintain an oxygen concentration below 12% in a Boeing 747 center wing tank (CWT) during typical commercial transport airplane operations. A series of ground and flight tests were performed, in conjunction with National Aeronautics and Space Administration (NASA) aircraft operations personnel, designed to evaluate the simplified inerting system and examine inerting of a compartmentalized fuel tank. Additionally, the flammability of both the center wing and one inboard wing fuel tank was examined. The FAA inerting system was mounted in the pack bay of a modified 747, operated by NASA for Space Shuttle Orbiter transportation, and used to inert the aircraft CWT during testing. The inerting system, CWT, and the number 2 wing tanks were instrumented to analyze system performance, inerting capability, and fuel tank flammability.

The results of the testing indicated that the FAA inerting system operated as expected. Any deviations in system performance from test to test could be explained by the difference in system warmup times on the day of the test. Using a variable flow methodology allowed for a greater amount of NEA to be generated on descent at a higher oxygen concentration (lower purity) as intended, but it had no measurable effect on the resulting average ullage oxygen concentration after each test when compared to a simple dual-flow system methodology. It did seem to improve inert gas distribution by decreasing the worst bay oxygen concentration. The highest average ullage oxygen concentration observed on any flight test correlated directly with the worst bay oxygen concentration. Oxygen diffusion between the bays of the tank was relatively rapid, and the overnight increase of the ullage oxygen concentration was measured to be very

small. Flammability measurements from both the CWT and the wing tank showed trends very similar to what was expected based on both experimental and computer model data. The equilibrium data agreed favorably with data from both the Fuel Air Ratio Calculator and the Condensation Model, while transient data trends matched closely with the Condensation Model, with some disagreement with flammability magnitudes at altitude. The measurements generated in these flight tests have been used to enhance the capability of these existing flammability models and will be used in the future to further improve the predictive flammability calculations.

1. INTRODUCTION.

1.1 BACKGROUND.

Significant emphasis has been placed on fuel tank safety since the TWA Flight 800 accident in July 1996. This has prompted the Federal Aviation Administration (FAA) to study methods that could limit the flammability exposure of the commercial transport fleet. The effort was focused on center wing and body-style fuel tanks that have been identified as being potentially hotter during ground operations and more flammable in general [1]. Extensive development and analysis has illustrated that flammability reduction using fuel tank inerting during aircraft operation could, potentially, be cost-effective if air separation modules (ASM) could be integrated into a system and used in an efficient manner. To illustrate this, the FAA, with the assistance of several aviation-oriented companies, developed a prototype onboard inert gas generation system (OBIGGS) with ASMs that used aircraft bleed air to generate nitrogen-enriched air (NEA) at varying flows and purities (NEA oxygen concentration) during a commercial airplane flight cycle. This system was designed to maintain an oxygen concentration below 12% in a Boeing 747 center wing tank (CWT) during typical commercial transport airplane operations. An ASM is made up of thousands of tiny, hair-sized, hollow-fiber membranes, which are fabricated into a vessel. When supplied with pressurized air, these modules will ventilate a waste stream of gas from a permeate vent that is rich in oxygen, carbon dioxide, and water vapor [2]. This allows the product gas passing through the ASM to be rich in nitrogen.

Early ASM OBIGGS work performed by the Department of Defense culminated in a study that highlighted the favorable life cycle costs of an on-demand (inert gas generation) system over a stored inerting agent system and explosive suppressant foam. This study concluded that an inerting system using ASMs with hollow-fiber membrane technology was cost-effective compared to other OBIGGS technologies with a relative performance increase of a factor of ten over previous ASM technology systems [3].

The initial FAA fuel tank inerting flight tests were performed in conjunction with The Boeing Company to examine the ability of a ground-based supply of nitrogen (ground-based inerting) to inert a commercial airplane CWT. This allowed for validation of the FAA's Onboard Oxygen Analysis System (OBOAS) during flight-testing, which was developed for the project and could continuously measure the oxygen concentration of a commercial transport fuel tank ullage using conventional laboratory oxygen analyzers and a pressure-controlled sample train [4]. Recent FAA flight tests were performed in conjunction with Airbus to test the FAA inerting system, which was mounted in the cargo bay of an A320 operated by Airbus, for the purpose of research and development. The system performance was degraded to examine the ability of a single ASM and two ASMs to inert the CWT of the test aircraft and to help develop a system performance model. The basic dual-flow system concept was validated and system scaling was examined. The effects of fuel and inert gas distribution were also studied, and a simply ullage inerting model was developed to calculate ullage oxygen concentration given a system performance and flight cycle [5].

Much of the flammability research performed by the FAA has focused on the determination of the limiting oxygen concentration (LOC), the oxygen content below which ignition of jet fuel

vapors can no longer be supported. The LOC is the main design criteria for any inerting system, because it determines the oxygen levels required to provide adequate fuel tank explosion protection. Traditionally, the military has used a value of 9 percent oxygen by volume as the inert limit of a fuel tank ullage. An experimental investigation performed by the FAA using a 9-cubic-foot test article illustrated, however, that no measurable pressure rise was observed when a spark was used to ignite a flammable ullage with an oxygen concentration less than 12 percent by volume at sea level and 10,000 feet. The LOC value increased in a linear fashion to approximately 14.5 percent oxygen at 40,000 feet [6]. The experiment used a small fuel pan, radiantly heated from underneath, with the test article in a vacuum chamber to study the ability of a simulated ullage to react to a spark source applied under a variety of conditions. Follow-on experiments studied a wide variety of fuel/air mass ratios and ignition sources/energies with no change in the resulting LOC. A review of previously published literature showed very good agreement with measured results.

1.2 SCOPE.

The FAA, with the assistance of National Aeronautics and Space Administration (NASA) aircraft operations, performed a series of ground and flight tests designed to study the simplified inerting concept developed by the FAA. The FAA developed a prototype inerting system, based on ASM technology, designed to maintain an inert ullage in the CWT of a 747 commercial transport during normal ground and flight operations using a dual-flow methodology. The inerting system was mounted in the pack bay of a NASA 747 Space Shuttle Orbiter Carrier Aircraft (SCA) to perform the FAA-managed test plan. The system was interfaced with the aircraft systems, and instrumentation was installed to measure the inerting system performance and fuel tank flammability during the flight tests. Both the CWT and the number 2 wing fuel tank (here after referred to as the wing tank) were instrumented with gas sample tubing and thermocouples to allow for real-time monitoring of total hydrocarbon concentration, temperatures, and CWT ullage oxygen concentration distribution during each test flight.

2. TEST ARTICLE AND PROCEDURES.

2.1 TEST ARTICLE.

The test article consisted of a NASA 747 SCA associated instrumentation and data acquisition system (DAS). The FAA OBIGGS with associated instrumentation was installed in the pack bay. The CWT was instrumented with eight gas sample tubes that were routed to the FAA's OBOAS, a heated gas sample port routed to the FAA Flammability Analysis System (FAS), as well as multiple temperature probes. The wing tank was instrumented with both a heated gas sample port for the FAS and multiple temperature probes as well.

2.1.1 Aircraft.

The test article was a 747-100, highly modified by NASA, as an SCA (figure 1). It has a basic operating weight of 318,053 lbs with a gross taxi weight of 713,000 lbs. It has a 195′ 8″ wing span and is 231′ 10″ long. The maximum cruise speed of the aircraft is 250 knots or Mach 0.6 with a ceiling of 35,000 feet.

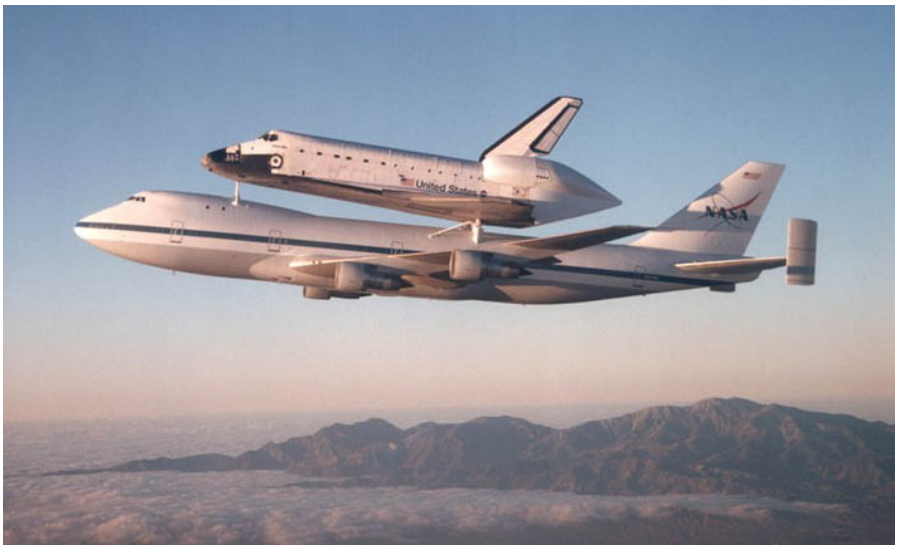

FIGURE 1. NASA 747 SCA AIRCRAFT WITH SPACE SHUTTLE ORBITER

Figure 2 shows the four main wing fuel tanks, the two wing tip reserve fuel tanks, and the large CWT of the NASA 747 SCA. The CWT has a capacity of 12,890 gallons of fuel and is between the wings of the aircraft, within the fuselage of the aircraft (center wing box). The CWT is approximately 242 inches long and 255 inches wide with a height varying from 78 inches to 48 inches and is partitioned into six bays, two bays are the full width of the fuselage, while another two full-length bays are bisected mid-way with a partial rib creating four bays. The empty CWT ullage volume was determined to be 1775 normal cubic feet for the purpose of inerting the tank with NEA. A large dry bay exists in the center wing box forward of the first tank bay. Immediately below the CWT, in an area known as the pack bay, are three air cycle machines (ACM) that provide conditioned air to the aircraft and rejects heat to the CWT.

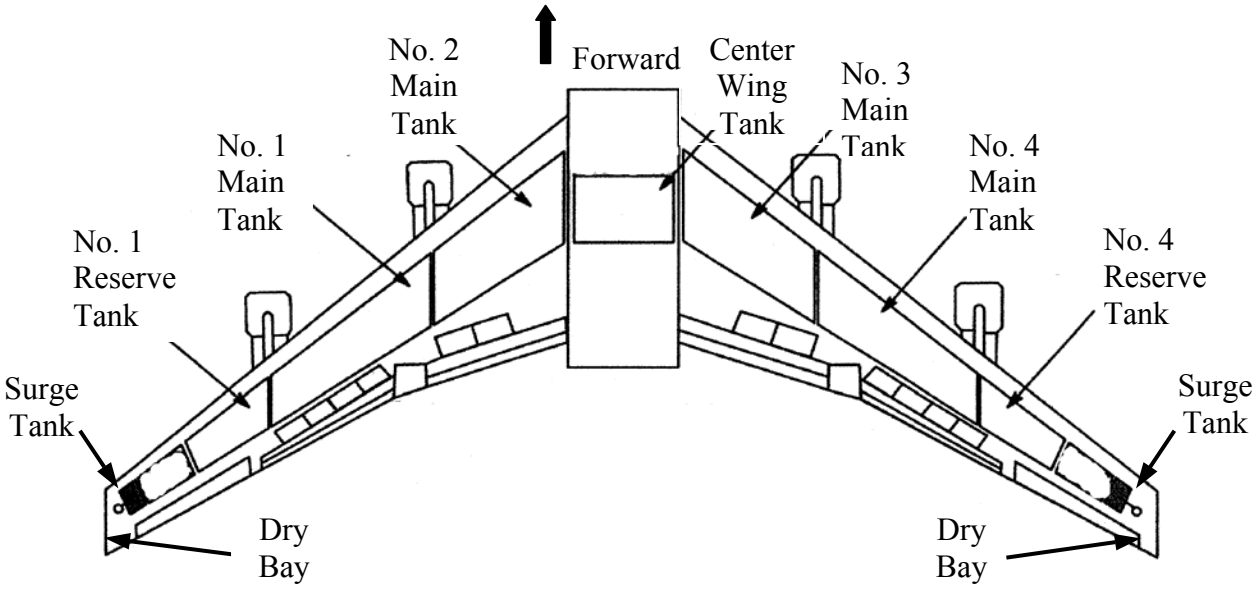

FIGURE 2. NASA 747 SCA FUEL TANK DIAGRAM

The CWT is vented to both wing tip surge/vent tanks via a vent channel in each wing that is plumbed to vent tubing contained within the tank. One vent channel travels along the top of bays 3 and 4, while the other travels along the top of bays 5 and 6. These channels vent crosswise to the exterior of the tank so that the vent channel plumbed on the right side of the tank (bays 5 and 6) is vented to the left wing surge/vent tank and vise-versa. Each vent channel is plumbed to a length of aluminum tubing on each side of the tank that travels forward perpendicular to the spanwise beams and midspar across the bays. A smaller tube travels aft within the vent channel bay. This plumbing configuration allows the CWT to vent pressure in various rolling and climb/dive scenarios. The vent channels from the CWT and all other fuel tanks terminate in one or both of the surge/vent tanks located near each wing tip. These surge/vent tanks catch fuel and prevent overflow, and are connected to the aircraft exterior via a NACA scoop located on the bottom surface of each wing.

2.1.1.1 Replacement of Ventilation Port With Instrumentation Panel.

The 747 has a ventilation port on the rear spar to ventilate the CWT with fresh air during maintenance operations. The FAA installed an instrumentation panel in place of the CWT ventilation purge door on the rear spar as shown in figure 3, allowing easy passage of instrumentation to and from the CWT. The instrumentation panel accommodated ten bulkhead fittings for the gas sample lines as well as two thermocouple bulkhead ports for sealing the thermocouples at the rear spar. There was also a 1-inch bulkhead fitting in the center of the panel for the NEA deposit line. The installation drawing for the instrumentation panel is shown in appendix A.

FIGURE 3. MODIFIED REAR SPAR PURGE DOOR

2.1.1.2 Modification to the Vent System.

As described above, the 747 aircraft vents the CWT to both wing tip surge (overflow) tanks. Cross venting is the process by which subtle pressure changes between these vents allow outside air to ventilate the ullage by passing through one vent channel, into the tank, and out of the other vent channel.

To prevent the loss of inert gas by this process, the FAA installed three blocking plates in the right side vent system (looking forward) of the NASA 747 SCA. One was installed by removing the vent flange that attached the vent tubing to the vent channel, placing a thin aluminum plate between the flange and the vent stringer and sealing it with fuel tank sealant. In addition, the 4-inch-diameter vent tube also had a thin, round aluminum plate installed in one connection fitting to prevent inert gas from transferring through the tube from one bay to another. It was not necessary to use fuel tank sealant on this blocking plate. The right side vent stringer also has a fuel drain with a float valve mounted on it. The float valve was removed and a blocking plate was installed in its place and sealed with fuel tank sealant. This modification prevents cross venting of the CWT ullage.

After the FAA completed the tests to examine inerting without cross venting, the vent system was restored to the original equipment configuration for a single baseline flammability test.

2.1.1.3 Gas Sample Fittings.

Two sample port tubes were installed through modified HiLok® fasteners, which were installed in place of specified existing fasteners in the wing structure, to allow for the measurement of total hydrocarbons in both the CWT and the wing fuel tank. In each case, an appropriate fastener was specified, modified with a 1/8-inch hole through the fastener center, and then installed in the appropriate location. The CWT fitting penetrated the top of the tank in the number 2 bay slightly left of centerline, while the wing tank fitting was located just outboard of the number 2 engine pylon on the front spar. The sample port tubes were later bonded into the fastener holes with aviation grade epoxy, and float valve assemblies were installed on the tube inside the tank to prevent sloshing fuel from entering the sample lines attached to the tubing outside of the tank. A drawing illustrating the hollow-fastener installation with float valve assemblies is shown in appendix B. There was a third tooling hole fastener modified on the left wing forward spar to accommodate the eight thermocouples installed in the number 2 main fuel tank. When completed, the installation was sealed with the appropriate fuel tank sealant.

2.1.2 Instrumentation.

The primary instrumentation centered around the heated and unheated gas-sampling tubing and thermocouples in both the CWT and the wing tank. Continuous measurement of oxygen concentration and total hydrocarbon concentration (THC) in the fuel tanks during each flight test were made using the FAA OBOAS and FAS. Additionally, the FAA OBIGGS was instrumented with pressure, temperature, oxygen concentration ports, and a flow sensor to analyze system performance and health monitoring for each test. Additional test parameters were also collected to aide in the analysis of the inerting process and progression of flammability during the flight tests. Appendix C contains a complete instrumentation diagram as well as a complete list of all instrumentation channels.

2.1.2.1 Onboard Oxygen Analysis System.

The FAA OBOAS was used to measure the oxygen concentrations at the eight specified locations within the CWT. The OBOAS was developed by the FAA to measure the oxygen concentrations in a fuel tank environment during a typical commercial-transport airplane flight

cycle using conventional oxygen analyzers. This system consists of a regulated sample train with flow-through, in-line oxygen sensors and ancillary equipment. Two identical four-channel systems were developed. Each four-channel system was self-contained in a 19-inch flight test half-rack. Each system has four independent sample trains that can draw an ullage sample at four different locations in the fuel tank, regulate the sample pressure, expose the sample to the oxygen sensor, and redeposit the sample back into the fuel tank. Each oxygen sensor has a companion analyzer mounted on the same 19-inch half-rack. Also mounted on each 19-inch half-rack is a four-channel inlet pressure controller and a single-outlet pressure controller electronic unit. These electronic units support the five pressure regulator/controllers in each four-channel system. Reference 7 gives a complete description of the measurement system with part lists, diagrams, and systems analysis.

2.1.2.2 Flammability Analysis System.

The FAA developed the FAS for the purpose of real-time, in-flight monitoring of the THC in both the CWT and wing tank. The FAS consists of a two-channel Rosemount Analytical NDIR analyzer, supplied by temperature-controlled, pressure- and flow-regulated sample streams. The NDIR analyzer was custom-designed and constructed by the manufacturer to safely measure fuel tank vapors in flight and housed in an explosion proof box.

All hydrocarbon gas samples must be maintained at a minimum 200°F temperature prior to entering the NDIR analyzer to eliminate any condensation of the hydrocarbon vapors prior to being measured. To that end, the sample stream external to the FAS consists of several heated sample tubes and a heated rack-mounted box, which houses the diaphragm pump heads, flash arrestors, float valves, sample control valves, and sample flow meters. A separate unheated, rack-mounted box houses the two inlet sample pressure regulators. For safety, both rack-mounted boxes are continuously purged with air in the same manner as the OBOAS to prevent the accumulation of explosive vapors in the event of a sample line leak. An additional rack-mounted panel houses all necessary electronics to maintain the proper sample conditions, including temperature controllers and the pressure controller electronic units.

Figure 4(a) shows a diagram of the rack-mounted installation of the pump, sample-conditioning boxes, and controller box, and figure 4(b) shows the NDIR analyzer.

2.1.2.2.1 Sample Train Flow.

After entering the FAS heated rack-mounted box, the samples pass through a flash arrestor and then a four-way selector valve. The selector valve enables the operator to draft a sample from the tank, cabin air, calibration gases, or to close off the sample inlet. Each sample then passes through a two-stage diaphragm pump. Prior to exiting the heated rack-mounted box, the samples are teed off to the inlet pressure regulators located in the sample-conditioning unit, which regulates the inlet pressure. On the other side of the tee, the samples pass through a sample flow meter prior to exiting the heated rack-mounted box. Another heated line then routes the samples to the NDIR analyzer. On the exit side of the NDIR analyzer, the two samples are joined together and dumped overboard after flowing through a manual backpressure regulator.

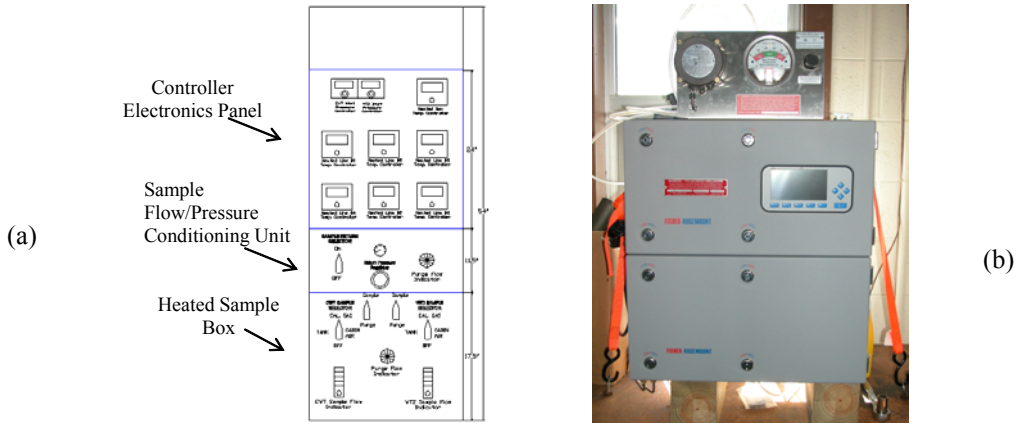

FIGURE 4. (a) RACK-MOUNTED FAS INSTALLATION AND (b) NDIR ANALYZER

In the event that a float valve is actuated and flow through that line is blocked, the operator has the capability to purge that line once it drops below the fuel level. This is accomplished by sampling from the cabin and circulating that sample back through the closed portion of the line until the float opens back up. A schematic of the sample train flow is shown in figure 5.

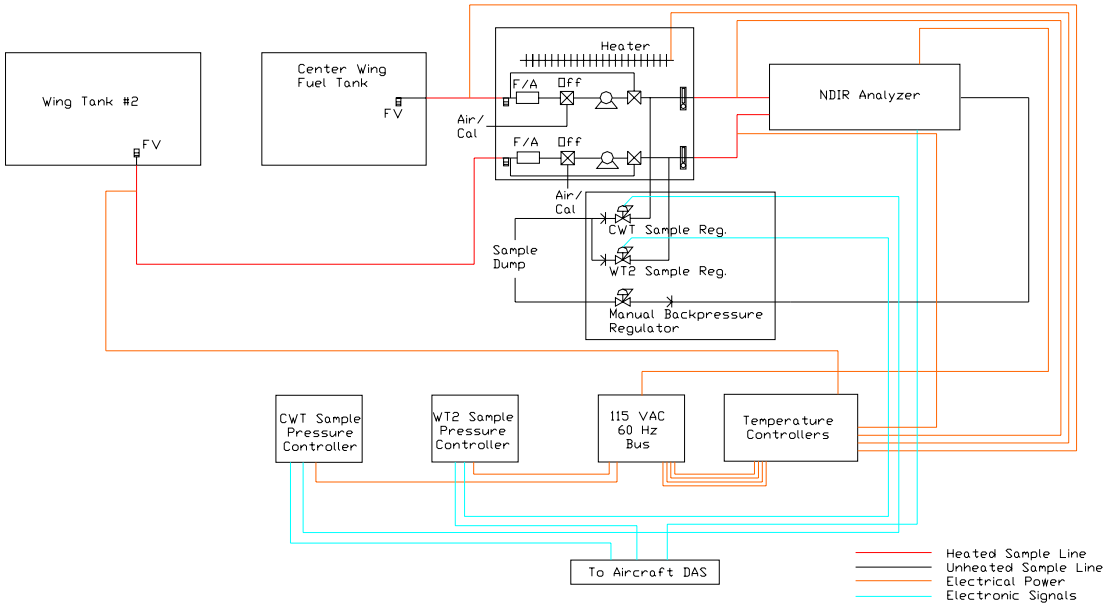

FIGURE 5. THE FAS SAMPLE STREAM FLOW SCHEMATIC

2.1.2.2.2 System Safety Features.

Careful measures were taken to ensure that the FAS operates in such a manner to minimize the operator's and crew's exposure to hazardous vapors as well as to preclude the ignition of any potentially flammable vapors that may be drafted through the FAS.

The NDIR analyzer is housed within a continuously purged housing with an impact-tested, intrinsically safe front panel. The electronics of the NDIR analyzer have been separated from the

sample stream to allow safe heating of all internal sample tubes to 200°F as well as to separate any potential ignition sources from the sample stream in the event of a leak of flammable vapors.

The purge system incorporated an easily observed indicator of a safe or nonsafe condition in the form of a rotary flow indicator. If purge pressure was unable to maintain a safe condition, the unit was immediately shutdown. The purge system for the rack-mounted sample-conditioning boxes used two ejectors each requiring a minimum of 3 standard cubic feet per minute (SCFM) of compressed air at 40 psi or greater. The ejector unit maintained a constant negative pressure on the inlet, drafting a volume of air from inside the boxes. The ejector inlet is plumbed through a rotary flow indicator, which allowed the operator to determine if the purge flow is functional at any point in time.

Likewise, the rack-mounted sample-conditioning boxes, housing the pump, flow meter, and sample pressure regulators, are continuously purged enclosures and are separated from the rack-mounted panel housing the control electronics (temperature controllers and pressure control electronic units). In addition, care has been taken to only mount the diaphragm pump head inside the heated box. The motor driving the diaphragm pump was kept external to the box, again to maintain separation between any electrical sources and the sample stream flow.

2.1.2.3 Gas-Sampling Lines.

Eight sample ports are located in the CWT at the eight locations identified in figure 6. The sample lines are made of PFA tubing routed from bay 6 to each location through the fuel seep holes at the top of the tank between the spars/spanwise beams and the side of body ribs. The tubing is terminated at a float valve that is attached to the tank through a mounting plate that was attached to a stiffening bracket between two stringers (with a stiffener) at the top of the tank. This small plate is attached to the stiffener bracket through a replaced rivet to minimize the necessary modification for the installation. Figure 7 shows one sample port mounting plate attached in the CWT with a float valve assembly.

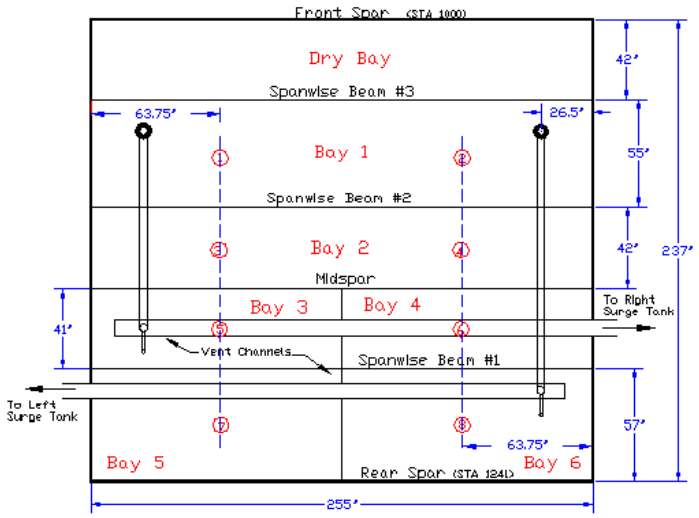

FIGURE 6. TOP VIEW OF A 747-100 CWT WITH SAMPLE PORT LOCATIONS

FIGURE 7. GAS SAMPLE FLOAT VALVE INSTALLATION

2.1.2.4 Heated Sample Lines.

The fuel vapor samples were drafted from the fuel tanks via the installed sample fittings (see section 2.1.1.3). After exiting the tanks, the samples were routed to the FAS using a series of heated sample lines maintained at a constant 200°F. For the CWT sample, a single 10-foot heated line was routed directly from a modified fastener at the top of the tank to the rack-mounted portion of the FAS. The sample from the wing tank was routed from a similarly modified fastener on the front spar, down the leading edge of the left aircraft wing with a 50-foot heated line. This line was routed to a fitting on the fuselage pressure bulkhead with a separate heated line routed from this fitting, into the front cargo bay, and to the FAS. The temperature of all heated lines along with the heated box was continuously monitored by the operator via panel-mounted displays. In addition, the 50-foot line was constructed to have additional thermocouples located every 5 feet along the line that were recorded by the DAS.

2.1.2.5 Fuel Tank Thermocouples.

There were 24 thermocouples mounted in the CWT positioned at the locations identified in figure 8. The T-type thermocouples were routed through compression fittings on the instrument panel and sealed with fuel tank sealant. Fourteen of these thermocouples were mounted on metallic surfaces with an epoxy-retaining patch (appendix D), while the remainder were suspended at the desired location. The thermocouples were mounted to the tank structure using fuel-compatible wire ties with some long runs being supported by additional epoxy patches. The thermocouples were 1/16-inch stainless steel sheathed and ran from the panel installed in bay 6 to each desired location through the fuel seep holes at the top and bottom of the tank between the spars/spanwise beams and the side of the body ribs.

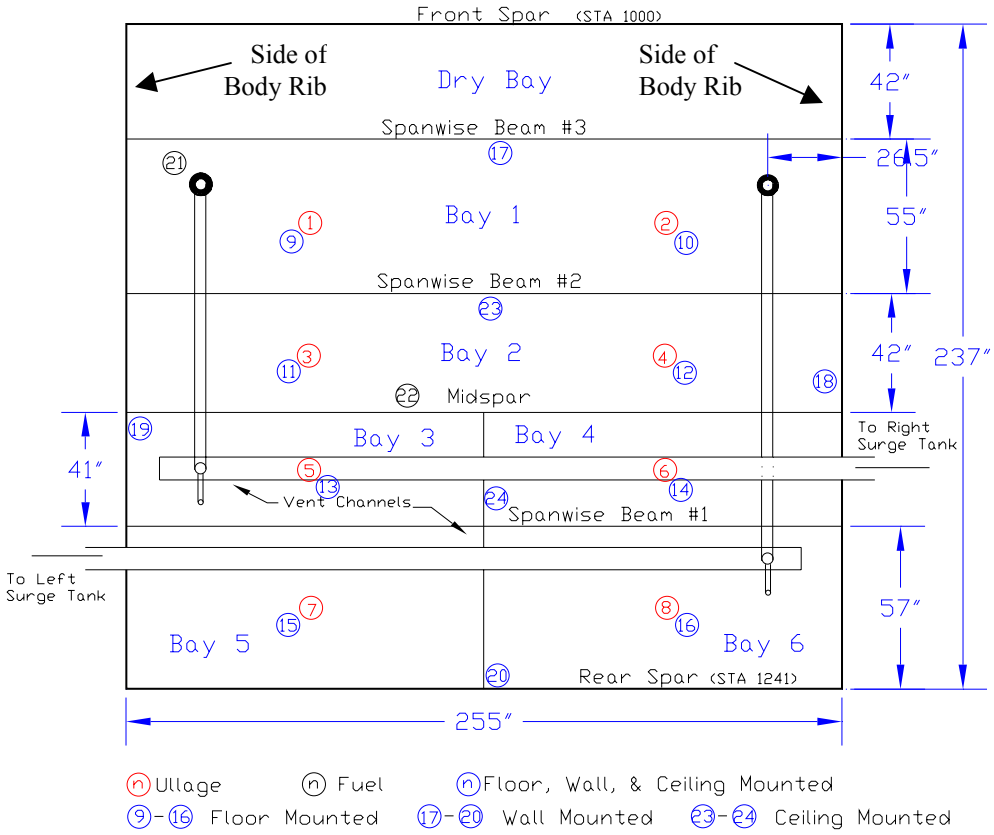

FIGURE 8. TOP VIEW OF A 747-100 CWT WITH THERMOCOUPLE LOCATIONS

The ullage thermocouples (1 through 8) were installed within 1 foot of the bottom of the caps of the ceiling stringers. The fuel thermocouples (21 and 22) were installed less than 1 inch from the tank bottom. Thermocouples 9 through 16 were mounted on the floor. Thermocouples 17-20 were mounted on the tank walls approximately half way between the bottom and the top of the tank. Thermocouples 23 and 24 were mounted on the ceiling of the tank.

There were eight thermocouples mounted in the wing tank, positioned as described in table 1. The thermocouples were the same type used in the CWT and were routed from the cabin, through the cargo bay, into the fairing area, along the leading edge, and through a drilled out tooling hole on the front spar of the wing approximately at wing station (WS) 400. Five of these thermocouples were mounted on surfaces in the same manner as in the CWT, with the remainder suspended at the desired location. Figure 9 gives a top diagram of wing tank number 2 with the approximate location of the thermocouples noted.

TABLE 1. WING TANK THERMOCOUPLE LOCATIONS

Temp No.	Description	Location
1	Wing tank forward spar surface temperature	Front spar surface, WS 455, 25″ from tank bottom
2	Wing tank inboard fuel temperature	4′ from front spar, WS 310, 6″ from tank bottom
3	Wing tank rear spar surface temperature	Rear spar surface, WS 435, 25″ from tank bottom
4	Wing tank ullage temperature	2″ from front spar, WS 650, 4″ from tank top
5	Wing tank mid-fuel/ullage temperature	25″ from front spar, WS 586, 13" from tank bottom
6	Wing tank outboard wall surface temperature	6′ from front spar, WS 715, 12″ from tank bottom
7	Wing tank bottom surface temperature	8′ from front spar, WS 455, tank bottom surface
8	Wing tank top surface temperature	8′ from front spar, WS 455, tank top surface

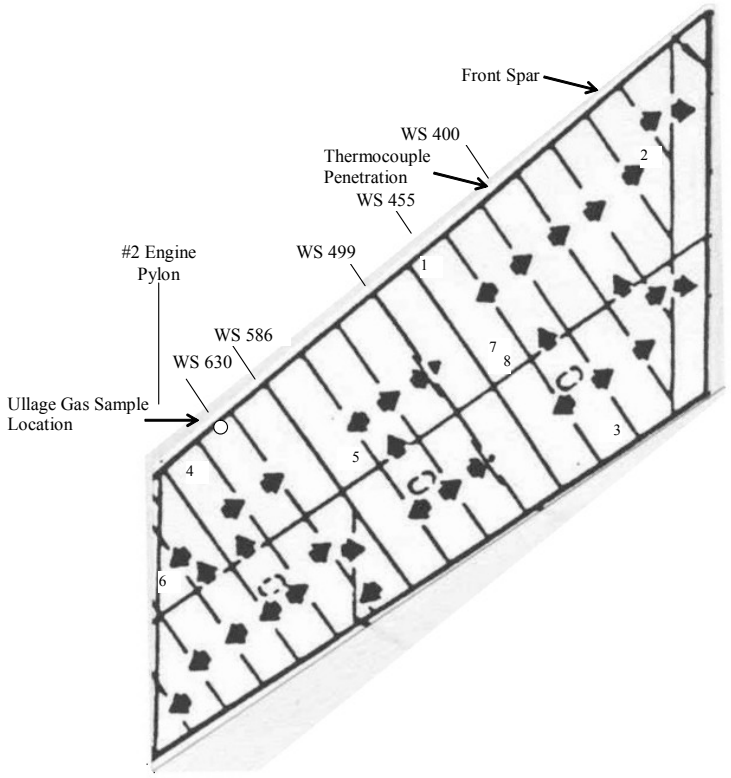

FIGURE 9. TOP VIEW OF A 747-100 WING TANK WITH THERMOCOUPLE LOCATIONS

2.1.2.6 Onboard Inert Gas Generation System Parameters.

The FAA OBIGGS was equipped with instrumentation that monitored and set system parameters. The instrumentation was routed from the OBIGGS mounted in the empty right side, rear pack bay area to the cabin. The inerting system was instrumented with six thermocouples and four pressure taps to monitor system health and performance. Pressure transducers, used to monitor the system pressures, were mounted on a panel in the cabin with pressure-sensing tubes routed from the pressure taps to the transducer panel. All OBIGGS pressure tap and temperature measurement locations are identified on the OBIGGS drawing given in appendix E. Additionally, ambient pressure was measured in the pack bay for data reduction.

The OBIGGS was also equipped with gas-sampling ports to measure both NEA and oxygen-enriched air (OEA) oxygen concentrations, also shown on the drawing in appendix E. These oxygen samples were monitored by a two-channel oxygen analyzer capable of sampling from altitude, which operated very similar to the OBOAS. This oxygen analyzer did not require fluid traps, flash arrestors, or containment box purging because the sample system did not acquire a sample from a potentially flammable source. Also, a flow meter was installed at the NEA output to measure the NEA flow rate. These parameters constituted the ASM performance at a given flight condition.

2.1.2.7 Additional Parameters Collected.

Additional instrumentation was employed to determine the validity of certain data and to better understand the fuel tank inerting process, in general, as it relates to the FAA concept. Static pressure was measured, allowing examination of the effect of altitude on the inerting process. The NEA temperature at the flow meter and the backpressure on the OEA line was also acquired. Thermocouples were also located in the pack bay (4), one of which was in the immediate area of the OBIGGS. An additional three thermocouples were installed in the area of the bleed air connection to the system. This allowed for redundant measurement of temperature in the area of the pack bay that could potentially be susceptible to a bleed air leak.

2.1.2.8 Data Acquisition System.

A DAS recorded all analog signals required for the test in a multiplexed method and stored the data on the flight test data acquisition computer. Some data were presented on a master display, in a block diagram format, to facilitate real-time monitoring of the more significant parameters during the testing. Figure 10 shows the master DAS display.

2.1.3 Aircraft Cabin Installation.

All instrumentation was routed to the cabin via several different cabin penetrations to an array of FAA-designed and built instrumentation racks installed in the central part of the pressurized cabin immediately above the CWT. All instruments, as well as the OBIGGS, were powered via an extensive power distribution panel wired to an existing work rack immediately forward of the FAA rack system.

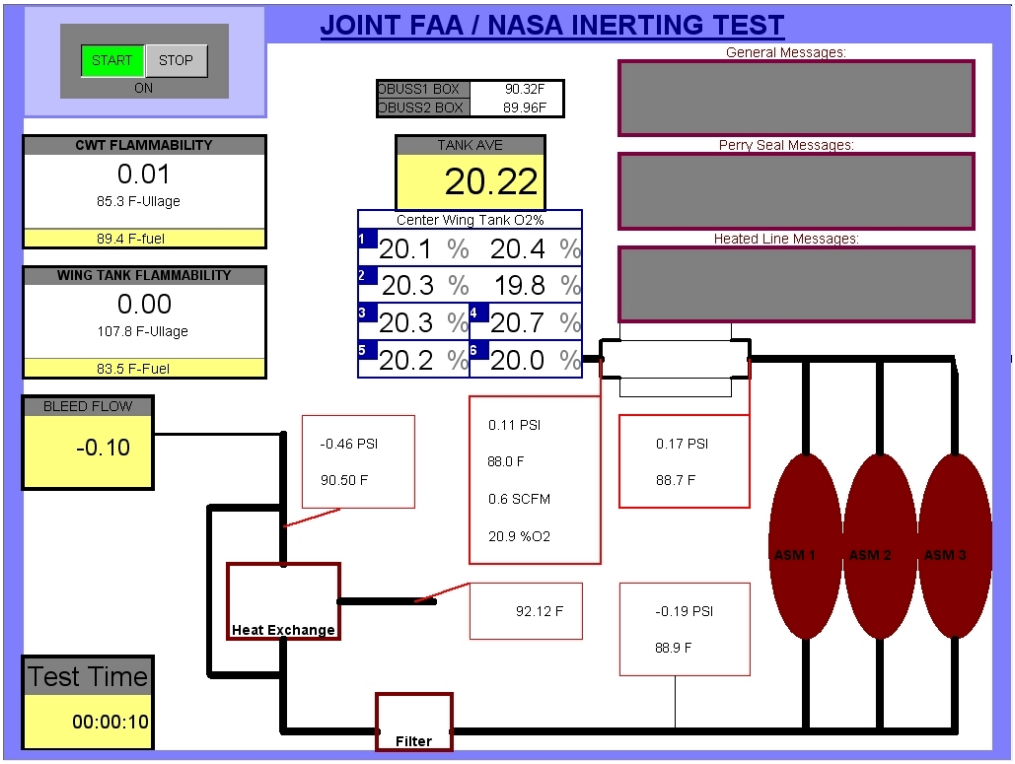

FIGURE 10. MASTER DAS DISPLAY

2.1.3.1 Power Distribution.

All power required to run the OBIGGS and the test instrumentation was obtained from an extensive power distribution bus located on an existing utility rack at station (STA) 990. The OBIGGS required both 115 Vac, three-phase 400 Hz and 28 Vdc power to operate. Each rack (2) in the OBOAS required 115 Vac, three-phase 400 Hz to operate an accompanying 115 Vac, single-phase 60-Hz power voltage converter rated for 20 amps. The two voltage converters are used to power the OBOAS as well as the OBIGGS oxygen analysis system with a power switching system attached to the OBOAS rack system.

An existing 60-cycle power converter was used in conjunction with an additional NASA power converter to power the FAS with the associated instrumentation. This included the NDIR analyzer, all heated lines, and pressure controllers. Additionally, the computer and DAS were powered by this set of power converters using an uninterruptible power supply. Figure 11 illustrates the distribution of power for the flight test instrumentation and DAS.

2.1.3.2 Instrumentation Routing.

The CWT thermocouples were routed from the modified rear spar purge door into the cabin through an existing wiring penetration in the right-hand wheel well at STA 1275. The DAS was located on the same rack with the OBIGGS control box and gas analysis equipment. The wing tank thermocouples were routed from a modified fastener in a tooling hole on the front spar, along the front spar into the fairing area, and into the fuselage through another wiring penetration

at STA 985. These thermocouples were routed to the DAS rack under the floor in the cargo bay to the right side of the cabin.

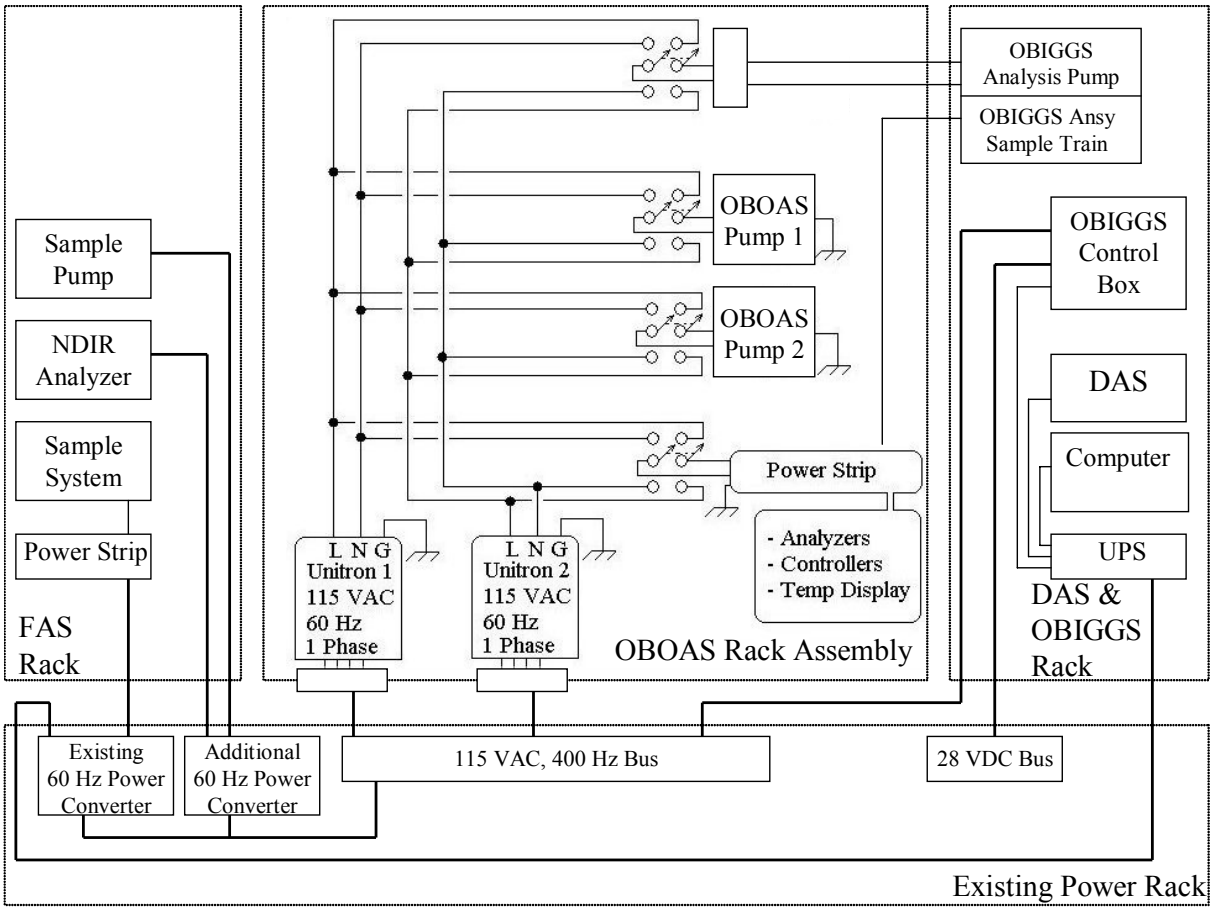

FIGURE 11. POWER DISTRIBUTION FOR THE NASA 747 SCA CABIN

The eight CWT gas-sample lines and two sample return lines were routed from the rear spar purge door fittings to the OBOAS in the cabin via a cabin penetration in the wheel well adjacent to the thermocouple penetration (approximate STA 1250). The CWT gas-sample lines were routed into the cabin through a mating fixture that terminated the shrouds of the eight sample lines and two returns in the cabin area. The lines were routed to the OBOAS location in the center of the aircraft adjacent to the DAS rack aft of STA 1080. Each four-channel system had a gas sample return routed to the tank through the same mating fixture to minimize the effect of the sample system on the ullage environment. The signals from the eight oxygen analyzers were routed to the DAS.

For the CWT THC gas sample, a single 10-foot heated line was routed directly from a modified fastener in the cabin near STA 1100 to the FAS rack located on the left side of the cabin near STA 1030. The sample from the wing tank was routed from a similarly modified fastener at WS 630 on the front spar to a 50-foot heated line routed down the leading edge of the left aircraft wing, through an existing hole between the leading edge and the fairing area, to a bulkhead fitting on the fuselage pressure bulkhead in the front cargo bay at STA 985. From this fitting,

another 10-foot heated line conveyed the sample to the rack-mounted portion of the FAS. The FAS also required two heated lines between the FAS rack and the NDIR analyzer immediately adjacent to the rack at approximately the same fuselage station. Signals from the FAS were routed across the cabin to the DAS rack.

The control cable for the OBIGGS was routed from the OBIGGS in the pack bay to the OBIGGS control box through a modified waste shoot that provided a conduit to the cabin from the aft bulkhead of the pack bay (figure 12). All OBIGGS instrumentation, including gas-sampling tubing, pressure-sensing tubing, and thermocouples, as well as all pack bay thermocouples were also routed in the same manner. The waste shoot was capped at the floor in the cabin area with an aluminum plate sealed in place, which had a slot to accommodate the instrumentation bundle. Additional sealant was used to seal the slot around the instrumentation bundle.

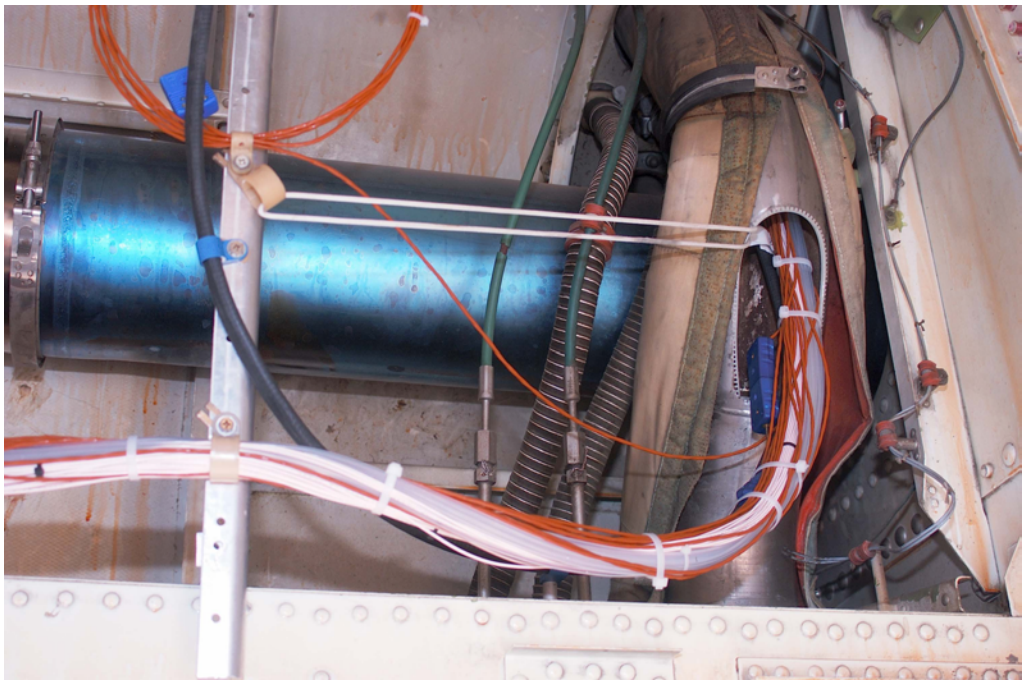

FIGURE 12. MODIFIED WASTE SHOOT USED AS A CONDUIT AT THE AFT PACK BAY AREA BULKHEAD

Figure 13 illustrates the cabin layout and equipment proximity as well as basic signal routing for the flight test setup.

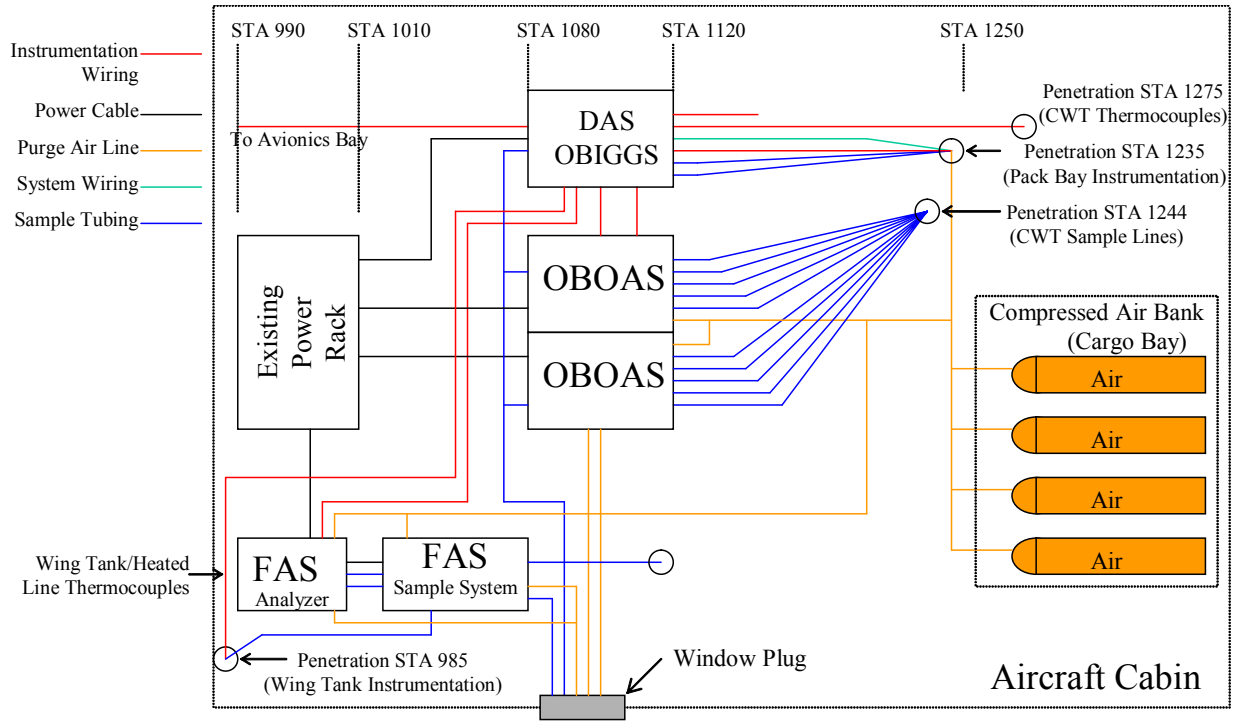

FIGURE 13. DIAGRAM OF INSTRUMENTATION INSTALLATION IN THE NASA 747 SCA CABIN

2.2 TEST PROCEDURES.

Nine flight tests were performed for a total of 29 hours. An additional 11 hours of ground testing was performed prior to and during the execution of the flight tests. All tests were performed from Ellington Field, TX, the center of NASA aircraft operations, with the exception of test 0, which departed from NASA Dryden, Edwards, CA. The ground operation between tests 4 and 5 occurred at Davis-Mothem Airbase in Tucson, AZ. The tests were performed during two different 2-week periods approximately 4 months apart. The primary focus of the testing was to study commercial transport fuel tank inerting using the FAA-simplified inerting system. Both the dual-flow and variable-flow operation was studied, with and without fuel in the CWT. Ullage flammability was measured under a variety of flight and ground conditions in both the CWT as well as in the wing tank. Additionally, flammability was measured during tests without inerting and with a conventional CWT vent configuration. Table 2 gives a list of flight tests performed on the NASA 747 SCA during the fuel tank inerting and flammability study.

TABLE 2. TABLE OF INERTING FLIGHT TESTS ON THE NASA 747 SCA

No.	FAA Designator	Date	Flight Hours	Description
1	Pretest 1	12/09/03	2.1	Preliminary OBIGGS proof of concept. CWT approx. 11% [O_2], run system gate to gate, ascend to FL 350, cruise until CWT [O_2] stable, descend per ATC. CWT no cross venting.
2	Pretest 8	12/10/03	2.9	OBIGGS performance evaluation. Stabilized system inputs at three altitudes for three different flows and two different temperatures. CWT no cross venting.
3	Test 0	5/13/04	3.8	FAS Evaluation. CWT not inert, OBIGGS off, operate FAS gate to gate. Operate ACMs on ground to generate flammability. CWT no cross venting.
4	Test 1	5/19/04	2.1	OBIGGS Demonstration–Dual Flow Mode. CWT approximate 10% [O_2], run system gate to gate, ascend to FL 350, cruise until CWT [O_2] stable, descend per ATC. CWT no cross venting.
5	Test 2	5/21/04	2.1	OBIGGS Variation 1–Variable Flow (small orifice). CWT approx. 10% [O_2], run system gate to gate, ascend to FL 350, Cruise until CWT [O_2] stable, descend same as test 1 within limits of ATC. CWT no cross venting.
6	Test 3	5/22/04	2.1	OBIGGS Variation 2–Maximum Flow (wide orifice). CWT approximate 10% [O_2], run system gate to gate, ascend to FL 350, cruise until CWT [O_2] stable, descend same as Test 1 within limits of ATC. CWT no cross venting.
7	Test 4	5/20/04	4.2	Flammability Reduction Demonstration Part 1–OBIGGS Variable Flow. CWT approximate 10% [O_2], 25% fuel load, run system gate to gate, ascend to max altitude, cruise until CWT fuel burned and [O_2] stable, descend per ATC, 3-hour turn-around running ACMs, CWT no cross venting.
8	Test 5	5/20/04	3.6	Flammability Reduction Demonstration Part 2–OBIGGS Variable Flow. CWT approximate 10% [O_2], 25% fuel load, run system gate to gate, ascend to max altitude, cruise until CWT fuel burned and [O_2] stable, descend per ATC, 3-hour turn-around running ACMs, CWT no cross venting.
9	Test 6	5/26/04	6.1	FAS Evaluation. CWT not inert, OBIGGS off, operate FAS gate to gate, operate ACMs on ground to generate flammability. CWT venting original configuration.

3. ONBOARD INERT GAS GENERATION SYSTEM.

The FAA prototype OBIGGS was designed to incorporate a dual-flow concept, developed by the FAA, that provides a low, relatively pure inert gas flow to the tank during taxi, takeoff, and cruise to obtain a low oxygen concentration. During descent, the system was switched to low-flow mode, which provides a low amount of less pure NEA to the tank to reduce the amount of air entering the tank through the vent system. The system was modified to allow for a variable/high flow during the system operation. This allowed the operator on some tests to increase the amount of flow at higher altitudes to decrease the total amount of air entering the ullage through the fuel tank vent system during descent.

The FAA OBIGGS consists of a single unregulated flow path that is plumbed to a manifold of three ASMs. The nitrogen-rich gas that passes through the modules is then plumbed to the CWT to reduce the oxygen concentration. The flow path has a heat exchanger that controls the ASM inlet temperature and a filter. The flow passes through the ASMs and through the flow control valves, which allows the system to flow in both low- and variable/high-flow modes. Figure 14 shows a block diagram of the primary components of the OBIGGS. The system is mounted on a relatively simple aluminum frame in a palletized manner for simplicity of assembly and installation.

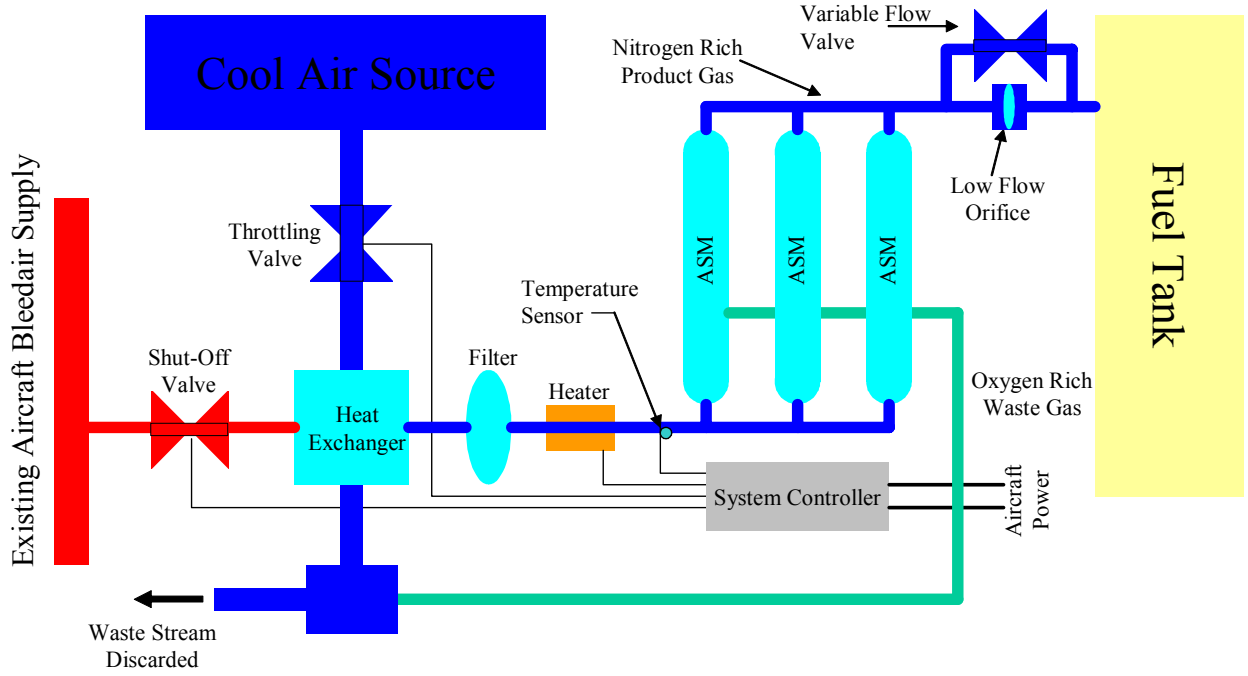

FIGURE 14. SYSTEM BLOCK DIAGRAM

3.1 SYSTEM FLOW.

The inerting system gets its bleed air from a modified main bleed air duct on the aft bulkhead of the 747 pack bay at STA 1245, which is reduced to a 2-inch-diameter tube for connection to the

system shutoff valve (SOV). When energized, the 18-32 Vdc SOV valve opens, allowing flow into the system, through the heat exchanger bypass Y, into the air/air heat exchanger. The heat exchanger accepts the 400°F bleed air and uses a 4-inch-diameter cooling bypass loop to cool the system flow to a temperature of 180°F ±10°. The cooling bypass uses a three-phase, 115 Vac, 400-Hz fan to draw outside ambient air through the heat exchanger and uses a 4-inch-diameter, 18-32 Vdc motor-operated, modulating valve to control the airflow through the heat exchanger. This modulating valve is operated by the system temperature controller, but is controlled manually with a switch box (referred to as the Parker box) by the system operator. The heat exchanger bypass Y allows a 1-inch-diameter line to bypass a portion of the system flow into the heat exchanger to decrease the effectiveness of the cooling loop, giving better control of the air temperature into the ASMs.

After the heat exchanger, the bleed air passes through a desiccating filter, past the temperature sensor used by the system operator to control the temperature, and through a section of pipe with a 187-watt clamp heater before entering the ASMs via a manifold. The clamp heater is designed to increase the temperature of the ASM inlet air significantly if the temperature should drop (due to system heat rejection) well below the target temperature obtained by the heat exchanger. However, it provided very little additional temperature when the air was maintained close to the specified temperature.

Once the 180°F cooled bleed air passes into the ASMs, the air is separated into the NEA and OEA constituents. The NEA portion passes through to the ASM outlet, while the OEA portion passes out the permeate (waste) port. The ASM waste flow is eliminated from the system through the OEA manifold plumbed into the heat exchanger exhaust box on the bottom side of the aircraft.

After the OEA is separated, the NEA passes through the flow control portion of the system, which allows the system to flow at either low-flow (low-oxygen concentration), or variable/high (higher-oxygen concentration) flow conditions. The variable-flow valve can be closed forcing all the flow through the low-flow orifice, or it can be opened to one of five distinct open conditions, of different backpressure, allowing the system to give a total of six different flow conditions. As the variable-flow valve is opened, the system backpressure will decrease, creating progressively more NEA flow, with the NEA oxygen concentration increasing (less pure) as flow increases. Two separate variable-flow valves were used; both were 1-inch, motor-operated, ball-type SOVs. One had a standard ball with a 1-inch-diameter hole, the other had a square slot with an effective 0.391-inch-diameter hole.

The NEA can be directed by means of counter-actuated SOVs to either “inert” the CWT or to “divert” the NEA overboard. When divert is selected, the NEA flows directly to the heat exchanger exhaust box where it mixes back with the OEA and is safely dumped overboard. If inert is selected, the NEA flows through a flow meter, a check valve, and finally to the NEA deposit line.

3.2 SYSTEM INTERFACES.

The primary inerting system physical interfaces are the attachment brackets that mount the system to the aircraft. The mechanical interfaces allow bleed air to interface with the system, NEA to be deposited into the CWT, OEA to be eliminated, and heat exchanger air to be used. Additionally, system electrical connections also provide an interface between the system and the aircraft power as well as between the system and the operator. The system diagram given as appendix E identifies each system interface.

3.2.1 System Mounting.

To allow a relatively simple interface with the aircraft, the system pallet was installed in the number 4 pack bay of the NASA 747 SCA, frequently referred to as the empty pack bay, using six attachment brackets. The brackets attached the aluminum angle pallet to the fairing support structure in the aft right-hand side of the pack bay area. The brackets were made of stainless steel and were attached using doublers with 1/4″ Steel A/N standard bolts. Figure 15 shows a three-dimensional rendering of the system mounted in the empty pack bay of a 747 with the main bleed air duct illustrated in blue as a spatial reference.

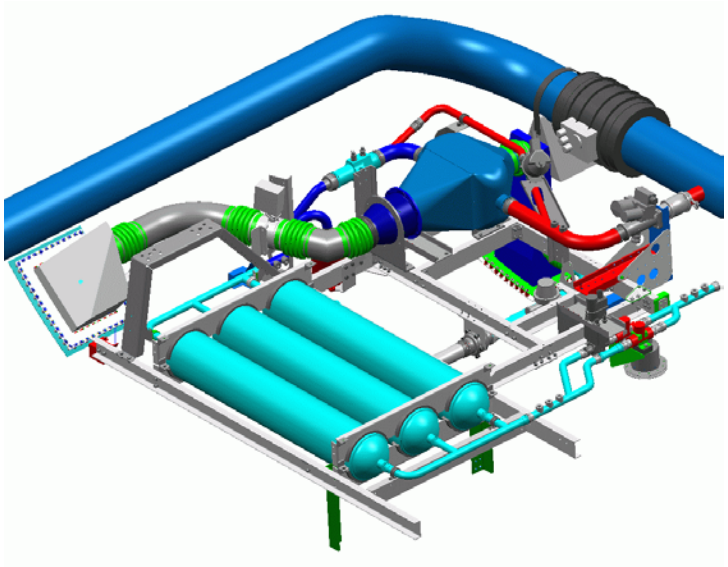

FIGURE 15. THREE-DIMENSIONAL RENDERING OF THE OBIGGS INSTALLED IN THE PACK BAY

3.2.2 Mechanical Interface.

The primary mechanical interfaces for system operation were the bleed air inlet, the NEA deposit, the OEA discharge, and the heat exchanger cooling air inlet and exit. Bleed air was supplied to the system by modifying the bleed air duct (Boeing part no. 69B41284-12) at STA 1245. The modification consisted of welding a 2-inch, commercially pure titanium BMS7-21 grade 3 tee into the main bleed air duct, and using a sealed sleeve assembly to connect the bleed air duct to the OBIGGS SOV assembly. The system SOV was a 2-inch-diameter, 28-32 Vdc

solenoid operated, mechanically closed valve, Parker part number 5940016 that had a 55-psig overpressure protection circuit. The overpressure protection feature closes the valve if the static pressure on the system exceeds 55 psi, protecting the system components in the event of a bleed air system over-pressurization.

The OBIGGS NEA output was a 1-inch Hydroflow™ 14J02 sleeve and coupling connection. The NEA inert/divert tubing assembly, described in section 3.1, was a series of 1-inch Hydroflow™ fittings with associated 1-inch SOVs adapted to a 16D A/N fitting for mating with the NEA deposit (see appendix F). The NEA was carried to the CWT through a 1-inch flexible AE701 wire-reinforced hose with stainless steel over braid lines using MIL-F-83798 specified 816-16D standard fitting ends. The 1-inch flexible line attached to an AN837-16D bulkhead fitting on the outboard, aft pack bay-canted bulkhead, which passes the NEA into the wheel well area. A second flexible line passed the NEA from the A/N bulkhead fitting to the rear spar purge panel. The NEA entered the CWT through a 1-inch-diameter SwageLok® bulkhead fitting on the rear spar purge panel (see figure 3). Adaptors were used to adapt the A/N fittings to the SwageLok bulkhead fitting. A third 1-inch flexible line was used to carry NEA to a nozzle mounted on a bracket at the top of bay 6 (right aft most bay) in the CWT. This nozzle consisted of a 90º elbow 16D A/N bulkhead fitting directing the NEA down, and a check valve was placed immediately before the nozzle to reduce the possibility of fuel seeping back into the inerting system. Appendix G contains an installation drawing of the NEA nozzle.

The OEA discharge was connected to the inboard side of the heat exchanger exhaust box via a 2-inch inner diameter (ID) aluminum tube and flexible coupling. A 2-inch check valve was also used to keep contaminants from entering the ASMs when not in operation.

The heat exchanger cooling air was interfaced with the pack bay exterior through two scoops on two separate fairing panels that were modified for the flight tests. The heat exchanger inlet door was located on fairing panel 192KR, between STA 1169 and 1181, and was approximately 10.5 inches above the bottom edge of the panel. The air inlet door had a semi-circular cross section or approximately 6 inches in diameter and was mounted in a 13.5- by 12- by 7-inch assembly. It was connected to a 4-inch motor-operated air inlet modulating valve using two flexible couplings and an aluminum tube, which had a 2-inch opening into the air inlet box. The heat exchanger cooling air exhaust door had a rectangular cross section approximately 6 inches by 3 inches and was located on access door 192NR, between STA 1223 and 1233, approximately 10.5-inches from the seam of panel 192KR. The cooling air exhaust door was mounted in an assembly 10.5 by 8 by 16 inches and was connected to the heat exchanger by a 4-inch flexible coupling that attached to an aluminum box fitted to the back of the exhaust door assembly. The NEA bypass line was connected with a 1-inch ID stainless steel flexible hose to a 16D AN fitting on this box.

Figure 16 shows the OBIGGS installed in the empty pack bay of the NASA 747 SCA test aircraft without the two panels described above.

FIGURE 16. ONBOARD INERT GAS GENERATION SYSTEM INSTALLED IN TEST AIRCRAFT PACK BAY

3.2.3 Electrical Interface.

Each system part had a specified electrical connector to communicate power and signals to the individual component. They were wired with aviation-grade wiring to a system connector, allowing the system to easily interface to the OBIGGS control box. The control box allowed the system and its components to be turned on or off and to switch the system from one flow mode to the other (see figure 17). It also provided the system operator with the ASM inlet temperature and a manual temperature control box. A complete wiring diagram of the system and control box is shown in appendix H.

FIGURE 17. FRONT PANEL OF OBIGGS CONTROL BOX

3.3 SYSTEM OPERATION.

The system is designed to operate during normal aircraft flight and ground operations, provided bleed air is available. The system low-flow and high-flow conditions were established by setting two different needle valves during ground operations. The needle valves provide the backpressure needed to give the necessary system variable performance throughout the flight profile. The aircraft's auxiliary power unit was used to power the bleed air system to approximately 30 psi, and the low-flow mode needle valve was adjusted to generate NEA with 5 percent oxygen at sea level conditions. The ASM inlet temperature was allowed to stabilize at

180°F before setting the needle valve with the variable/high-flow valve closed. For the first test, the high-flow mode needle valve was set to generate NEA with 11 percent oxygen at sea level. After the first test, the variable-flow valve was installed, and the high-flow needle valve was removed. Instead of a fixed needle valve configuration, the NEA conditions (flow/purity) were changed by opening and closing the valve in increments. The low-flow mode was primarily used for taxi, takeoff, climb, and cruise phases of flight, while the variable/high-flow mode was used primarily for the descent phase of flight and during the ground-taxi back to the gate.

It is considered essential that the OBIGGS be maintained at 180°F ±10° for efficient performance. The system operator controls the ASM inlet temperature manually using the system temperature controller. The operator adjusts several potentiometers that control the position of the 4-inch-diameter cooling air modulating valve for the heat exchanger. This modulating valve needed to be continually adjusted due to constantly changing conditions (altitude, bleed air pressure, pack bay temperature) on the aircraft during a typical flight. The operator used the temperature readout display on the OBIGGS control box to monitor cooling system performance. The readout display received its signal from a T-type thermocouple that was installed just before the ASM inlet manifold.

The operator could use the heat exchanger bypass valve if necessary to bypass a small amount of flow (10%-20%) around the heat exchanger to decrease the affectivity of the heat exchanger. This made controlling the temperature on the ASMs easier under some conditions.

During system warmup, maintenance, and testing, there was a need not to effect or disrupt the CWT environment, so a NEA divert valve was used to direct the NEA product away from the CWT. The inert/divert switch was located on the OBIGGS control panel and operates two opposing 1-inch-diameter, 28-32 Vdc motor-operated SOVs (see appendix F). When divert was selected, the inert SOV closes, and the divert SOV opens and deposits the NEA overboard. When inert was selected, the divert SOV closes, and the inert SOV opens, allowing the NEA to travel to the CWT.

The system required the operator to change from low to variable/high-flow mode manually. Low-flow mode gave the most pure (lowest oxygen concentration) NEA the system could generate with the fixed low-flow orifice and the given aircraft conditions. Variable/high-flow mode was adjusted by incrementing an “Increase/Decrease” switch on the OBIGGS control panel. The increase/decrease switch controlled a 1-inch-diameter, 28-32 Vdc motor-operated SOV. The variable/high-flow mode can allow the system to produce higher volumes of NEA of greater oxygen concentrations (less pure) at higher altitudes. This system feature allows greater flow into the tank during aircraft descent to minimize air entry into the ullage due to increasing static air pressure. This creates lower resulting ullage oxygen concentration than if the low-flow mode was simply employed the entire flight cycle.

4. ANALYSIS.

Data analysis was performed in two different categories: inerting calculations and flammability calculations.

4.1 INERTING CALCULATIONS.

The primary calculations performed to analyze the inerting test data were to determine the quantity of bleed air consumed by the system and the bulk average oxygen concentration. Additionally, a simple inerting model was used to calculate the oxygen concentration in a tank volume, given a flight profile and performance schedule of the OBIGGS.

4.1.1 Bleed Air Consumption.

System bleed air flow was calculated using an equation developed from flow in and out of the ASM and a mole balance of oxygen in and out of the ASM. The combination of these equations gives the following equation for bleed air flow in terms of NEA flow.

$$\dot{Q}_{Bleed} = \dot{Q}_{NEA} \cdot \frac{([O_2]_{NEA} - [O_2]_{Perm})}{(0.21 - [O_2]_{Perm})} \quad (1)$$

With: $[O_2]_{NEA}$ = NEA Oxygen Concentration
$[O_2]_{Perm}$ = OEA Oxygen Concentration

A more complete derivation of the equation is given in reference 5.

4.1.2 Average Fuel Tank Oxygen Concentration.

To allow for a fair comparison between different flight tests, it is critical to express the oxygen concentration of the tank as a whole, even though the concentrations of the individual bays often vary. To achieve this, a weighted average by volume was calculated, given the oxygen concentration distribution at a given time. This average weighed the oxygen concentration of each bay with the total tank volume percentage of each bay.

$$\begin{aligned} Average[O_2] = {} & .31[O_2\,Bay1] + 0.23[O_2\,Bay2] + 0.10[O_2\,Bay3] \\ & + 0.10[O_2\,Bay4] + 0.13[O_2\,Bay5] + 0.13[O_2\,Bay6] \end{aligned} \quad (2)$$

4.1.3 Inerting Model.

A simple analytical model was developed to calculate the average tank ullage oxygen concentration, given a specific tank volume and system performance schedule, to compare to the measured tank average oxygen concentration data. The model calculates the mass of oxygen in the tank at the start of the mission, given a starting tank oxygen concentration, and tracks the mass of oxygen in and out of the tank, given the changing system performance and flight conditions including the appropriate net oxygen entering the tank as a result of descent. The following equation governs the model process.

$$m_{O_2}(t) = m_{O_2}(t-1) + \dot{m} * IGOF - \dot{m} * UGOF(t-1) - (\Delta\rho * V_{Tank}) * UGOF(t-1) + (\Delta\rho * V_{Tank}) * .21 \quad (3)$$

In this equation, $UGOF(t\text{-}1)$ is the fraction of oxygen in the ullage gas. It is calculated by dividing the mass of oxygen in the tank at t-1 by the mass of gas in the tank ullage or:

$$UGOF(t-1) = m_{O_2}(t-1)/m_{Tank}(t-1) \quad (4)$$

Where:

$m_{O_2}(t)$ = Mass of oxygen in tank at time t
$\dot{m}$ = Mass flow rate of inerting gas (in terms of t)
$IGOF$ = Fraction of oxygen in inerting gas
$\Delta\rho$ = Change in ullage density due to altitude change
V_{Tank} = Volume of tank ullage
m_{Tank} = Mass of gas in tank
m_{air} = Mass of air entering tank

A more detailed description of the model process is given in reference 5.

4.2 FLAMMABILITY CALCULATIONS.

The primary calculations performed to analyze the flammability test data were simplified fuel air ratio (FAR) calculations using an FAA-developed model. Additionally, a more complex ullage flammability model was employed.

4.2.1 Estimation of the Vapor Generation in the CWT.

The vapor generation model used by the FAA has been developed by Professor C. E. Polymeropoulos of Rutgers University, and is still in its validation phase. The model employs free convection heat and mass transfer correlations in a fully mixed tank. It requires experimental data on the liquid fuel temperature, the tank walls, the ambient temperature and pressure, and generates, numerically over time, the total mass of vapor generated and the vapor masses of the component species used to characterize the liquid fuel. The user is able to input pressure, liquid fuel, and wall temperatures as functions of time, and can select from the compositions of several different flashpoint fuels. Part of the model can also calculate the equilibrium vapor concentrations at different pressures and temperatures. More detailed information about this model can be found in reference 8.

4.2.2 Fuel Air Ratio Calculator.

The FAR calculator, developed by the FAA's Chief Scientific and Technical Advisor for fuel system design, is by comparison a much simpler model, but it still provides a great amount of useful data. This model predicts fuel vapor pressure, and therefore, FAR for a wide range of fuels over a wide range of altitudes, temperatures, and mass loadings. This model, however, only calculates equilibrium values occurring under isothermal conditions and, therefore, is a conservative estimate of the FAR. The model also offers several other features, such as being able to enter ASTM D 2887 distillation curve and flashpoint data to generate a customized fuel for use in the model and predicting such things as the flashpoint of a given fuel, molecular weight of the vapor, and the temperature needed to arrive at a stoichiometric mixture. The model

and further associated information can be found online at www.fire.tc.faa.gov/systems/fueltank/downloads.stm.

5. DISCUSSION OF RESULTS.

The results of the flight tests are presented for two areas of analysis: fuel tank inerting and fuel tank flammability.

5.1 FUEL TANK INERTING.

The primary focus of the fuel tank inerting data is the changing system performance, given different flow modes and orifice settings. Additionally, the effect of these flow conditions on OBIGGS bleed air consumption was examined. Also, the ability of the system to inert the given aircraft CWT was examined for both the average fuel tank oxygen concentration and the distribution of oxygen within the compartmentalized tank.

5.1.1 Inerting System Performance.

The primary factors affecting the inerting system flow and purity are the pressure on the system and the altitude (pressure) at the OEA vent. Figure 18 illustrates these two parameters for the OBIGGS NEA flow and purity for a test using the basic dual-flow methodology. As expected, increases in pressure on the ASM resulted in greater NEA flow and a lower NEA oxygen concentration (more pure), given a fixed orifice. The NEA oxygen concentration will decrease with increased flow when the NEA deposit orifice is fixed. This is due to the fact that an increase in flow across a fixed orifice will result in a greater pressure drop and an increase in pressure drop across this system flow orifice will result in a decrease in oxygen concentration.

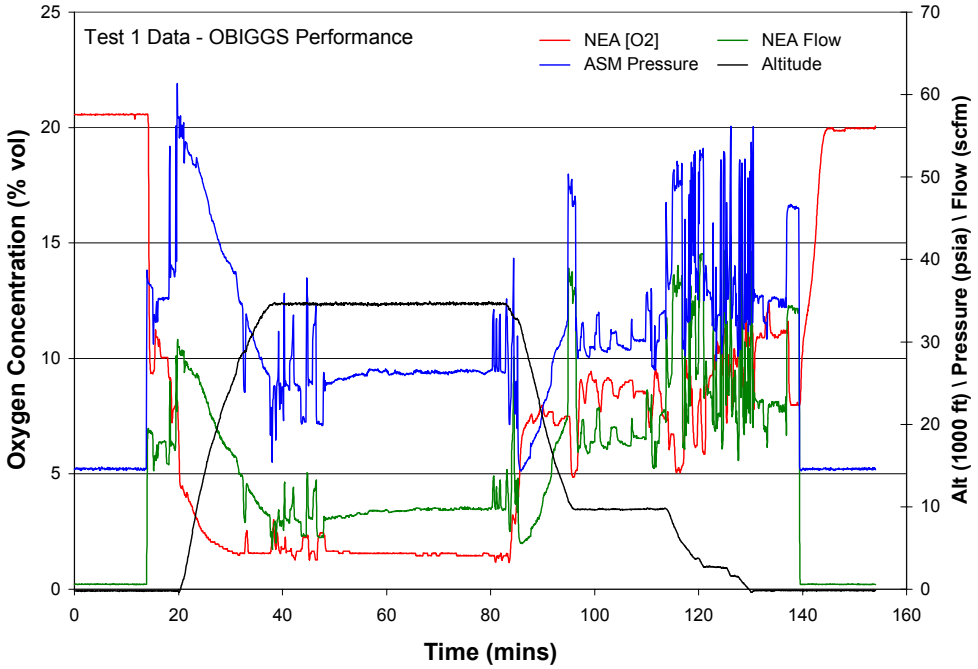

FIGURE 18. SYSTEM PERFORMANCE DATA FOR A TYPICAL FLIGHT TEST

Figure 19 illustrates the ASM pressure for the taxi/takeoff portion of three different tests with three different ascent rates. This graph illustrates the very similar pressure profiles the system was exposed to at the inception of each test, particularly the period just after takeoff for approximately 4 minutes. Figures 20 and 21 illustrate the NEA purity and flow, respectively, for the same three tests during the same time period. Each test had an adjusted time to allow for comparison of the parameters. Figures 20 and 21 illustrate the somewhat wider range of performance for this same time period.

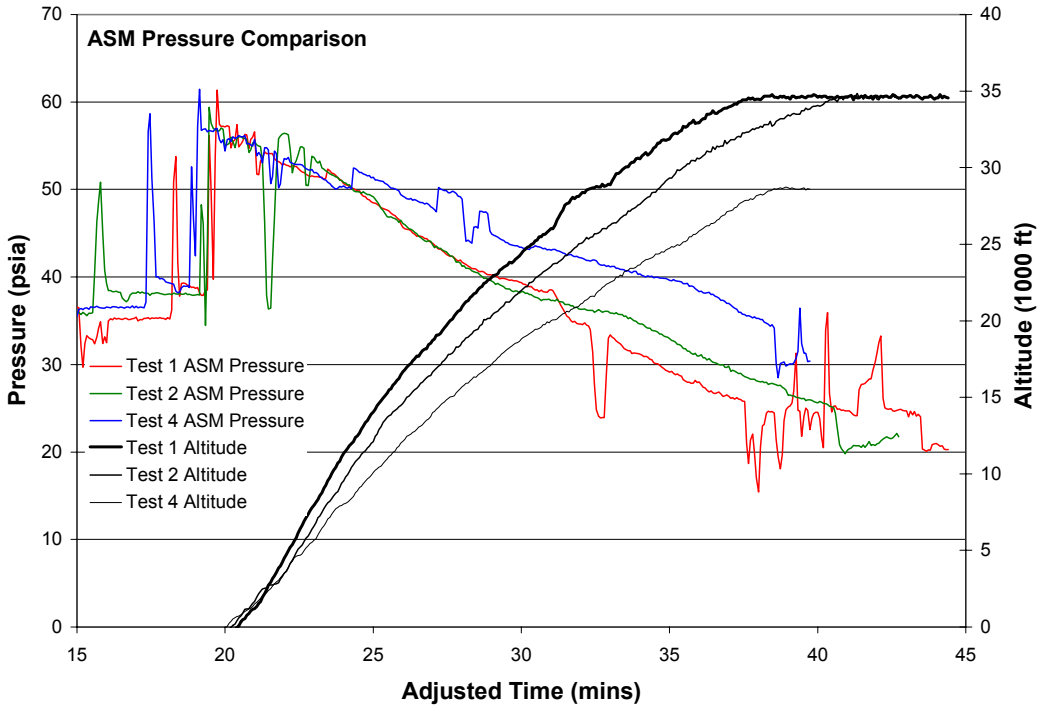

FIGURE 19. COMPARISON OF ASM PRESSURE DURING THE INCEPTION OF THREE DIFFERENT FLIGHT TESTS WITH ALTITUDE

Further examination of the system input conditions illustrates that the system input temperature was consistent for each test, but each had a significantly different output temperature, indicating a different level of heat soaking in the ASMs. For each test, the system was run prior to the test, but for different periods of time, each test having the system off prior to taxi (system on for test) for a different amount time. Also, the ACMs were run in different ways prior to each test, creating different temperature conditions in the pack bay area where the system was housed. All these factors had an effect on how heat soaked (steady temperature operation) the ASMs are, which created these unique performance conditions for the initial part of each system operation. This is evident in figure 22, which illustrates a similar ASM temperature input range for each of the tests during this time period (21 to 25 minutes) but very different NEA temperatures (ASM output). ASM temperature changes the permeability characteristics of the ASM, which causes these marked changes in system performance observed in figures 20 and 21. Presumably, these variations would be greater if the ambient temperatures were colder. Ambient temperatures ranged from 80º to 95ºF with varying amounts of sun and wind for these three tests.

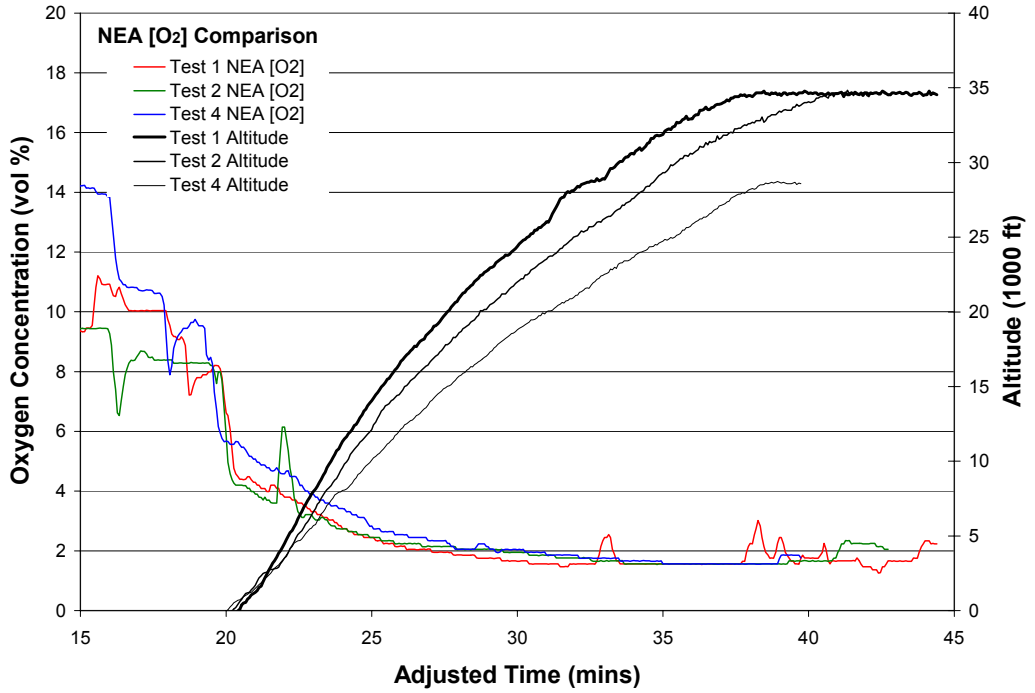

FIGURE 20. COMPARISON OF NEA PURITY DURING THE INCEPTION OF THREE DIFFERENT FLIGHT TESTS WITH ALTITUDE

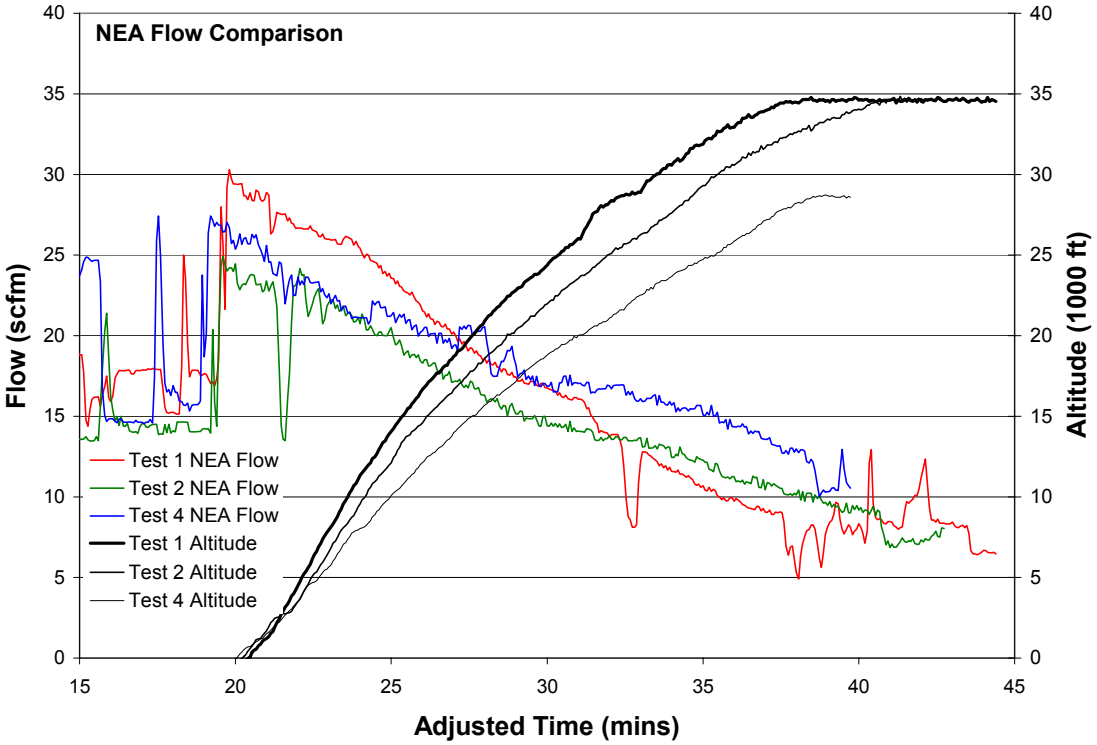

FIGURE 21. COMPARISON OF NEA FLOW DURING THE INCEPTION OF THREE DIFFERENT FLIGHT TESTS WITH ALTITUDE

Figure 23 illustrates the ASM inlet pressure for the descent/landing portion of three different tests with three similar descent profiles. Each test used a different valve and methodology for the variable/high-flow portion of the flight. As previously discussed, test 1 had a fixed high-flow orifice, while tests 2 and 3 varied the high-flow orifice to maximize flow at the top of descent. This graph illustrates the very similar pressure profiles the system was exposed to at the beginning of each descent, marked by periods of high variation in pressure during the altitude hold and completion of descent. All three tests exhibited the same range of pressures with similar trends.

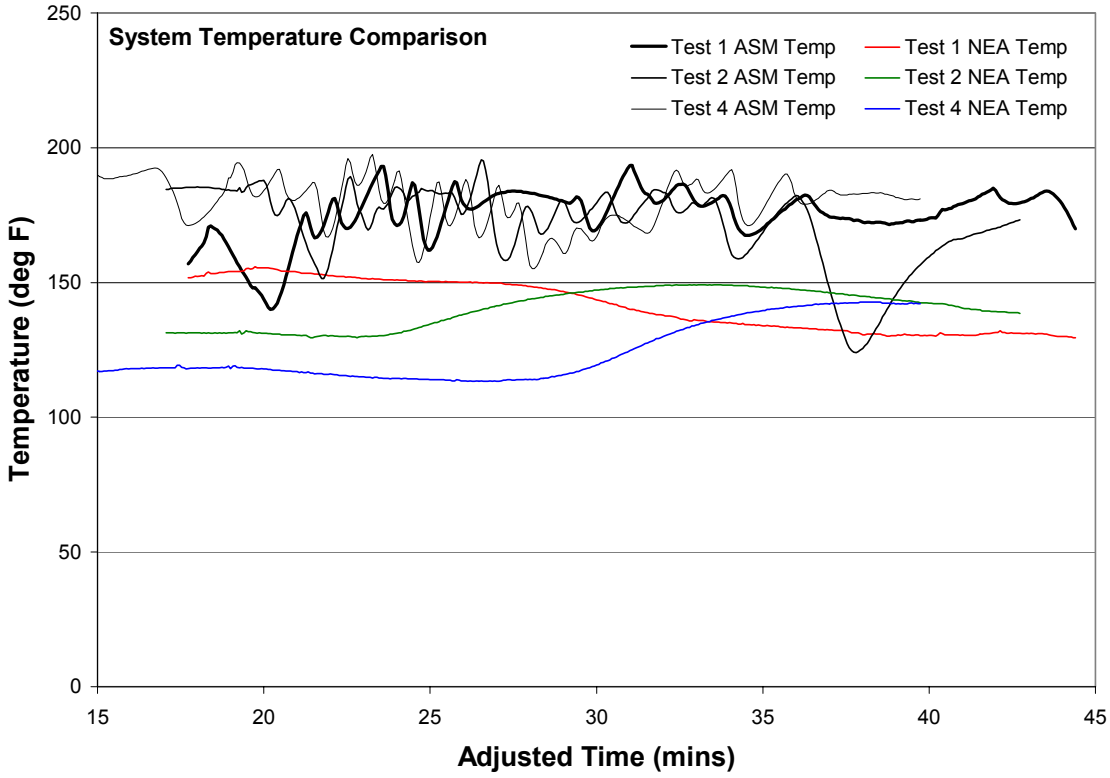

FIGURE 22. COMPARISON OF ASM INPUT AND OUTPUT CONDITIONS DURING THE INCEPTION OF THREE DIFFERENT FLIGHT TESTS

Figures 24 and 25 illustrate the NEA purity and flow, respectively, for the same three tests illustrated in figure 23. Each test had an adjusted time to allow for comparison of the parameters. Figures 24 and 25 show the expected result that tests 2 and 3, with potentially wider high-flow orifices, delivered a resulting higher volume of NEA with a resulting higher oxygen concentration (less pure), particularly at the bottom of descent. The result of this system performance change should be less ambient air flowing into the CWT through the vent system, and thus, a net lower oxygen concentration in the tank after the completion of descent. Note the erratic nature of the ASM pressure and flow at the end of descent, making it difficult to judge what tests had a greater net flow into the CWT. This is due to the very dynamic nature of the engine throttle settings during the final stages of flight.

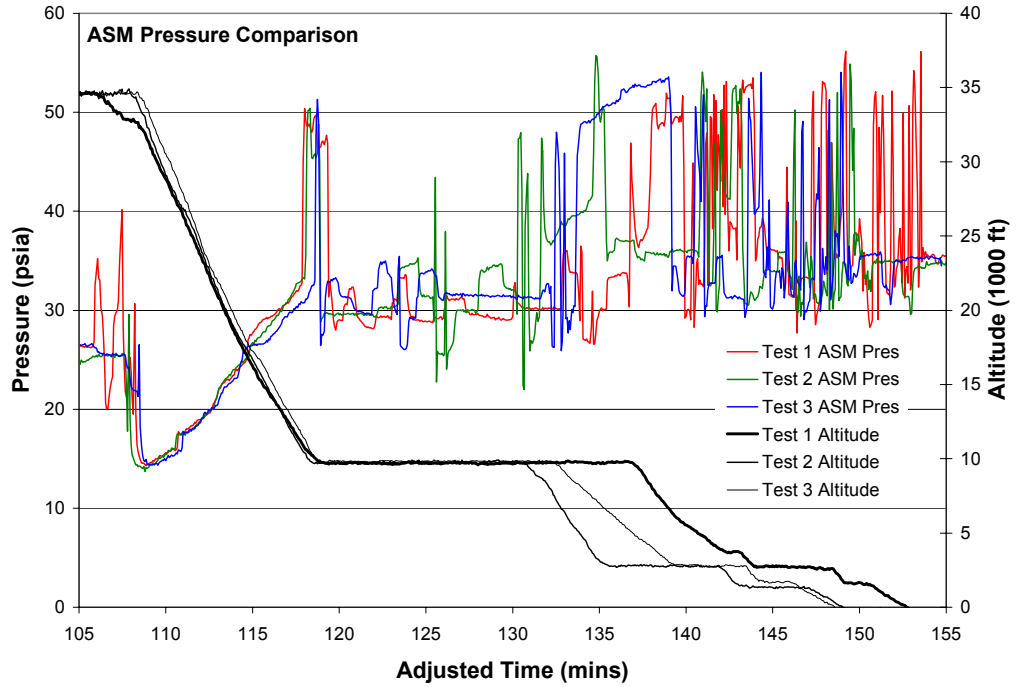

FIGURE 23. COMPARISON OF ASM PRESSURE DURING THE DESCENT PHASE OF THREE DIFFERENT FLIGHT TESTS WITH ALTITUDE

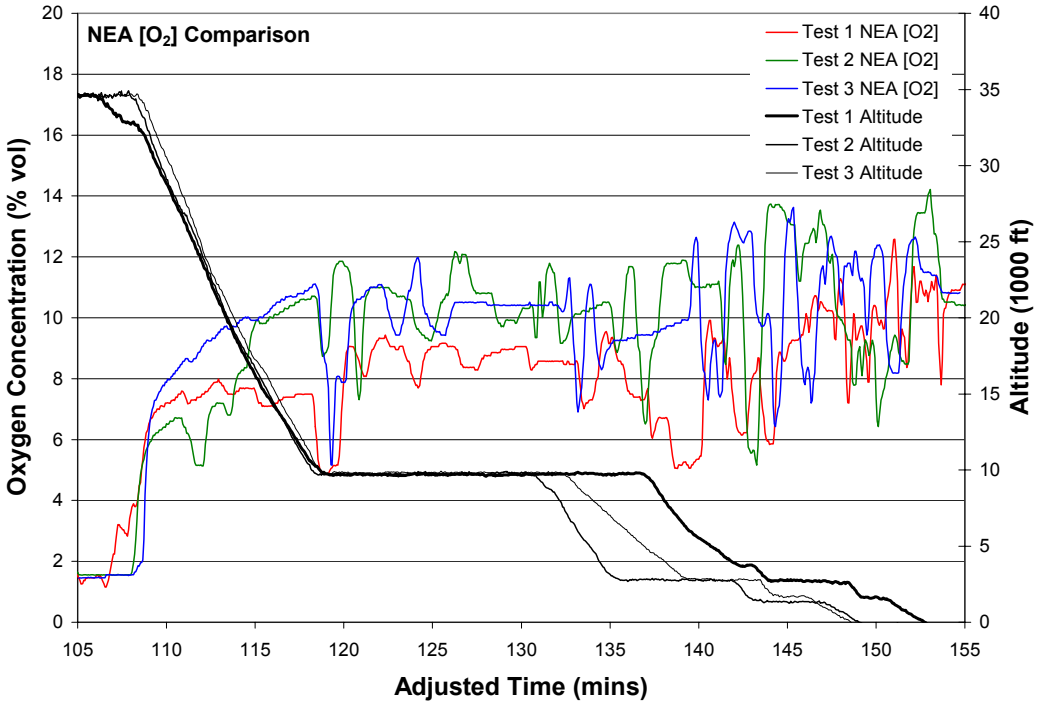

FIGURE 24. COMPARISON OF NEA PURITY DURING THE DESCENT PHASE OF THREE DIFFERENT FLIGHT TESTS WITH ALTITUDE

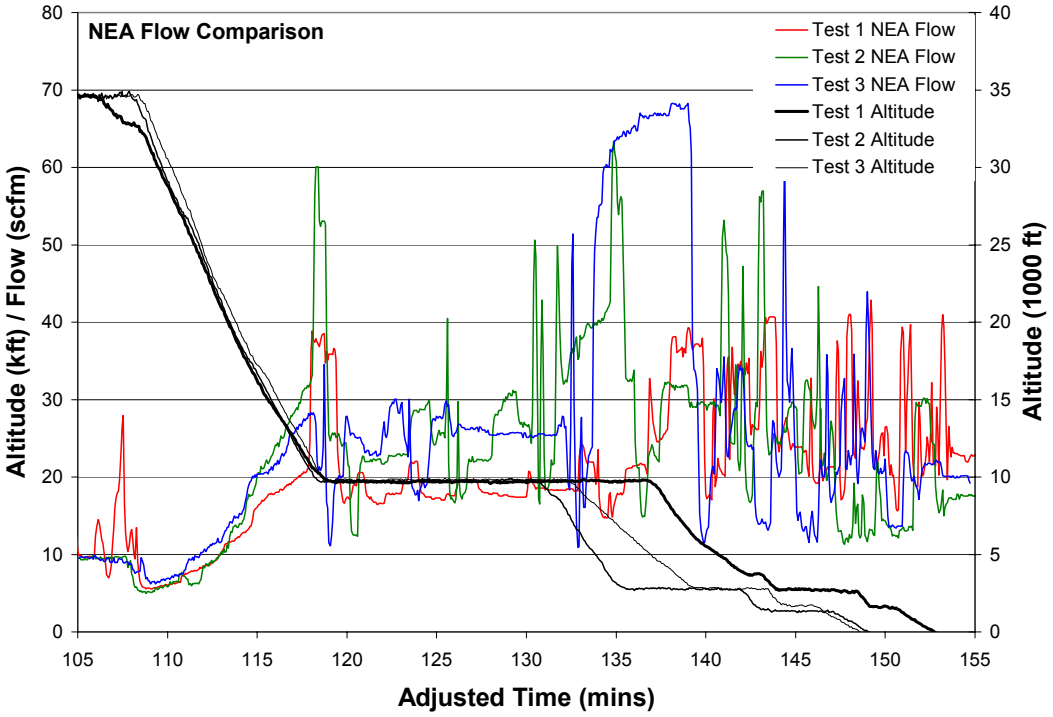

FIGURE 25. COMPARISON OF NEA FLOW DURING THE DESCENT OF THREE DIFFERENT FLIGHT TESTS WITH ALTITUDE

Bleed air flow consumption for the taxi/takeoff and descent/landing phases of the above-mentioned tests was also examined. The taxi/takeoff bleed air consumption (figure 26) shows a marked variation between the three tests, similar to the comparison of NEA flow. This is consistent with the analysis that temperature variations in the ASMs caused these differences. Any difference in ASM temperature will manifest itself in terms of changes in permeability, which will affect the NEA flow (recovery) by changing the bleed air consumption (permeability). The descent/landing bleed air consumption (figure 27) shows no significant deviation between the three tests, unlike the comparison of NEA flow. This is consistent with the ASM permeability characteristics that generally give constant ASM input flow, given a fixed ASM pressure and permeate pressure, assuming a heat-soaked bundle at a constant temperature. With each test operating with the same pack settings at the same altitude conditions for approximately the same time, somewhat constant temperature conditions would be expected. The NEA flow is a function of orifice pressure drop, as dictated by orifice size. The differences shown in NEA flow in figure 25, during the second half of the first part of descent, are due to changes in the high-flow orifice size from test to test, or by mechanically changing the effective orifice diameter during a test to increase flow and decrease purity. These tend to have little or no effect on the bleed air consumed by the OBIGGS during the observed high-flow conditions.

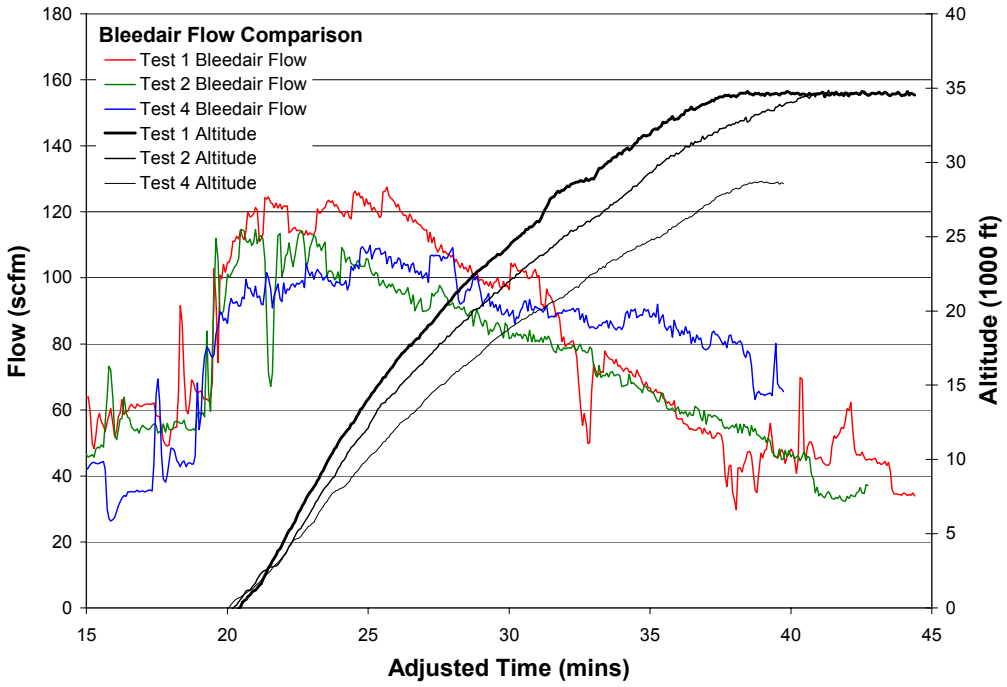

FIGURE 26. COMPARISON OF BLEED AIR CONSUMPTION DURING THE INCEPTION OF THREE DIFFERENT FLIGHT TESTS WITH ALTITUDE

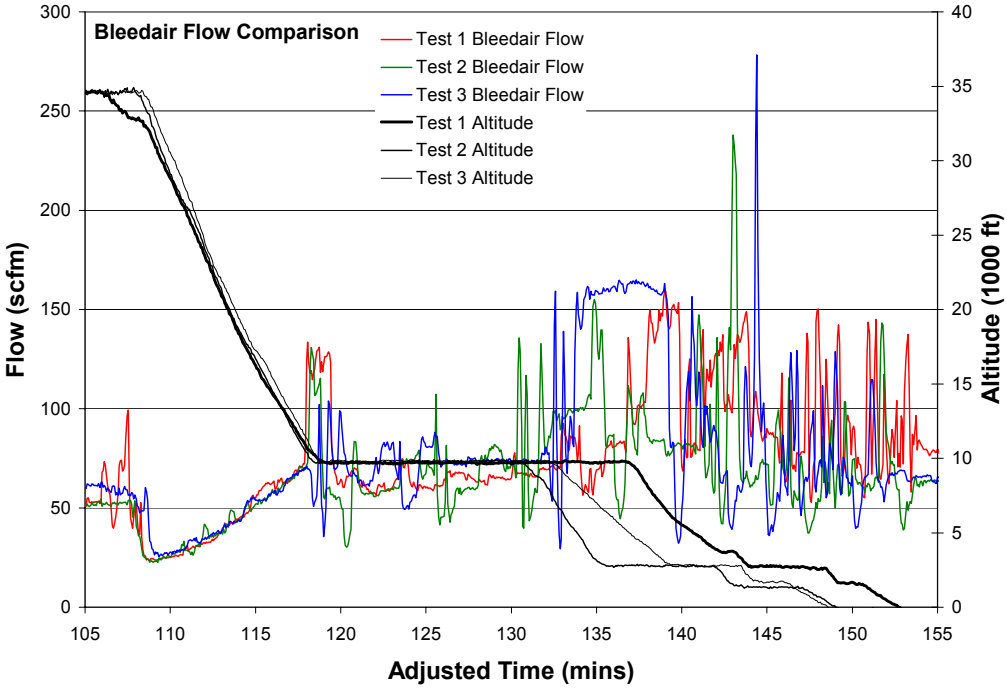

FIGURE 27. COMPARISON OF BLEED AIR FLOW DURING THE DESCENT OF THREE DIFFERENT FLIGHT TESTS WITH ALTITUDE

A correlation of system NEA flow and pressure was made for selected portions of the ascent and descent to characterize the system performance. It is important to note that these relationships are only valid for a single orifice setting and a narrow range of altitudes. Each specified altitude relates to a wide range of data around that altitude to make generalizations about system flow versus ASM pressure. Figure 28 shows how sensitive the NEA flow is to ASM pressure, even in the low-flow mode. The excellent correlation was due to the fact that the low-flow orifice settings remained constant during the entire flight test. The deviations in slope between the data from test 1 and the test 2 and 4 are probably due to the difference in system warmup times causing the deviations in system performance.

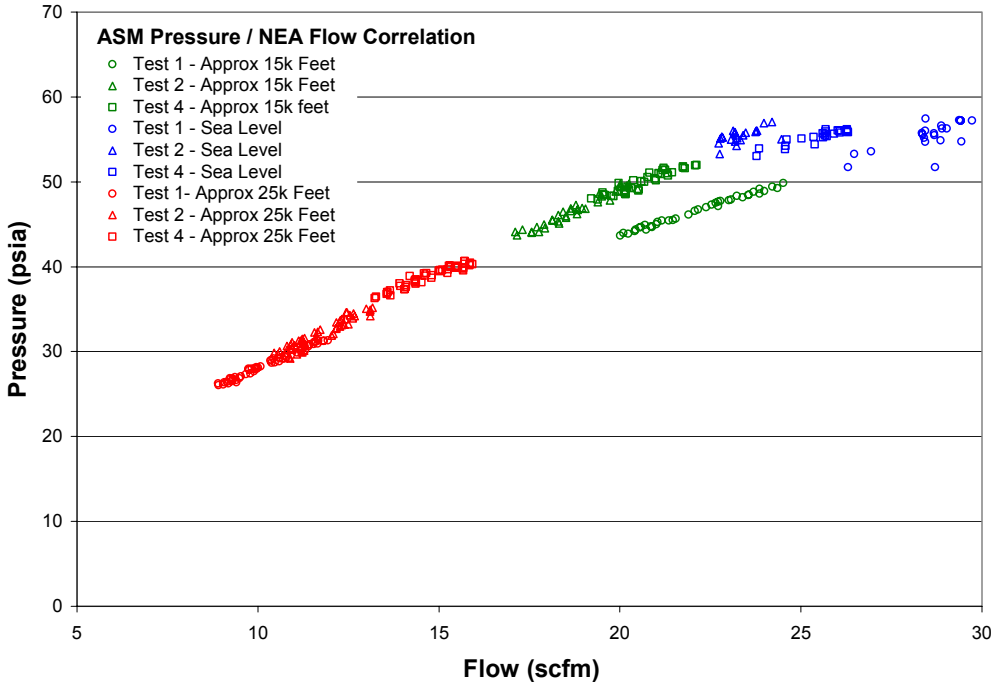

FIGURE 28. CORRELATION OF NEA FLOW WITH ASM PRESSURE FOR THE SYSTEM LOW-FLOW MODE FOR THREE DIFFERENT FLIGHT TESTS

Figure 29 gives the correlation between ASM pressure and NEA flow using the variable/high-flow mode. Although the data represents a wide range in orifice settings, better correlation is expected. The poor correlation in the graph is most likely due to the difficulty in obtaining consistent ASM pressure and orifice setting during the descent. The advantage of the variable-flow orifice used by the system operator for tests 2 through 5 was difficult to gage because of problems obtaining stable observable parameters (NEA purity, NEA flow, ASM pressure) with which to schedule the orifice setting. These problems were exacerbated because the operator did not have the ability to gage the existing orifice setting during the descent, but rather, changed the orifice setting continually to obtain the flow and purity desired.

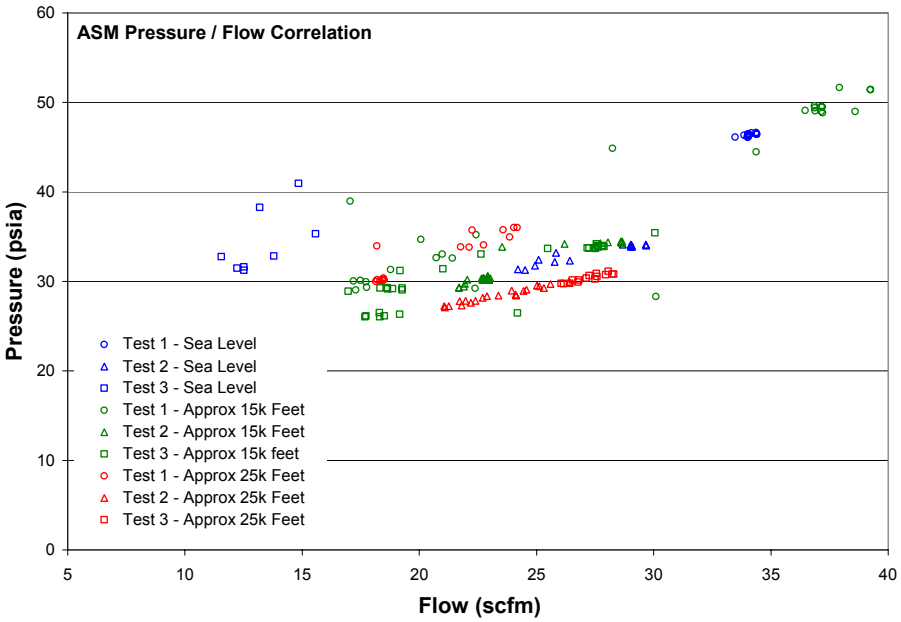

FIGURE 29. CORRELATION OF NEA FLOW WITH ASM PRESSURE FOR THE SYSTEM VARIABLE/HIGH-FLOW MODE FOR THREE DIFFERENT FLIGHT TESTS

5.1.2 Ullage Oxygen Concentration Data.

The result of the system performance on the oxygen concentration in the ullage of the CWT was analyzed by examining the oxygen concentration in each of the six bays in the tank. Figure 30 shows that there is considerable difference in the highest and lowest oxygen concentration in the ullage, particularly during descent. Bay 1 has a consistently higher oxygen concentration than the rest of the bays, primarily because it is the farthest from the bay where the NEA is deposited (bay 6), and it is where most of the air is deposited from the vent system during descent.

5.1.2.1 Average/Worst Bay Oxygen Concentration.

The primary focus of the fuel tank inerting analysis was to determine the ability of the system to maintain an average ullage oxygen concentration less than 12 percent oxygen in the CWT. Figure 31 gives the average ullage oxygen concentration measured in the CWT, as calculated from the data in figure 30, with the altitude flight profile for a reference. This profile was typical of the tests performed that had the tank oxygen concentration starting between 9 and 12 percent oxygen, which quickly decreased to about 3 percent after approximately 1 hour of cruise. At the time of descent, the oxygen concentration in the tank spikes, due to air entering the tank, and each hold at altitude allows for the tank oxygen concentration to decrease again. The average oxygen concentration in the tank settles out briefly after touchdown. It is important to note how quickly the oxygen concentration in the tank drops after takeoff. Although the normalized volume flow of NEA from the system in low-flow mode only changes a relatively small amount from taxi and takeoff to cruise, the impact of the actual volume flow at cruise altitude on the CWT oxygen concentration was much greater than at sea level when considering the mass of gas in the tank (to be ullage washed) is less than 1/3 the mass at sea level.

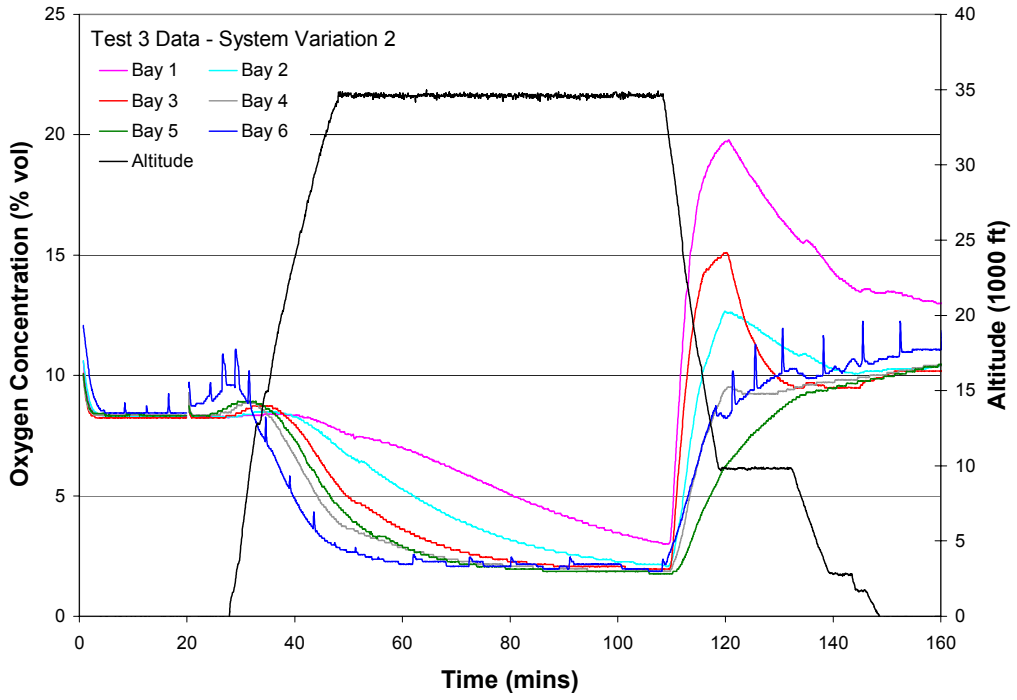

FIGURE 30. OXYGEN CONCENTRATION DATA FROM ALL SIX BAYS WITH TEST ALTITUDE FOR A TYPICAL FLIGHT TEST

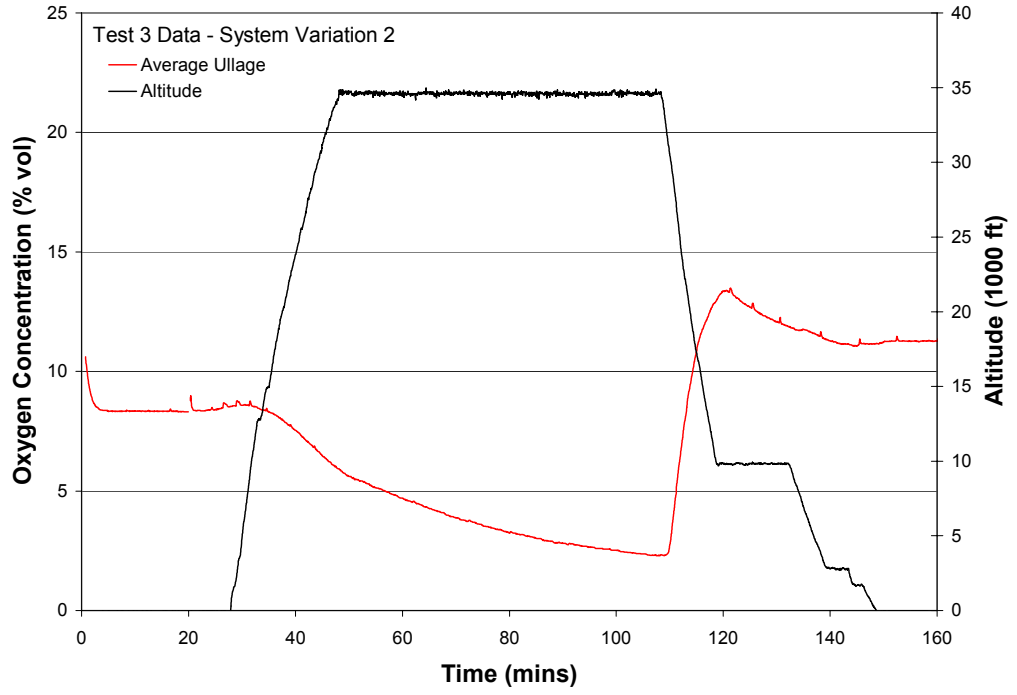

FIGURE 31. AVERAGE ULLAGE OXYGEN CONCENTRATION DATA CALCULATED FROM SIX BAY MEASUREMENTS WITH TEST ALTITUDE FOR A TYPICAL FLIGHT TEST

Figure 32 compares four descent profiles (altitude) with the measured average ullage oxygen concentration. Each test has a different flight profile with similar features. As evident from the graph, the total change in altitude (pressure) and the time to descend are the key factors when considering the increase in ullage oxygen concentration during descent. The same can be said of the worst bay oxygen concentration, described previously as bay 1. Figure 33 illustrates the bay 1 oxygen concentration for the same four descent profiles and illustrates the very same trends observed in figure 32 with greater magnitude. Although the greatest observed ullage average peak was 13.5 percent for a descent from 35,000 feet in 41 minutes, the corresponding bay 1 peak was approximately 19.5 percent oxygen by volume. However, on a 64-minute descent from 33,000 feet, the average ullage oxygen concentration peak was estimated to be approximately 10 percent, while the corresponding bay 1 peak was estimated to be less than 14 percent by volume. The peaks for test 5 were estimated due to a loss of data during the final stages of the flight. These estimates were made by calculating the peak oxygen concentration using a simple ullage model and observing the peaks of a similar flight test. This illustrates that an effective way to decrease the peak oxygen concentration in the worst observed bay is to decrease overall average ullage oxygen concentration at the duration of the flight. This is illustrated in figure 34, which gives the average ullage oxygen concentration correlated with the worst bay oxygen concentration for the four tests presented in figures 32 and 33.

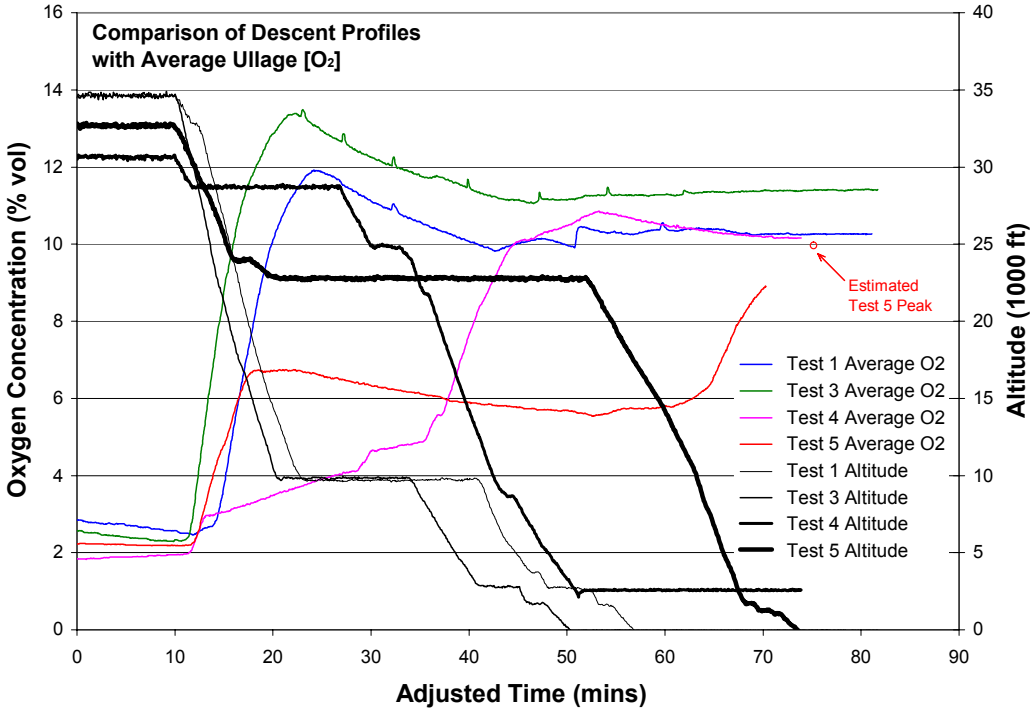

FIGURE 32. COMPARSION OF AVERAGE ULLAGE OXYGEN CONCENTRATION WITH FOUR DIFFERENT TEST DESCENT PROFILES

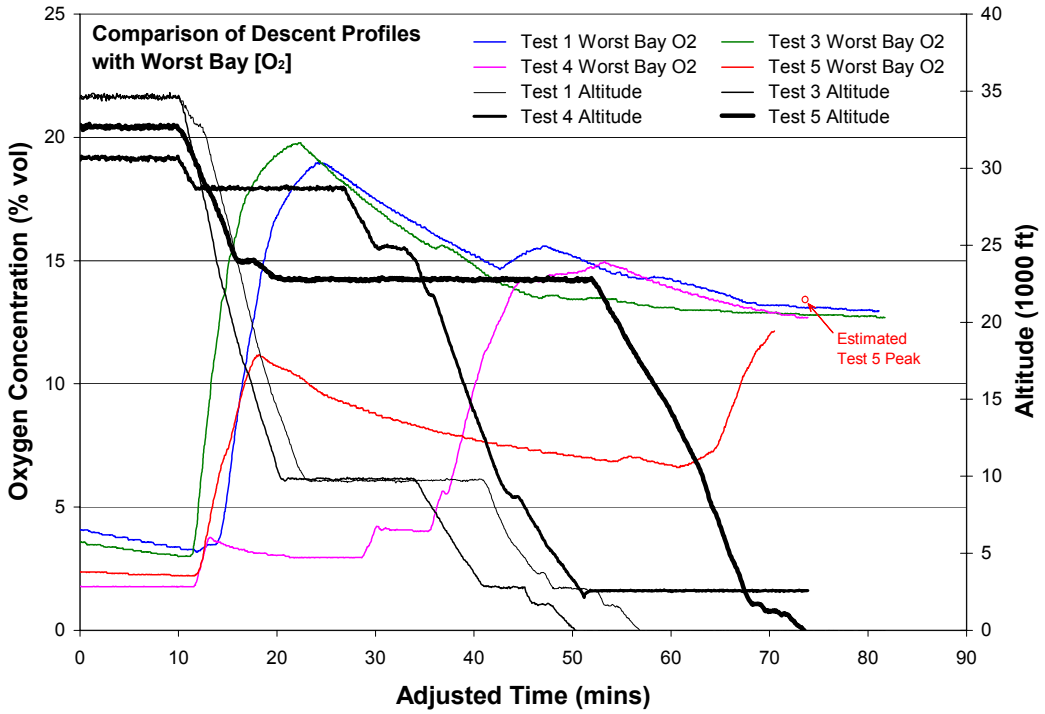

FIGURE 33. COMPARSION OF THE WORST BAY OXYGEN CONCENTRATION WITH FOUR DIFFERENT TEST DESCENT PROFILES

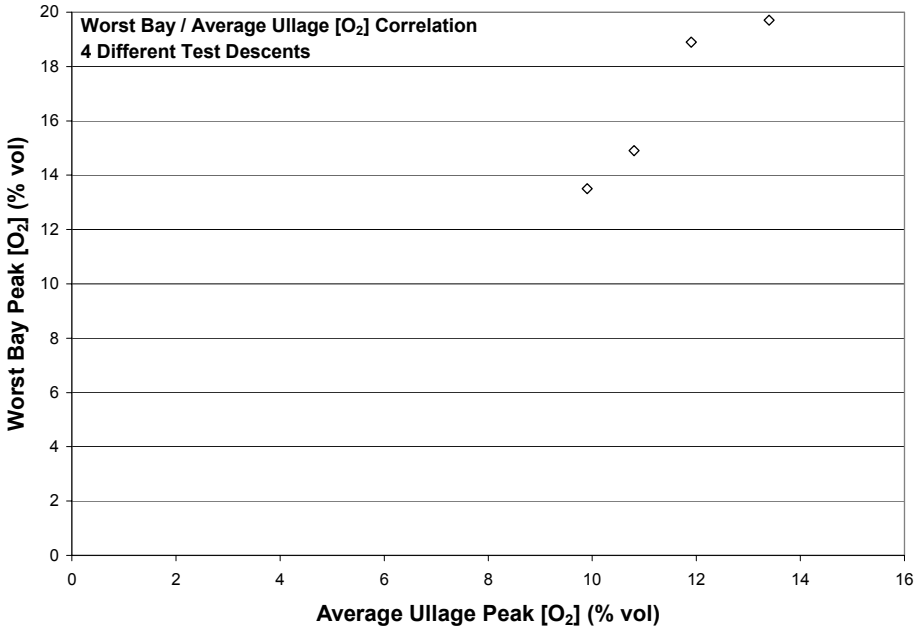

FIGURE 34. CORRELATION OF THE PEAK WORST BAY OXYGEN CONCENTRATION WITH THE PEAK AVERAGE ULLAGE OXYGEN CONCENTRATION FOR FOUR DIFFERENT TEST DESCENT PROFILES

5.1.2.2 Inerting Model Comparison.

To gage the ability of a simple ullage inerting model to predict average oxygen concentration, the model discussed in section 4.1.3 was applied to the data. The model uses the measured system performance and flight data to generate the ullage oxygen concentration. The model assumes a single, well-mixed bay in the tank vented to atmospheric pressure. Figure 35 shows the results of the model compared to the average ullage oxygen concentration calculated from the individual bay measurements. A comparison of the data shows good agreement with the data trends, with some disagreement between the peak oxygen concentrations. The maximum and minimum values agree within 1 oxygen percent, with some discrepancy between the time at which the peaks occur. Any deviation in peak times can be explained by the long delay in the OBOAS sample system, which takes as much as 2-3 minutes to completely respond to rapid changes in the ullage oxygen concentration. The differences in peak values can be explained by the efficiency of the inerting process when comparing a single deposit inerting a six-bay tank versus a single-bay rectangular tank. Previous studies of inerting compartmentalized fuel tank models on the ground exhibited an increase in inerting efficiency when using single- deposit methods [9]. This increased efficiency would manifest itself as a lower oxygen concentration achieved for the same gas deposited, similar to what is observed in figure 35.

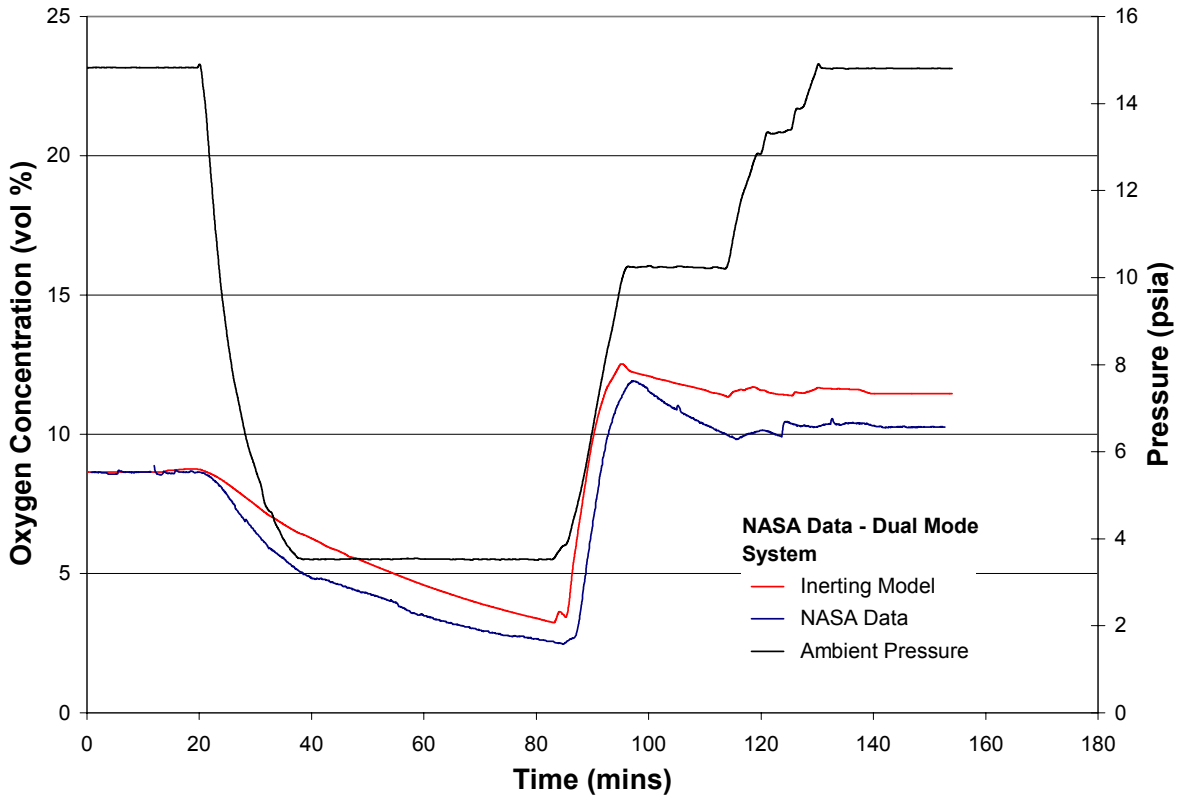

FIGURE 35. AVERAGE ULLAGE OXYGEN CONCENTRATION DATA FOR A TYPICAL FLIGHT TEST COMPARED TO A SIMPLE ULLAGE INERTING MODEL

5.1.2.3 Inert Gas Distribution.

The most challenging part of the distribution of inert gas in the CWT was during descent. Figure 36 shows the measured oxygen concentration in six bays of the CWT while the inerting system was operating in the variable-flow mode. This mode made it possible to create even higher flows at the top of the descent than the ordinary high-flow mode. Although most tests varied in starting altitude and descent time, they all exhibited similar trends with comparable distribution of the inert gas at the end of the test, with respect to the different bay oxygen concentrations.

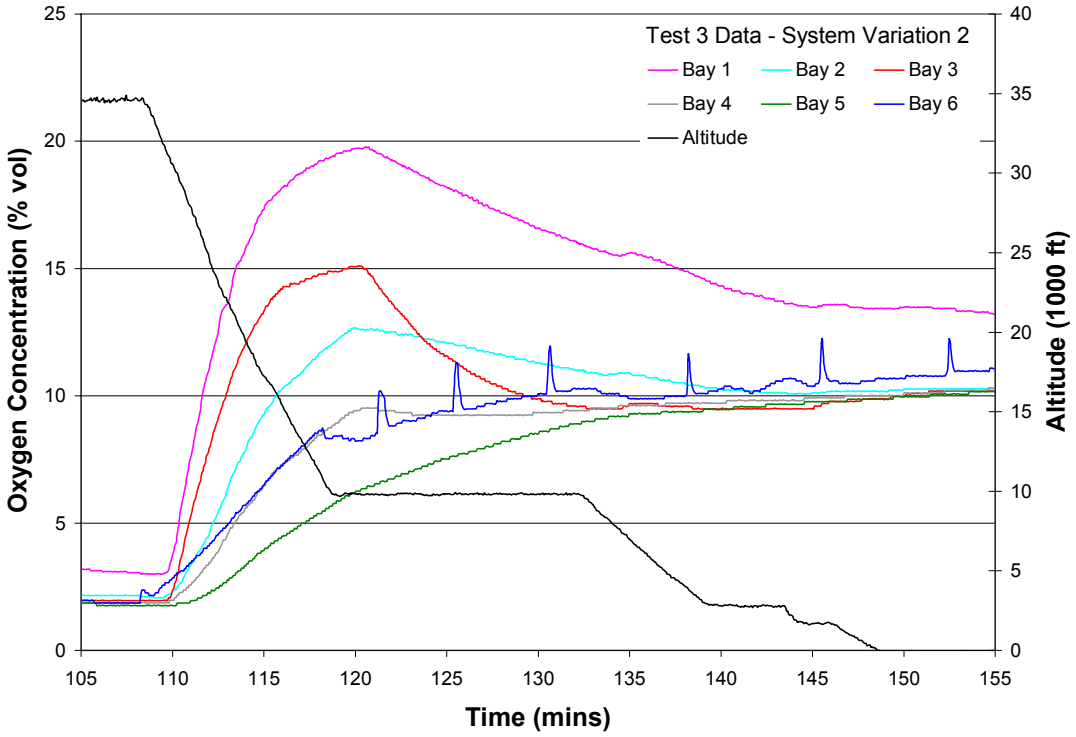

FIGURE 36. OXYGEN CONCENTRATION DATA FOR THE SIX BAYS OF THE CWT DURING THE DESCENT OF A TYPICAL FLIGHT TEST

Three different system operation methodologies were used for three different test descents, numbered test 1, 2, and 3. Test 1 used the traditional dual-flow mode, while tests 2 and 3 used two different scheduling methods for the variable-flow mode. Test 3 used the variable-flow mode to maximize flow, while test 2 used the variable-flow mode to target a particular oxygen concentration, which tended to give more flow than test 1. Figure 37 compares the distribution of inert gas at the end of each test, 5-10 minutes after touchdown. Each test started descent with approximately 2.5 percent average ullage oxygen concentration. A subtle trend was the variable-flow mode seemed to improve distribution, but it was difficult to tell as all three tests did not use the same descent time. Qualitatively, it appears that if test 1 had a 41-minute descent as in the case of tests 2 and 3, test 1 would have a greater average ullage oxygen concentration and a greater bay 1 (worst bay) oxygen concentration. This would imply that the more flow on descent, the better the distribution of inert gas at the completion of descent, but apparently this had little or no effect on the average ullage oxygen concentration after touchdown.

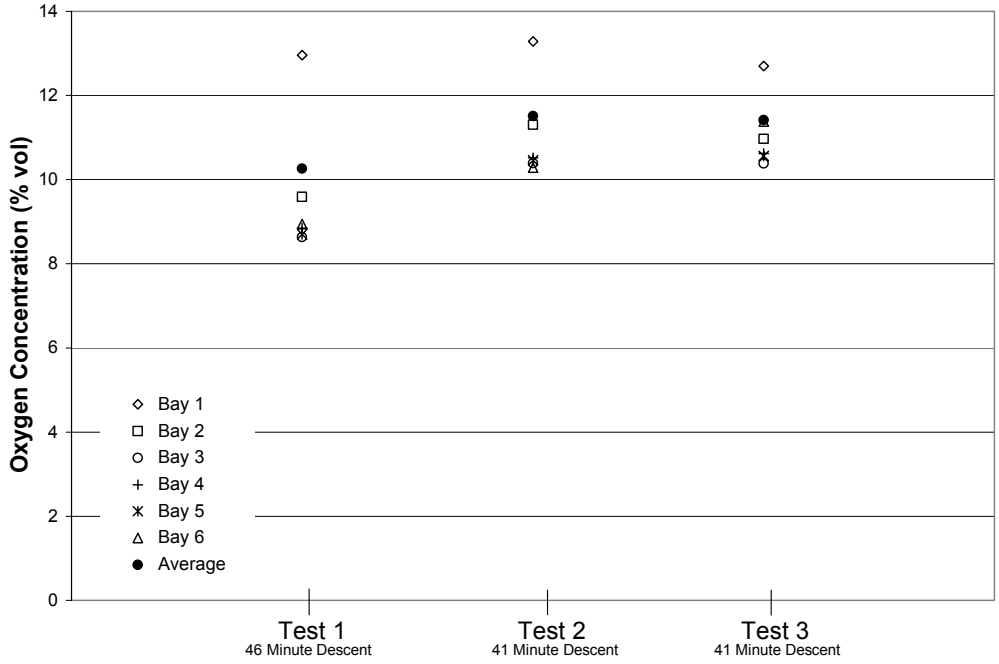

FIGURE 37. VARIATION IN THE OXYGEN CONCENTRATIONS IN THE SIX BAYS OF THE CWT DURING THREE FLIGHT TESTS

5.1.2.4 Inert Gas Diffusion.

To determine the potential flammability exposure of an aircraft landing with one or more tank bays above 12 percent oxygen, but with the average tank ullage oxygen concentration being less than 12 percent, a 3-hour ground turnaround test was performed in a warm dry climate (figure 38). The aircraft was parked after landing and the instrumentation was turned off briefly for maintenance purposes. One hour later, the instrumentation was turned on again and the oxygen concentration of the ullage was monitored. It took approximately 1 hour for the worst bay (bay 1) to go from 13 percent to 12 percent, with an average ullage oxygen concentration of 11 percent oxygen. During the ground turnaround, the ACMs were operated continuously to keep the cabin air conditioned, which heated the CWT. The average ullage oxygen concentration increased from approximately 10 percent at time zero, just after landing, to approximately 11 percent at time 1 hour. This is most likely due to slight vertical gradients in the individual bay oxygen concentrations from the mixing of different temperatures of ullage gases, NEA, and ambient air. Since the ullage gas samples are taken entirely at the top of the tank, any vertical nonhomogeneities in a bay will result in a biased reading. Similar behavior was observed on a 747SP ground test article used by the FAA for ground-based inerting and OBIGGS development and testing [10]. In this case, large quantities of NEA were deposited in a quiescent tank over a relatively short period of time while oxygen samples were taken continuously. After the NEA was stopped and a brief settling period ensued, the ACMs were turned on, and the average tank ullage oxygen concentration would rise and then stabilize over a period of several minutes. Any nonhomogeneities occurring during the flight test, did so during ACM operation, but were apparently more subtle in nature.

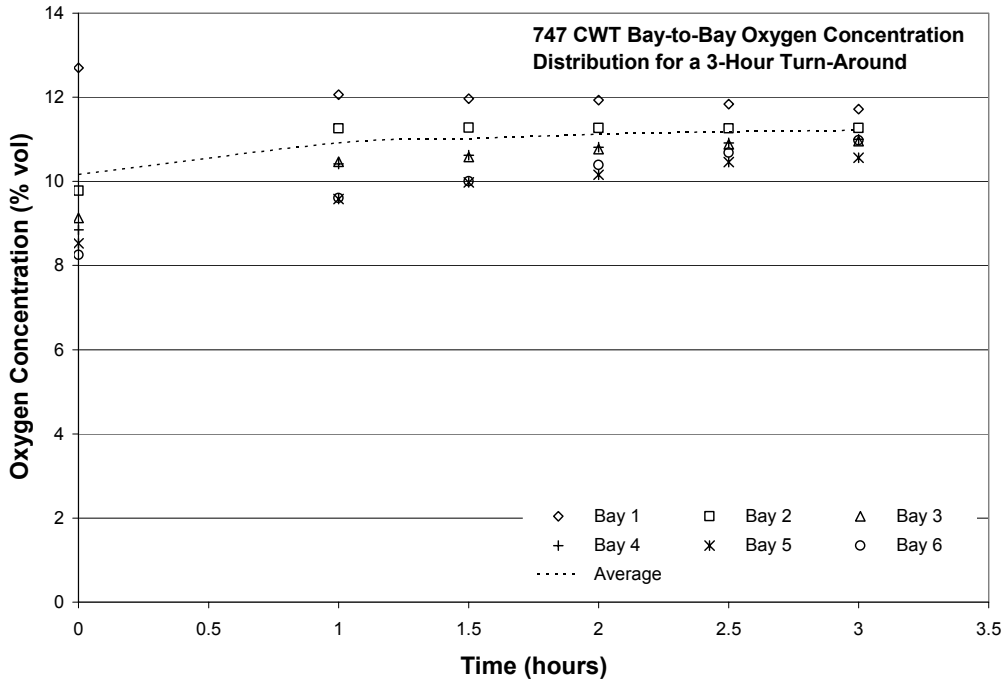

FIGURE 38. COMPARSION OF THE ULLAGE OXYGEN CONCENTRATION FOR ALL SIX BAYS DURING A 3-HOUR TURNAROUND

To examine the effects of air entering the ullage during overnight periods, the ullage oxygen concentration and distribution was recorded at the completion of a test, and then again the next morning after the instrumentation was warmed up and calibrated. The CWT was not cross-vented to both wing vent tanks, as is typical of the 747 model. Cross venting has been associated with air ventilating the inert ullage of Boeing type aircraft [4], and a modification was performed on the vent system to eliminate this venting process (section 2.1.1.2). Figure 39 shows the distribution of oxygen concentration of the six bays of the tank after touchdown one afternoon and then again early the next morning. As expected, the distribution of bay oxygen concentrations came completely to equilibrium. During the 12-hour overnight period, the average ullage oxygen concentration rose slightly over 1 percent, even though fuel was transferred during the instrumentation warmup period. Assuming the time zero average oxygen concentration is an unbiased reading and the fuel transfer deposited no air in the tank, this still represents a small increase in ullage oxygen concentration. This is consistent with the theory that thermal cycling of the tank is the source of air penetration because this particular night was almost as warm as the previous day. It is just as likely that virtually no air entered the tank during the overnight period, and the increase in oxygen concentration is strictly due to the final equilibration of the inert gas in the tank, as observed in the first hour of the 3-hour turnaround test and/or the transfer of fuel from tanks 2 and 3.

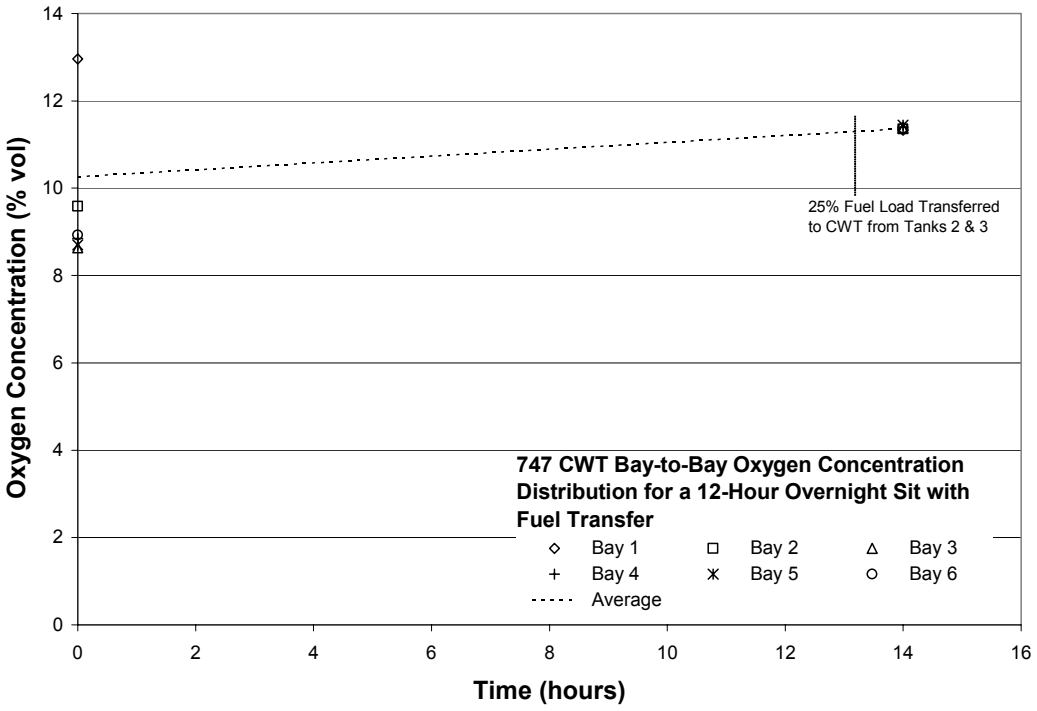

FIGURE 39. COMPARSION OF OXYGEN CONCENTRATION FOR ALL SIX BAYS DURING A 24-HOUR OVERNIGHT PERIOD WITH A FUEL TRANSFER

5.2 FUEL TANK FLAMMABILITY.

The primary focus of the fuel tank flammability measurements was to generate real-time, in-flight THC data for comparison to predicted results from the FAA's fuel tank flammability models. The results of these measurements, including environmental and flight effects are first discussed in the following sections followed by a comparison of the data to the calculated results. The flashpoint and ASTM D 2887 distillation data on the fuels for each test are shown in appendix I.

5.2.1 General Flammability Trends.

Though the data from each flight test is quite different, there are certain trends in the data that are seen throughout. As an example of these trends, figure 40 shows the THC and ambient pressure data for both the CWT and the wing tank from flight test 5. Initially, during ground operations with the ACMs on, the CWT THC reading rises slowly, but steadily, prior to takeoff. During takeoff, the effects of the change in vapor pressure are seen, as the hydrocarbons evolve faster, overcoming the corresponding condensation effects due to reduced temperatures. This effect is reversed at the approximate time of the start of level flight, as the condensation effects now begin to drive the THC readings. Finally, during descent, incoming air causes the THC to drop at a slightly increased rate. Similar trends are seen in the wing tank flammability data; however, the condensation effects in this tank are much more substantial as its ullage tends to follow the ambient temperature more closely. As a result, there is little if any increase in the wing tank flammability measurements during the climb phase of flight.

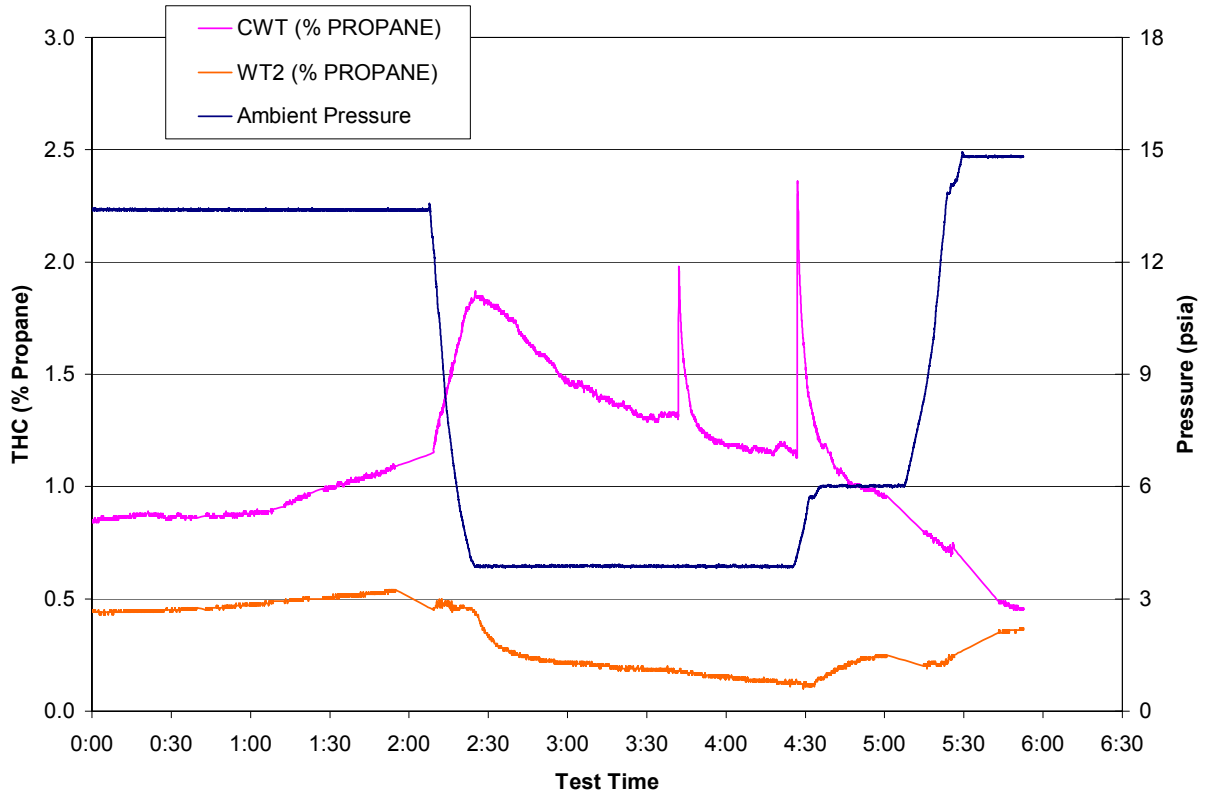

FIGURE 40. FLIGHT TEST 5 THC AND AMBIENT PRESSURE MEASUREMENTS

5.2.2 Temperature Effects.

Temperature effects on the THC readings throughout testing were quite noticeable in both tanks. Figures 41 and 42 show the temperature and THC data from flight test 5 for the CWT and wing tank, respectively. The approximate times of takeoff and start of descent are labeled on each for reference. In each figure, it is clear that the THC readings in each tank closely follow the trends of temperature. The only exception to this is in the CWT during the climb phase of flight, as the vapor pressure effects overcome the effects of condensation. During ground operations prior to takeoff, as fuel, surface, and ullage temperatures slowly increase, both from operation of the ACMs and ambient heating, so does the THC readings in each tank. In the cruise phase of flight, as temperatures drop due to the cold ambient temperature, the THC readings closely follow the trend of all fuel tank temperatures as condensation causes the THC levels to decline. Likewise, as temperatures in the wing tank begin to increase once again during descent and landing, so too does the wing tank flammability.

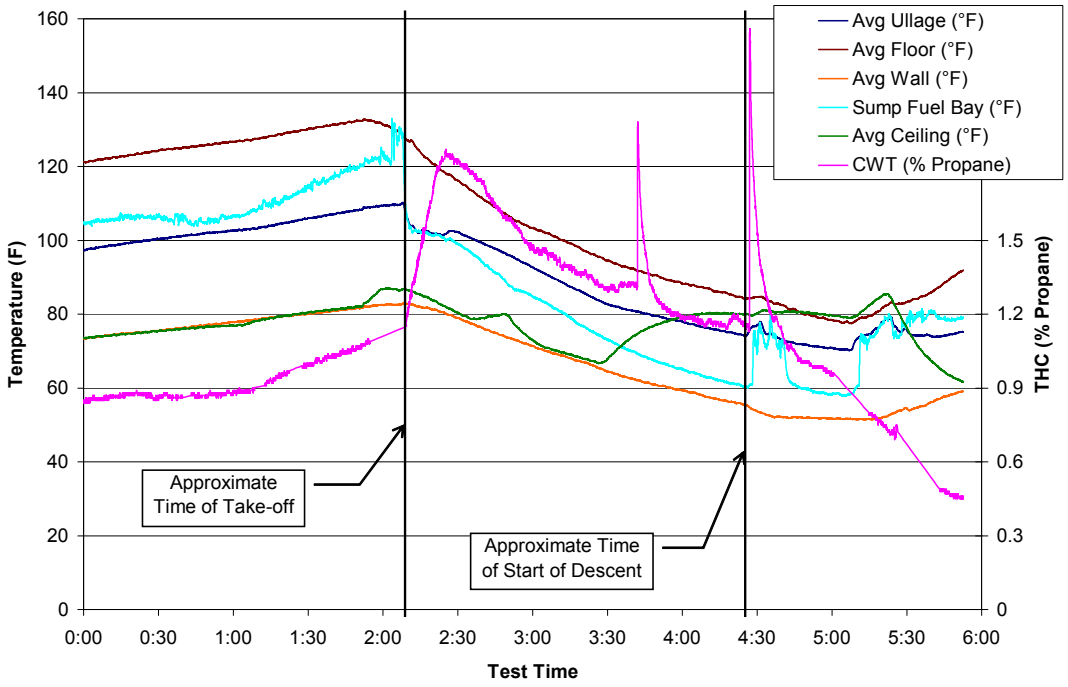

FIGURE 41. FLIGHT TEST 5 CWT THC AND TEMPERATURE MEASUREMENTS

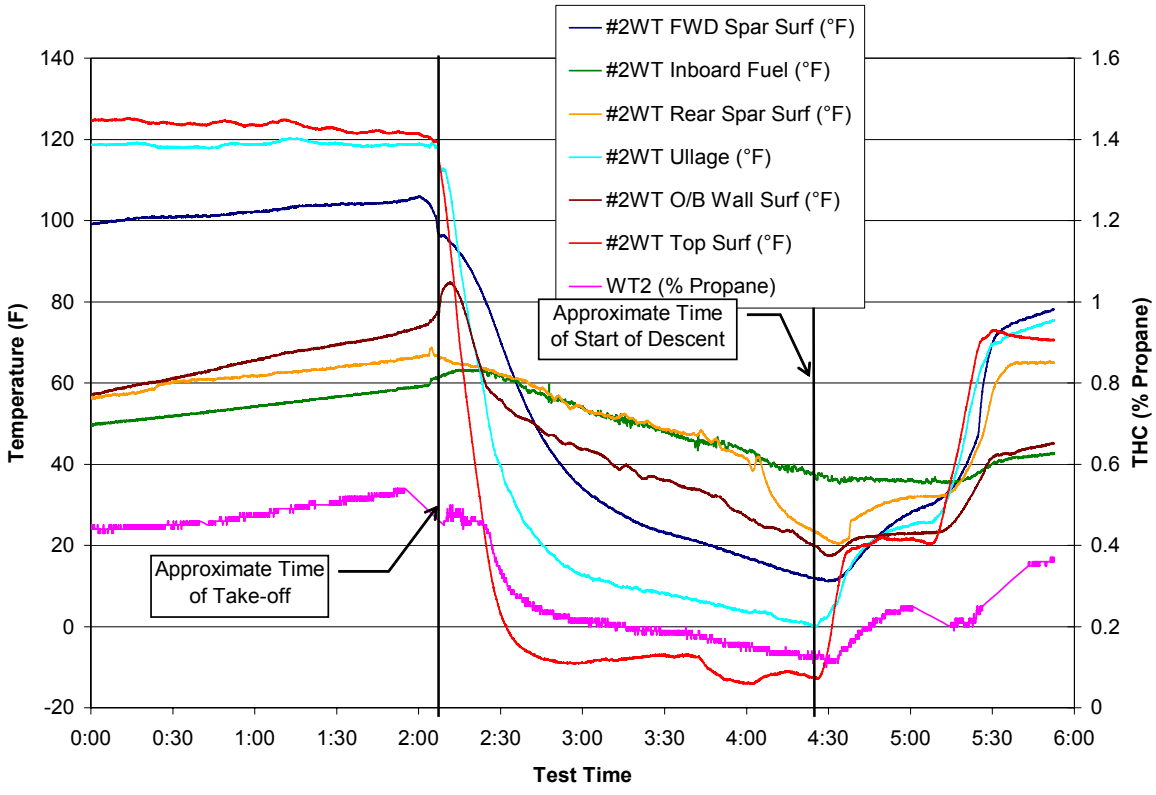

FIGURE 42. FLIGHT TEST 5 WING TANK THC AND TEMPERATURE MEASUREMENTS

To further exhibit the close relationship between tank flammability and various tank temperatures, figure 43 shows the CWT temperature and THC data from flight test 4. Because this test was performed with a 25% fuel load in the CWT, the changes in temperatures in flight are relatively small, with the exception of the tank wall temperatures. As the tank temperatures remain relatively stable, so do the THC readings in the tank, although it is evident that the drop in the tank wall temperatures still has an effect on the THC, causing a slow decrease in the flammability readings throughout the cruise phase of flight.

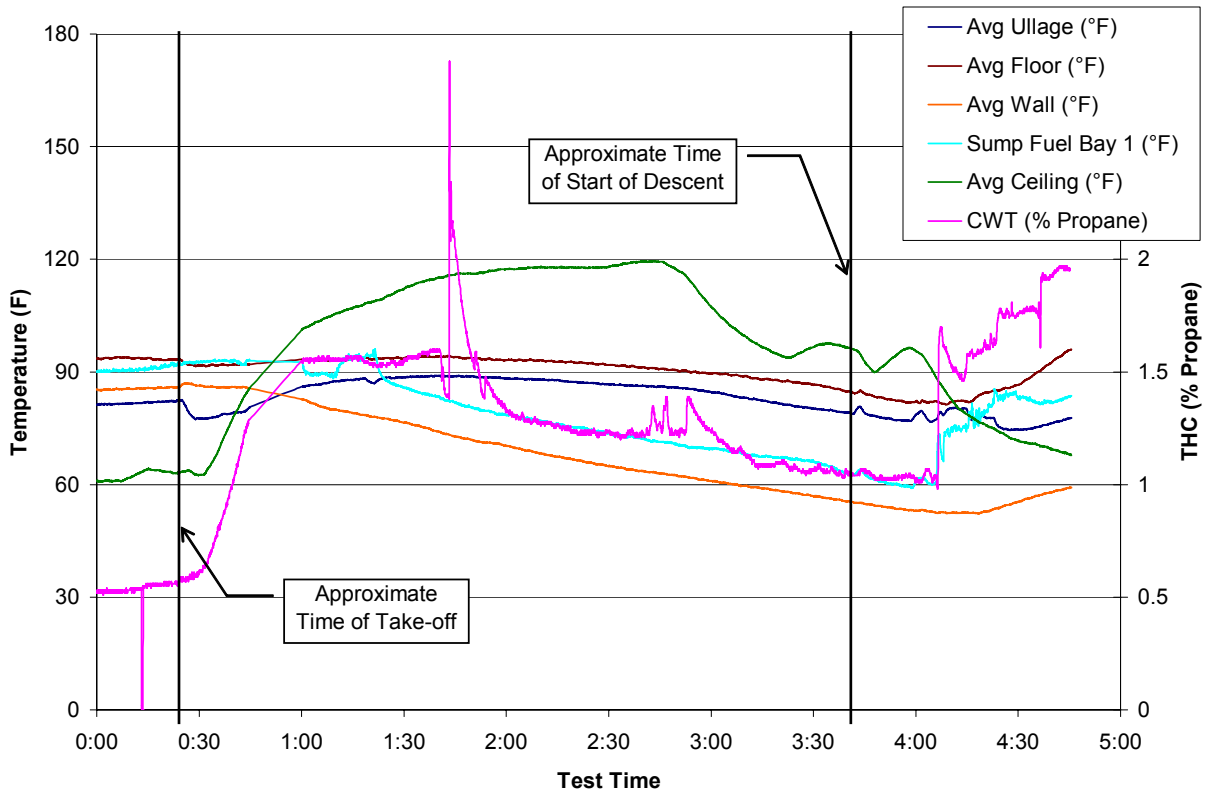

FIGURE 43. FLIGHT TEST 4 CWT THC AND TEMPERATURE MEASUREMENTS

5.2.3 Cross-Venting Effects.

The effects of cross venting (see section 2.1.1.2) on CWT flammability are shown in figures 44 and 45. These figures depict CWT THC and ambient pressure readings in tests 0 and 6, respectively. Both flights consisted of a similar flight profile without the OBIGGS running and showed similar trends in CWT temperature readings, as shown in figures 46 and 47.

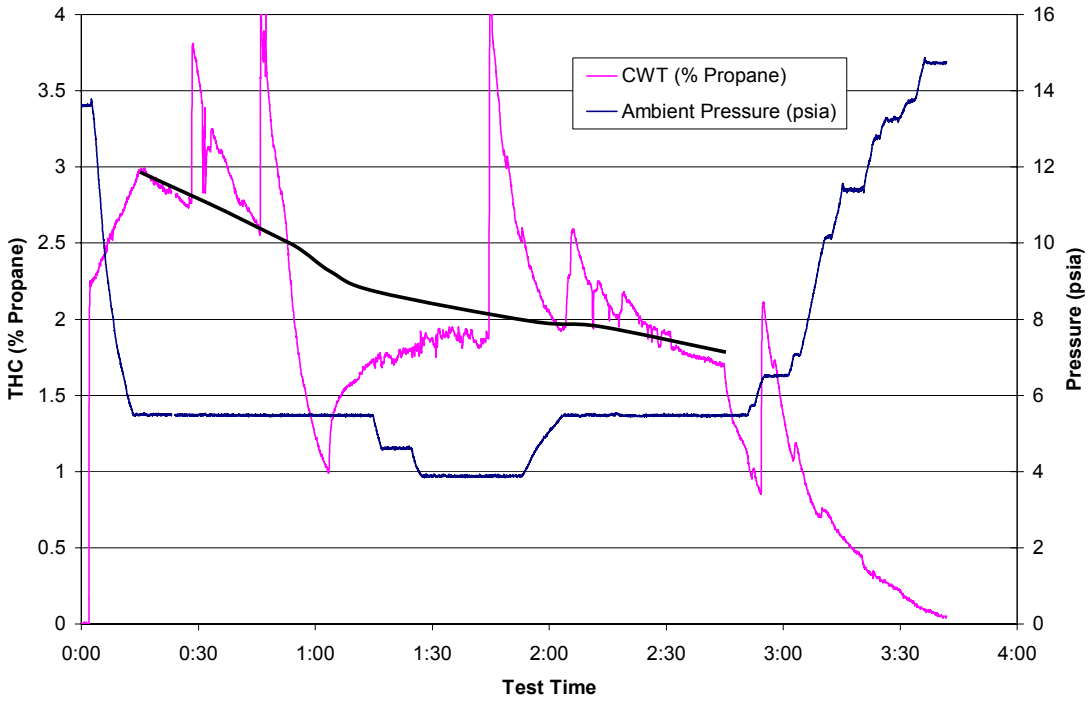

FIGURE 44. FLIGHT TEST 0 CWT THC AND AMBIENT PRESSURE MEASUREMENTS

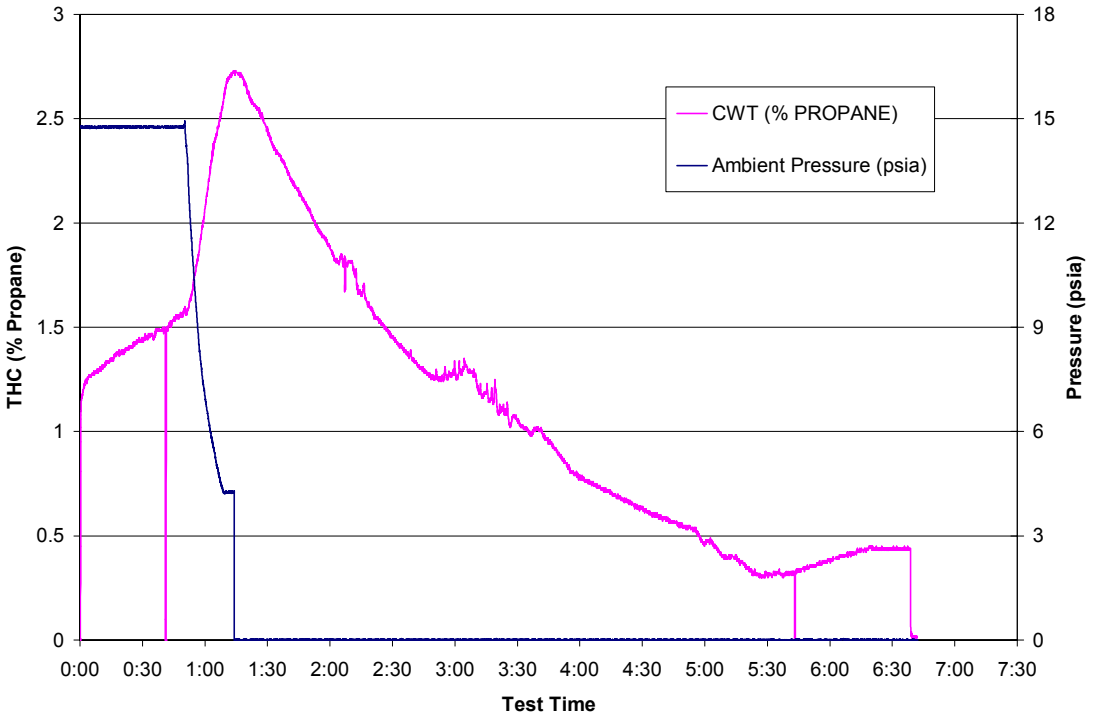

FIGURE 45. FLIGHT TEST 6 CWT THC AND AMBIENT PRESSURE MEASUREMENTS

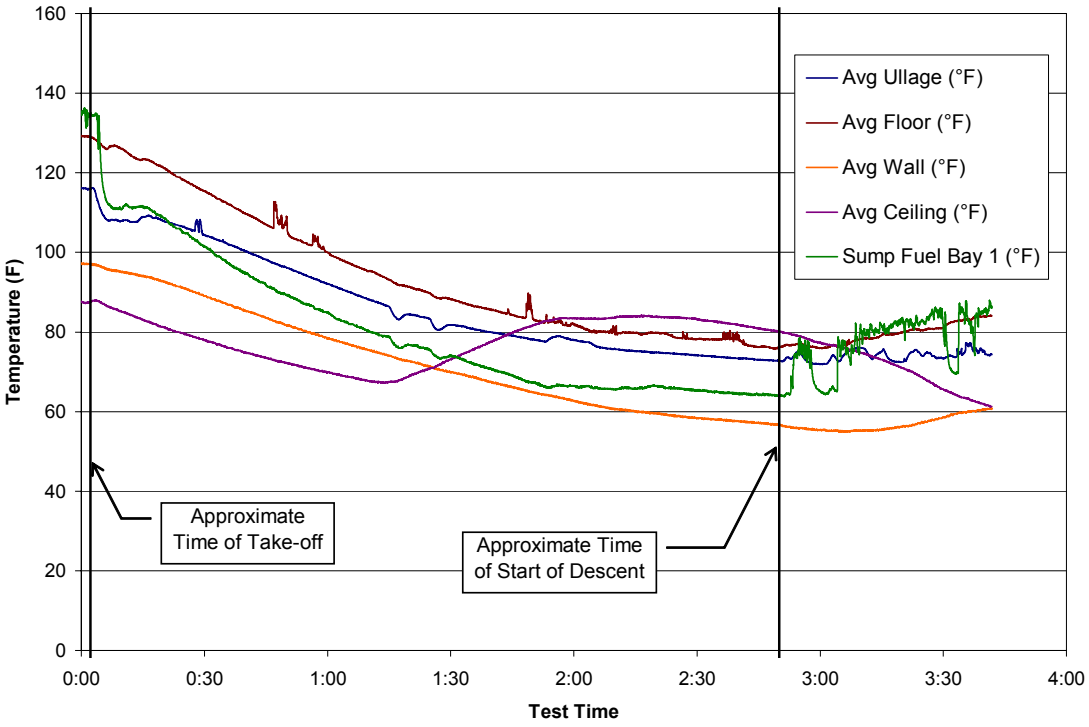

FIGURE 46. FLIGHT TEST 0 CWT TEMPERATURE MEASUREMENTS

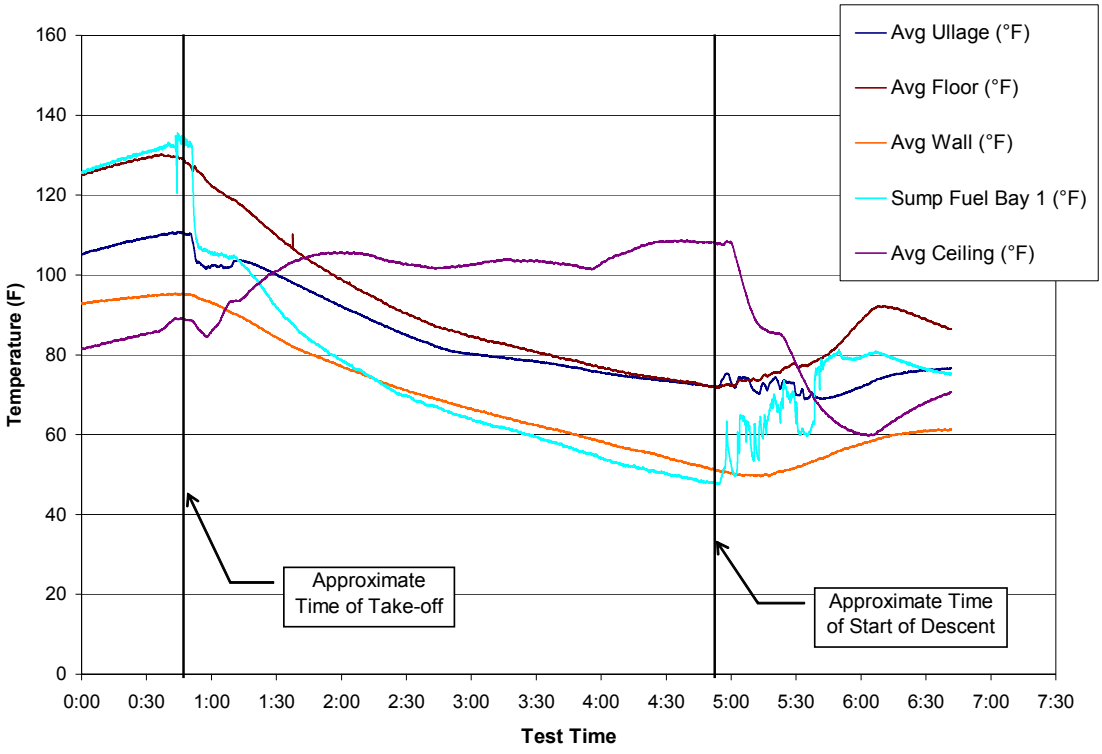

FIGURE 47. FLIGHT TEST 6 CWT TEMPERATURE MEASUREMENTS

Flight test 0 was conducted with half of the venting system blocked, eliminating all cross venting, whereas the venting system was in the original configuration through flight test 6, thus allowing cross flow through the CWT. Data from flight test 0 was somewhat scattered due to various issues during the flight, which caused the system to be diverted from fuel tank sampling at several points through the test. Using the data and test notes taken during the flight, a trend line of the data during the cruise phase of flight has been drawn, depicting the trend of the available data. Pressure data from test 6 was unavailable through much of the flight because the ambient pressure transducer failed shortly after takeoff. It was noted however, that the cruise altitude was approximately 31,000 ft (4.17 psia) for nearly the entire flight.

From figures 44 and 45, the same trends discussed in section 5.2.1 are shown; however, during cruise, the CWT flammability readings drop much more rapidly when cross flow is present, despite the similarities in flight profile and tank temperature data. It is also interesting to note that these two tests, the only two conducted without the OBIGGS running, exhibited the highest peak THC readings. Presumably, when the OBIGGS is operating, the incoming NEA displaces a sufficiently high amount of ullage vapors to produce a net lower flammability in the tank. Therefore, the OBIGGS can potentially protect against ignition not only by reducing the fuel tank ullage oxygen concentration, but also by reducing the resulting fuel/air mass ratio in the ullage through ventilation.

5.2.4 Comparison of Calculations.

Equilibrium THC values for each test were calculated with both models using the start of test thermal conditions as model inputs, as these were shown to be fairly stable conditions. This data is shown in figure 48 along with the measured THC at the start of each test. Also shown on the chart are the corresponding temperatures that were used for model inputs. All CWT calculations were performed using an assumed 3% fuel load, except test 4 which used a fuel load of 25 percent, as per the test plan.

The FAR calculator, as expected, overpredicts the THC in the CWT, due to its assumption of isothermal fuel tank conditions with a given fuel temperature. Thus, this model provides consistently conservative estimates of the FAR in the CWT, with noticeably increased predictions as the fuel temperature is increased. Using the FAR calculator for the wing tank estimates however, at times, underpredicts the THC in the tank. This is due to the lower fuel temperature that is observed in the wing tank. Assuming an isothermal condition, using the fuel temperature, provides a low estimate because the increased skin and ullage temperatures provide for reduced condensation effects and increased vapor generation in the tank.

Because the vapor generation model is currently configured to work solely with CWTs, wing tank calculations are not shown. Looking at the CWT data, however, one can see that this model provides a more accurate prediction of the THC than the FAR model. The ability of the user to input separate fuel and tank wall temperatures allow more accurate modeling of the thermodynamic processes in the tank. The highest variation from the measured values observed with the vapor generation model was just 0.38% propane.

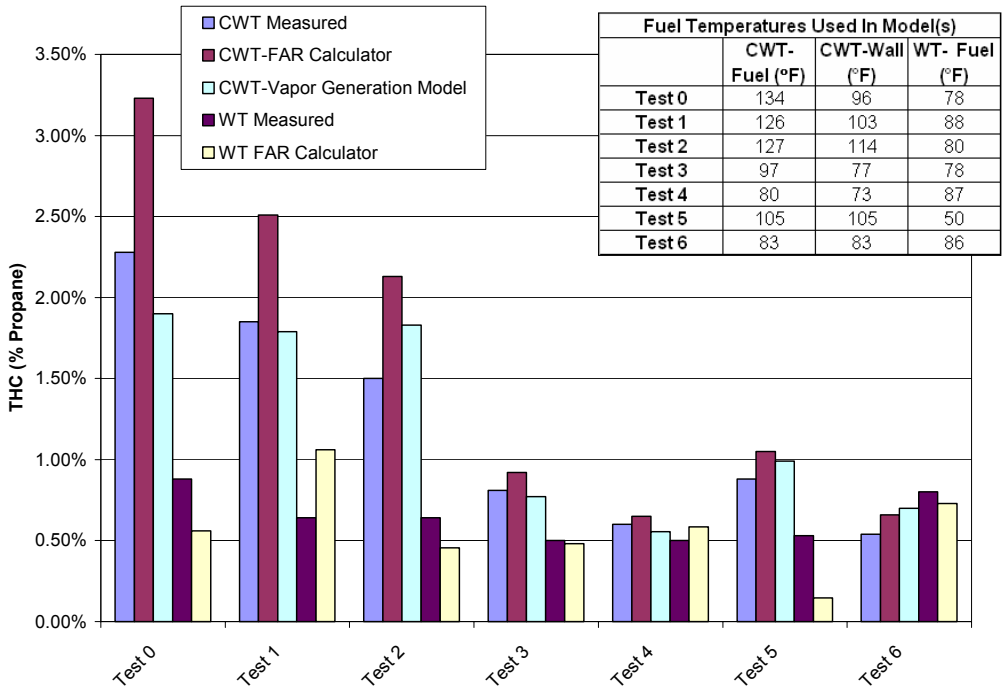

Fuel Temperatures Used In Model(s)			
	CWT-Fuel (°F)	CWT-Wall (°F)	WT- Fuel (°F)
Test 0	134	96	78
Test 1	126	103	88
Test 2	127	114	80
Test 3	97	77	78
Test 4	80	73	87
Test 5	105	105	50
Test 6	83	83	86

FIGURE 48. MEASURED AND COMPUTED EQUILIBRIUM THC VALUES

Because the vapor generation model is currently configured to work solely with CWTs, wing tank calculations are not shown. Looking at the CWT data, however, one can see that this model provides a more accurate prediction of the THC than the FAR model. The ability of the user to input separate fuel and tank wall temperatures allow more accurate modeling of the thermodynamic processes in the tank. The highest variation from the measured values observed with the vapor generation model was just 0.38% propane.

Figure 49 shows the measured and predicted CWT THC results from test, using the vapor generation model, with all systems running on the ground. The model was run using two different flashpoint fuels: 130° and 135°F. The actual flashpoint of the test fuel, as given in appendix I, was 131°F. As expected, the two different computed results closely bracket the measured data, thus providing confidence in the models ability to accurately track the THC evolution in the CWT.

Figures 50 through 52 show the computed and measured results of several of the flight tests through the entire flight profiles. Each of the calculated results were computed using fuel compositions according to the measured flashpoints (appendix I), matched with Woodrow's compositions at the same flashpoint [11]. The pressure data from each flight test were modified to remove any fluctuations that were occurring in flight, because these were found to have adverse effects on the results. The overall trend of the computed data matches closely with the measured results in all three cases, with the exception of the descent portion of figure 51. The magnitude of the THC at the cruise altitude, however, is overestimated in each case by the model. It is believed that this is attributable either to differences in the ambient pressure readings and the tank pressure due to vent flow or a reduction in the accuracy of the mathematical relationships used at reduced pressures. This issue is currently being evaluated,

and changes to the model will be made as needed. The trends of figure 51, as mentioned, match quite closely through the entire flight, with the exception of descent. At this point, the measured data rises, while the calculated results decrease. In this case, the measured data appears to be incorrect for an undetermined reason, as this trend was not observed in any of the other flights and is not what would be expected.

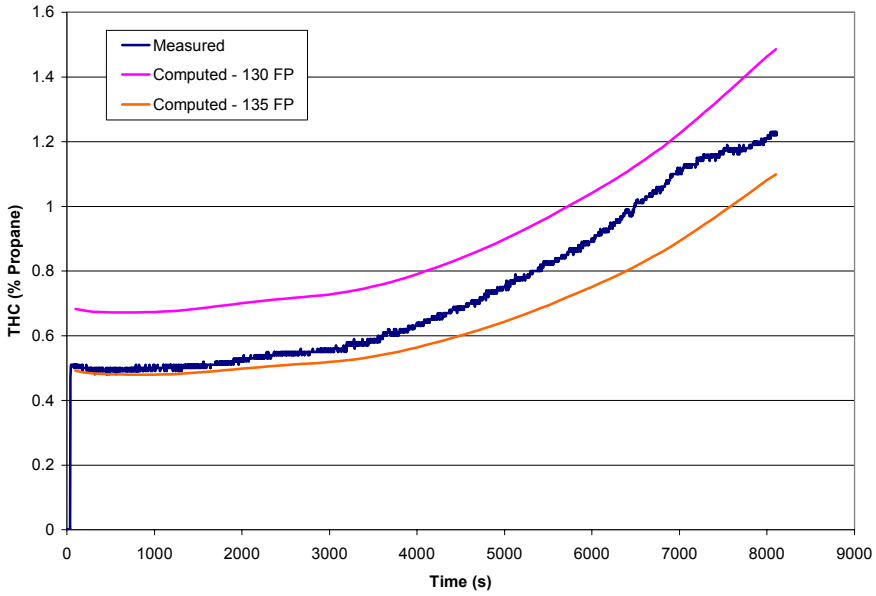

FIGURE 49. CENTER WING TANK THC MEASURED AND COMPUTED RESULTS FOR A GROUND TEST

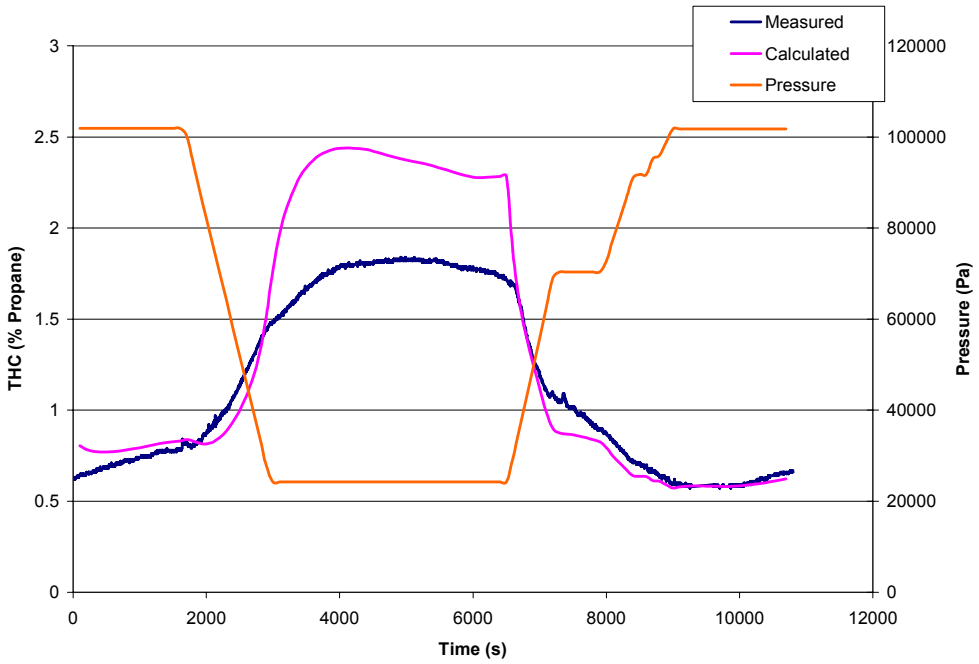

FIGURE 50. MEASURED AND CALCULATED THC MEASUREMENTS FOR FLIGHT TEST 3

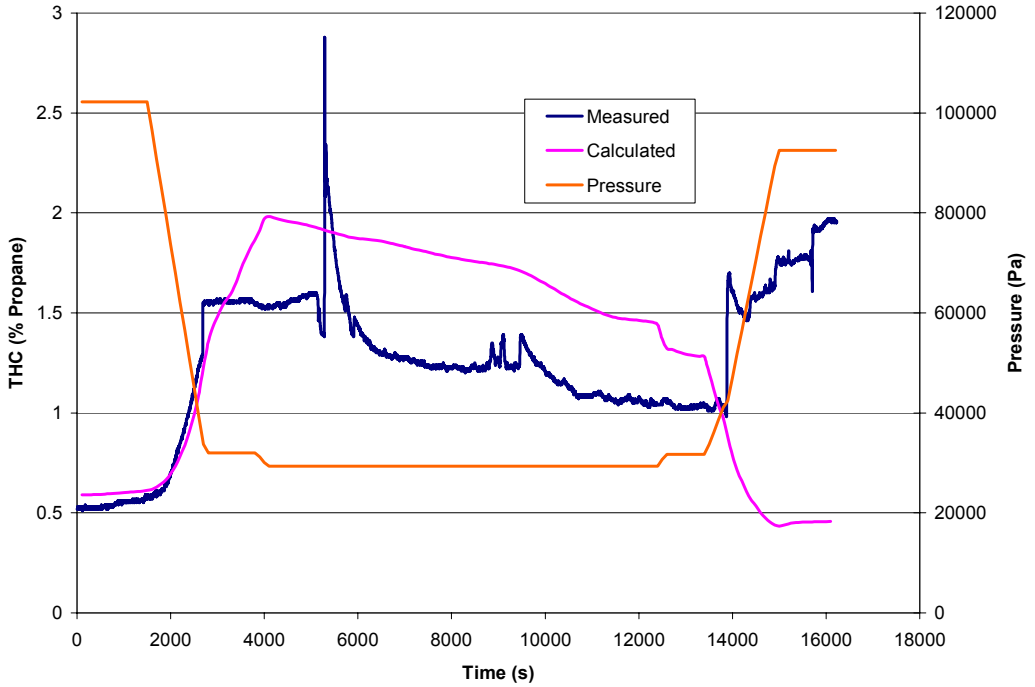

FIGURE 51. MEASURED AND CALCULATED THC MEASUREMENTS FOR FLIGHT TEST 4

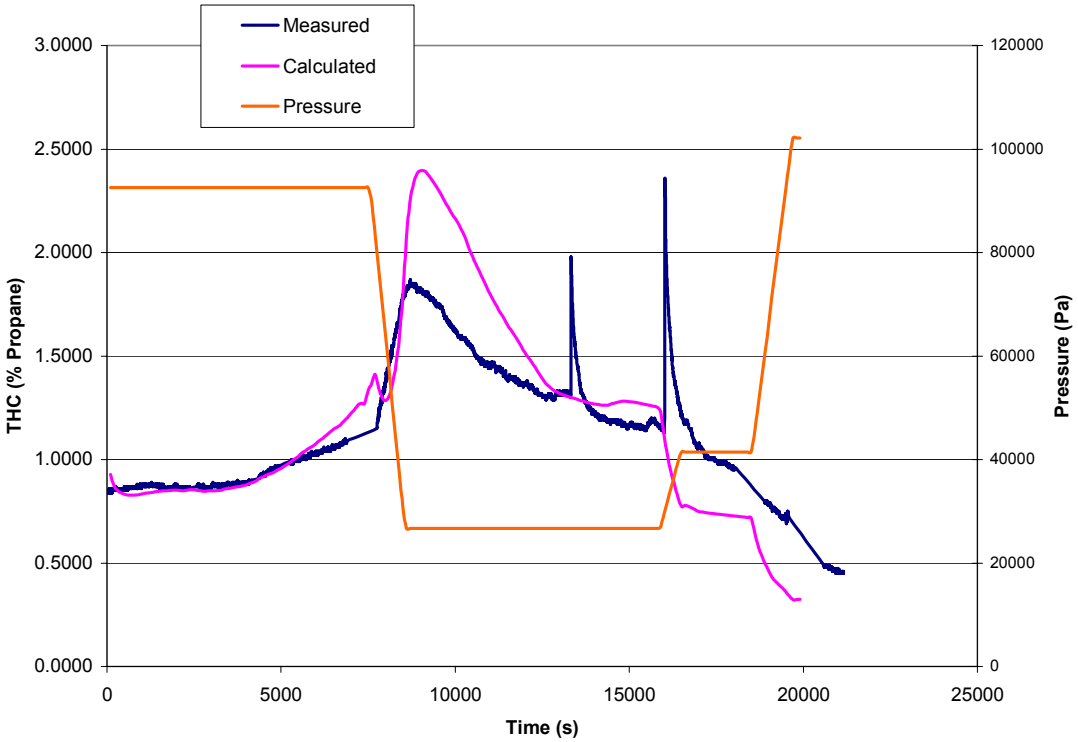

FIGURE 52. MEASURED AND CALCULATED THC MEASUREMENTS FOR FLIGHT TEST 5

6. SUMMARY OF FINDINGS.

The results of the tests indicated that the inerting system operated as expected, and the dual-flow methodology allowed the system to maintain an ullage oxygen concentration below 12% for the flight tests performed. Any deviations in system performance from test to test could be explained by the difference in system warmup times on the day of the test. Using the variable-flow methodology allowed a greater amount of nitrogen-enriched air to be generated on descent at a higher oxygen concentration with flow being as much as 50% greater for short periods of time, but it had no measurable effect on the resulting average ullage oxygen concentration after each test when compared to the dual-flow methodology. The higher flow rates did seem to help inert gas distribution by decreasing the worst bay oxygen concentration. The highest average ullage oxygen concentration observed on any flight test correlates directly with the worst bay oxygen concentration, illustrating the importance of maintaining a low average ullage oxygen concentration for good inert gas distribution. Oxygen diffusion between the bays of the tank was relatively rapid and showed that diffusion would reduce the oxygen concentration in bay 1 (worst bay) from 13 to 12 percent in approximately 1 hour with the air cycle machines running. Overnight dispersion of the ullage oxygen concentration was measured to be very small when considering other effects that could affect an increase in oxygen concentration overnight such as fuel transfer and vertical gradient diffusion.

Flammability measurements from both the center wing tank and number 2 wing tank showed trends very similar to what was expected, based upon both experimental and computer model data. The equilibrium data agreed favorably with the data from both the Fuel Air Ratio Calculator and Condensation Model, while transient data also matched closely with that of the Condensation Model. The measurements generated in these flight tests are being used to enhance the capability of these existing flammability models and will be used in the future to further improve upon predictive flammability calculations.

7. REFERENCES.

1. "Fuel Tank Harmonization Working Group Final Report," Aviation Rulemaking Advisory Committee, July 1998.

2. Burns, Michael and Cavage, William M., "Inerting of a Vented Aircraft Fuel Tank Test Article With Nitrogen-Enriched Air," FAA report DOT/FAA/AR-01/6, April 2001.

3. Clodfelter, R.G., Anderson, C.L., and Vannice, W.L., "OBIGGS for Fighter Aircraft," SAE Technical Paper 871903, *Aerospace Technology Conference and Exposition*, Long Beach, California, October 5-8, 1987.

4. Burns, Michael and Cavage, William M., "Ground and Flight Testing of a Boeing 737 Center Wing Fuel Tank Inerted With Nitrogen-Enriched Air," FAA report DOT/FAA/AR-01/63, August 2001.

5. Burns, Michael et. al., "Flight Testing of the FAA Onboard Inert Gas Generation System on an Airbus A320," FAA report DOT/FAA/AR-03/58, June 2004.

6. Summer, S., “Limiting Oxygen Concentration Required to Inert Jet Fuel Vapors Existing at Reduced Fuel Tank Pressures—Final Phase,” FAA report DOT/FAA/AR-04/8, August 2004.

7. Burns, Michael and Cavage, William M., “A Description and Analysis of the FAA Onboard Oxygen Analysis System,” FAA report DOT/FAA/AR-TN03/52, June 2003.

8. Ochs, Robert and Polymeropoulos, C.E., “Vaporization of Jet A in a Simulated Aircraft Fuel Tank Including Sub-Atmosphere Pressures and Low Temperatures,” *Proceedings from the International Fire and Cabin Safety Conference*, Lisbon, Portugal, November 15-18, 2004.

9. Cavage, William M. and Kils, Ole, “Inerting of a Boeing 747SP Center Wing Tank Scale Model With Nitrogen-Enriched Air,” FAA report DOT/FAA/AR-02/51, May 2002.

10. Cavage, William M., “Ground-Based Inerting of Commercial Transport Aircraft Fuel Tanks,” RTO-MP-103 26, *Proceedings from RTO AVT Specialists’ Meeting on Fire Safety and Survivability*, Aalborg, Denmark, September 23-26, 2002.

11. Woodrow, J.E., “Flash Point and Chemical Composition of Aviation Kerosene (Jet A),” NTSB Docket SA-516, Exhibit No. 20S, May 2000.

APPENDIX A—CENTER WING TANK INSTRUMENTATION PANEL INSTALLATION DRAWING

Detail 2:

Instructions:

Remove Aft CWT Purge Door (65B10812-3),
Reference Maintenance Manual 28-11-00 Page 3
Remove Leash and Install Instrumentation Plate

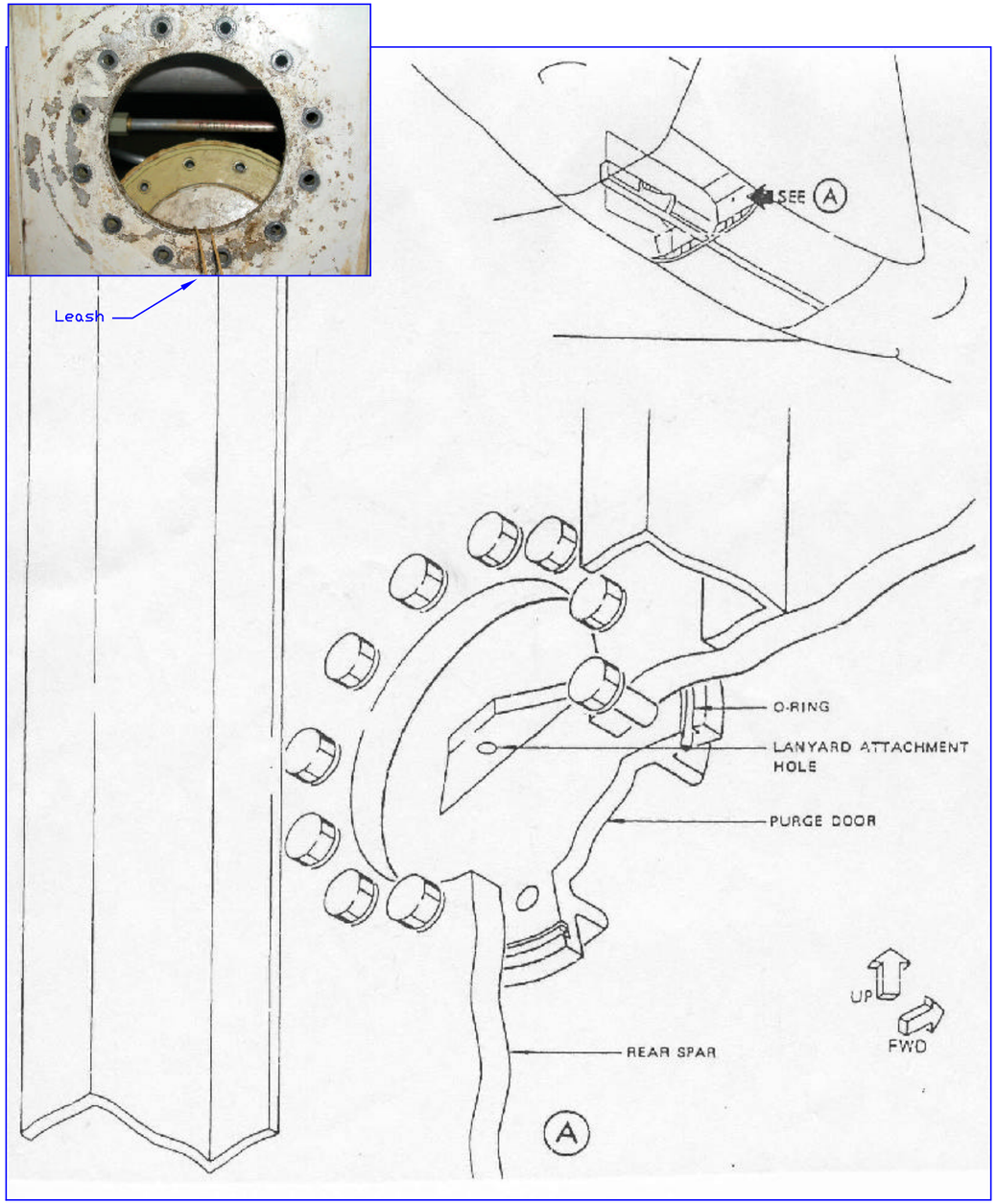

Instrument Panel

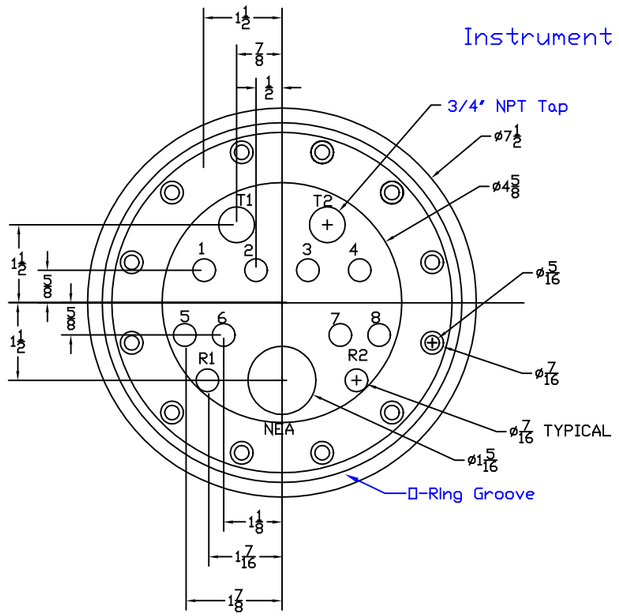

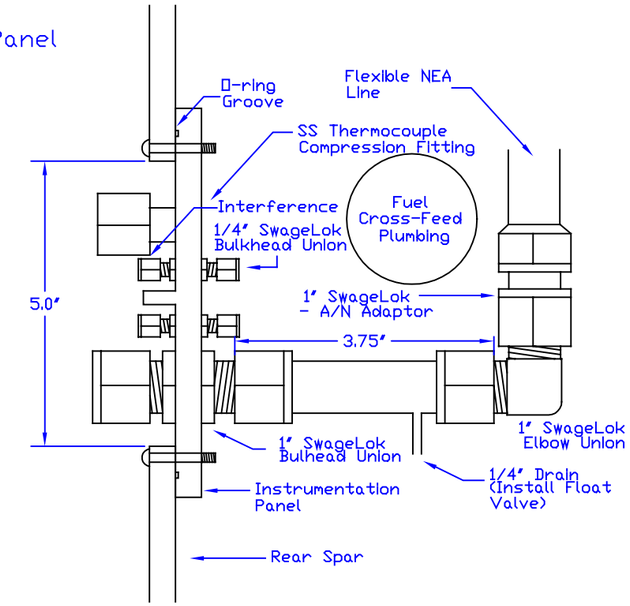

Instructions:

Install SS 304 NEA Deposit Extension/Elbow with Nipple

Install Tubing Extensions on Bulkhead Fittings 2 and 3 to Correct Interference

Note:
Instrumention Plate is Modified Ventilation Port
See Manual for Part Mat'l and Specification

Detach Door Leash, Remove from Tank and Save for Later Reinstallation

Attach Modified Float Valve with Tapered Thread Adaptor to 1/4" Drain on NEA Deposit Extension per Detail 3

Seal Thermocouple Compression Fittings and Threads with BMS5-23 Sealant

After Installation Coat Fittings on Inside of Plate with BMS5-23 Sealant

Inspect Purge Door O-Ring for Integrity Before Reusing to Install Instrumentation Plate

	Parts List
Part #	Part Description
AAR1-06	Instrument Panel
AAR1-07	NEA Extension Line
SS-1610-9	NEA Elbow
AAR1-08	NEA Line
AAR1-03	Modified Float Valve
A-400-61	1/4" Bulkhead Union
SS-1610-61	1" Bulkhead Union
MFT-116-16	Thermocouple Fitting
AAR1-11	1" SwageLok-A/N Adaptor

Federal Aviation Administration
Technical Center Atlantic City Airport, NJ

FAA BIGGS Flight Test Instrumentation Installation

Dwg No. AAR440-023 rev G

APPENDIX B—HEATED GAS SAMPLE FITTINGS INSTALLATION DRAWING

Install Float Valve Assembly Inside #2 Wing Tank per Detail Shown on 1/8th Inch Tube Bonded into Modified Fastener on Front Spar at FSS 630 at Top of Wing Cord

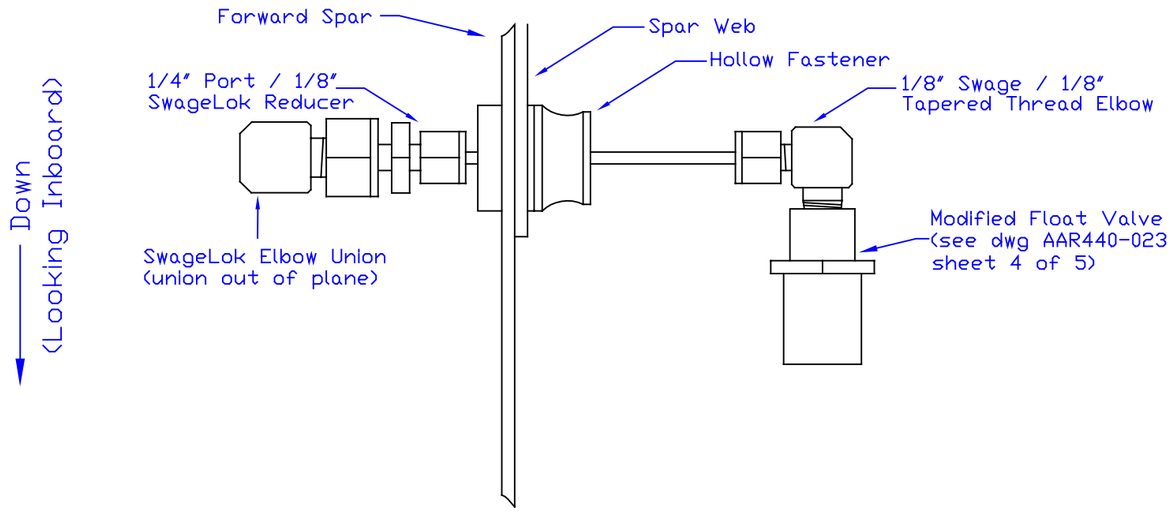

Install Float Valve Assembly Inside Center-Wing Tank per Detail Shown on 1/8th Inch Tube Bonded into Modified Fastener at STA 1098 (str 19) Left of BL 11.33

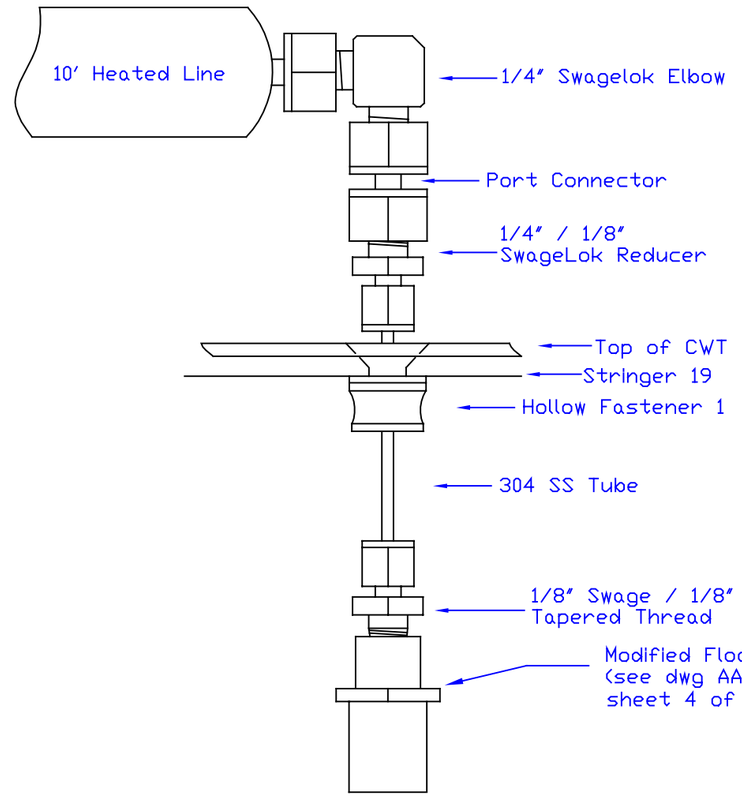

Note:

Bond 304 SS Tube in Modified Fastener with Loc Tite Epoxy, BMS 5-123, Type 1, Class 2 or Equivalent Mil-Std

Saftey All Connections with Sealant as Recommended by FAA Guidance

Float Valve is Allen Aircraft 8F111-101 Modified per Dwg AAR440-023 sheet 4 of 5

All SwageLok Fittings Aluminum

Parts List	
Part #	Part Description
A-401-PC	Port Connector
A-400-6-2	1/4" Swage / 1/8th" Swage
A-400-9	Elbow Union
A-200-1-2	1/8th" Swage / 1/8" NPT
212-4-10	10' Heated Line
A-200-R-4	1/8th" Swage / 1/4" Port
HL63PBB-*	Modified Fastener 1
AN960PD416	Nut 1
BACB30NX*K*	Modified Fastener 2
BACN10TN*	Nut 2
AAR1-02	Modified Float Valve
A-200-2-2	1/8th" Swage / 1/8" NPT Elbow

Federal Aviation Administration
Technical Center Atlantic City Airport, NJ

FAA BIGGS Flight Test Heated Sample Line Installation

Dwg No. AAR440-027 rev D

Sheet 2 of 2

APPENDIX C—INSTRUMENTATION DIAGRAM WITH CHANNEL LISTING

Aircraft Cabin

Existing Power Rack

Harness #TBD

Harness #TBD

Harness #7&8

Harness #5&6

DAS

- CWT Temps Ch. 19-42
- Sys Pressures Ch. 59-63,
- Sys O2 Ch. 70-71
- Sys O2 Pres Ch. 62-64
- Sys Flow Ch. 75
- System/Pack Bay Temps Ch. 66-73
- CWT Oxygen and THC Analyzers Ch. 1-8 Ch. 43
- OBOAS/FAS Pressures Ch. 9-18, 44-45
- OBOAS/FAS Temperatures Ch. 46-48
- Misc Temps Ch. 76-91
- Wing Tank Temps Ch. 51-58

Pressure Transducers

OBIGGS

OBOAS

OBOAS

FAS Analyzer

FAS Sample System

Penetration STA 1275

Modified Waste Tube, STA 1235

H/X Bypass Shut-Off

Ejector Supply Shut-off

Air

Air

Air

Air

Compressed Air Bank (Cargo Bay)

Cabin Temperature

Window Plug

Modifed Fastener WS400

#2 Wing Tank

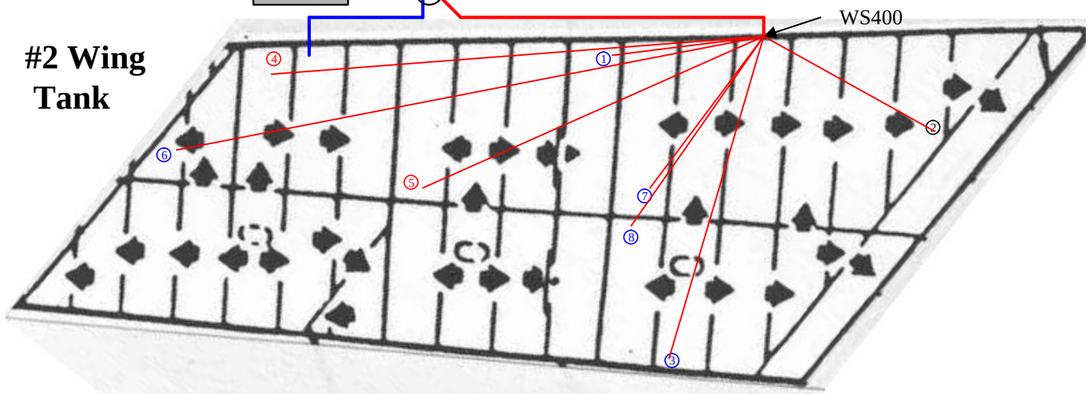

Instrumentation Wiring

Power Cable

Purge Air Line

System Wiring

Sample Tubing

Thermocouples

(n) Ullage & (n) Fuel (n) Floor, Wall, & Ceiling Mounted

Sample Ports

Center-Wing Tank

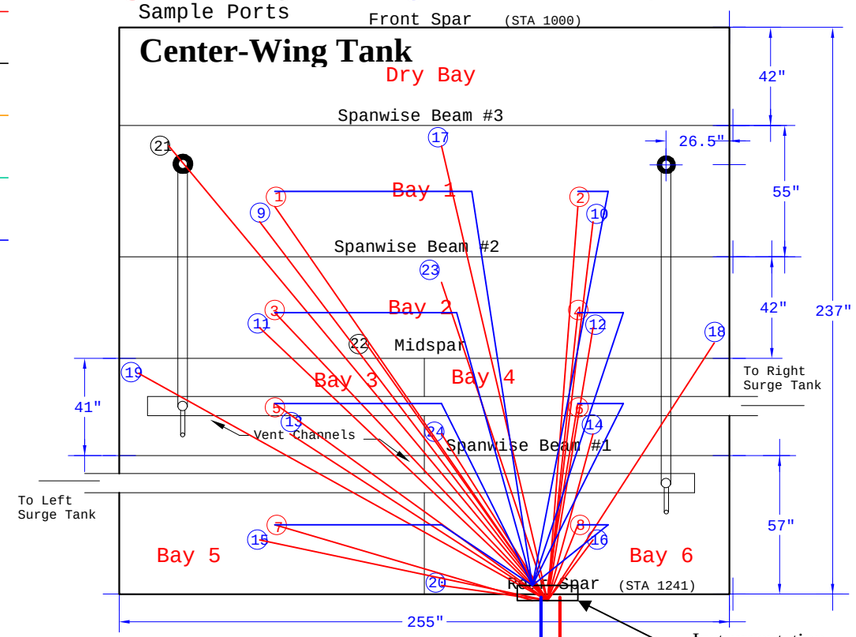

Instrumentation Panel

Empty Pack Bay

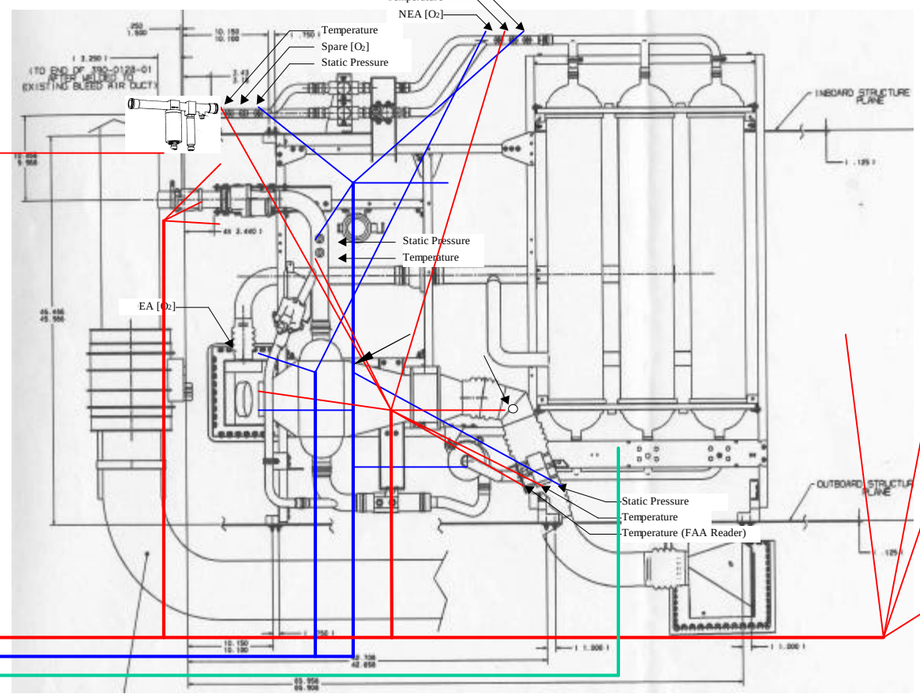

- Pack Bay 1
- Pack Bay 2
- Pack Bay 3

Listing of Specified Data Acquisition Channels

Item	Description	Range	Output	Designator
	Fuel Tank / OBOAS Instrumentation			
1	Oxygen Channel - Bay 1 Right	0-25%	0-10 vdc	
2	Oxygen Channel - Bay 1 Left	0-25%	0-10 vdc	
3	Oxygen Channel - Bay 2 Right	0-25%	0-10 vdc	
4	Oxygen Channel - Bay 2 Left	0-25%	0-10 vdc	
5	Oxygen Channel - Bay 3	0-25%	0-10 vdc	
6	Oxygen Channel - Bay 4	0-25%	0-10 vdc	
7	Oxygen Channel - Bay 5	0-25%	0-10 vdc	
8	Oxygen Channel - Bay 6	0-25%	0-10 vdc	
9	Bay 1-R O2 Anylz Inlet Pressure	0-500 Torr	0-1 vdc	
10	Bay 1-L O2 Anylz Inlet Pressure	0-500 Torr	0-1 vdc	
11	Bay 2-R O2 Anylz Inlet Pressure	0-500 Torr	0-1 vdc	
12	Bay 2-L O2 Anylz Inlet Pressure	0-500 Torr	0-1 vdc	
13	Bay 3 O2 Anylz Inlet Pressure	0-500 Torr	0-1 vdc	
14	Bay 4 O2 Anylz Inlet Pressure	0-500 Torr	0-1 vdc	
15	Bay 5 O2 Anylz Inlet Pressure	0-500 Torr	0-1 vdc	
16	Bay 6 O2 Anylz Inlet Pressure	0-500 Torr	0-1 vdc	
17	OBOAS 1 Outlet Pressure	0-1000 Torr	0-1 vdc	
18	OBOAS 2 Outlet Pressure	0-1000 Torr	0-1 vdc	
19	Ullage Temp - Bay 1 Right	0-450 F	T-Type	
20	Ullage Temp - Bay 1 Left	0-450 F	T-Type	
21	Ullage Temp - Bay 2 Right	0-450 F	T-Type	
22	Ullage Temp - Bay 2 Left	0-450 F	T-Type	
23	Ullage Temp - Bay 3	0-450 F	T-Type	
24	Ullage Temp - Bay 4	0-450 F	T-Type	
25	Ullage Temp - Bay 5	0-450 F	T-Type	
26	Ullage Temp - Bay 6	0-450 F	T-Type	
27	Fuel Temp - Bay 1 Sump Area	0-450 F	T-Type	
28	Fuel Temp - Bay 2 Middle	0-450 F	T-Type	
29	Floor Temp - Bay 1 Right	0-450 F	T-Type	
30	Floor Temp - Bay 1 Left	0-450 F	T-Type	
31	Floor Temp - Bay 2 Right	0-450 F	T-Type	
32	Floor Temp - Bay 2 Left	0-450 F	T-Type	
33	Floor Temp - Bay 3	0-450 F	T-Type	
34	Floor Temp - Bay 4	0-450 F	T-Type	
35	Floor Temp - Bay 5	0-450 F	T-Type	
36	Floor Temp - Bay 6	0-450 F	T-Type	
37	CWT Wall Temp - Forward Tank Wall	0-450 F	T-Type	
38	CWT Wall Temp - Left Tank Wall	0-450 F	T-Type	
39	CWT Wall Temp - Right Tank Wall	0-450 F	T-Type	
40	CWT Wall Temp - Left Tank Wall	0-450 F	T-Type	
41	CWT Ceiling Temp - Forward	0-450 F	T-Type	
42	CWT Ceiling Temp - Aft	0-450 F	T-Type	
43	THC - CWT (FAS1)	0-50K PPM	0-10 vdc	
44	THC - Wing Tank (FAS2)	0-50K PPM	0-10 vdc	
45	FAS 1 Inlet Pressure	0-500 Torr	0-1 vdc	
46	FAS 2 Inlet Pressure	0-500 Torr	0-1 vdc	

Item	Description	Range	Output	Designator
	Fuel Tank / OBOAS Instrumentation (cont'd)			
47	Spare Outlet Pressure	0-1000 Torr	0-1 vdc	
48	OBOAS Temp 1	0-450 F	T-Type	
49	OBOAS Temp 2	0-450 F	T-Type	
50	FAS Temp	0-450 F	T-Type	
51	Wing Tank Forward Spar Surface Temp	0-450 F	T-Type	
52	Wing Tank Inboard Fuel Temp	0-450 F	T-Type	
53	Wing Tank Rear Spar Surface Temp	0-450 F	T-Type	
54	Wing Tank Ullage Temp	0-450 F	T-Type	
55	Wing Tank Mid Fuel/Ullage Temp	0-450 F	T-Type	
56	Wing Tank Outb'rd Wall Surface Temp	0-450 F	T-Type	
57	Wing Tank Bottom Surface Temp	0-450 F	T-Type	
58	Wing Tank Top Surface Temp	0-450 F	T-Type	
	System Instrumentation			
59	Pack Bay Static Pressure	0-15 psia	0-5 vdc	
60	Bleed Pressure	0-100 psia	0-5 vdc	
61	ASM Inlet Pressure	0-50 psia	0-5 vdc	
62	ASM Exit Pressure	0-50 psia	0-5 vdc	
63	Post Orifice Pressure	0-25 psia	0-5 vdc	
64	Bleed Temperature	0-450 F	T-Type	
65	ASM Inlet Temperature	0-450 F	T-Type	
66	ASM Exit Temperature	0-450 F	T-Type	
67	Post Orifice Temperature	0-450 F	T-Type	
68	Heat Exchanger Inlet Temp	0-450 F	T-Type	
69	Heat Exchanger Outlet Temp	0-450 F	T-Type	
70	NEA Oxygen Concentration	0-25%	0-10 vdc	
71	OEA Oxygen Concentration	0-100%	0-10 vdc	
72	NEA O2 Analyzer Inlet Pressure	0-500 Torr	0-1 vdc	
73	OEA O2 Analyzer Inlet Pressure	0-500 Torr	0-1 vdc	
74	NEA/OEA Analyzer Outlet Pressure	0-1000 Torr	0-1 vdc	
75	NEA Flow Meter	.8-80 SCFM	.5-5 vdc	
	Additional			
76	Pack Bay 1 Temp	0-450 F	T-Type	
77	Pack Bay 2 Temp	0-450 F	T-Type	
78	Pack Bay 3 Temp	0-450 F	T-Type	
79	OBIGGs Bay Temp	0-450 F	T-Type	
80	Bleed Duct Area Temp 1	0-450 F	T-Type	
81	Bleed Duct Area Temp 2	0-450 F	T-Type	
82	Bleed Duct Area Temp 3	0-450 F	T-Type	
83	Heated Line Temp 1	0-450 F	T-Type	
84	Heated Line Temp 2	0-450 F	T-Type	
85	Heated Line Temp 3	0-450 F	T-Type	
86	Heated Line Temp 4	0-450 F	T-Type	
87	Heated Line Temp 5	0-450 F	T-Type	
88	Heated Line Temp 6	0-450 F	T-Type	
89	Heated Line Temp 7	0-450 F	T-Type	
90	Heated Line Temp 8	0-450 F	T-Type	
91	Cabin Temp	0-450 F	T-Type	

APPENDIX D—SURFACE-MOUNTED THERMOCOUPLE DRAWING

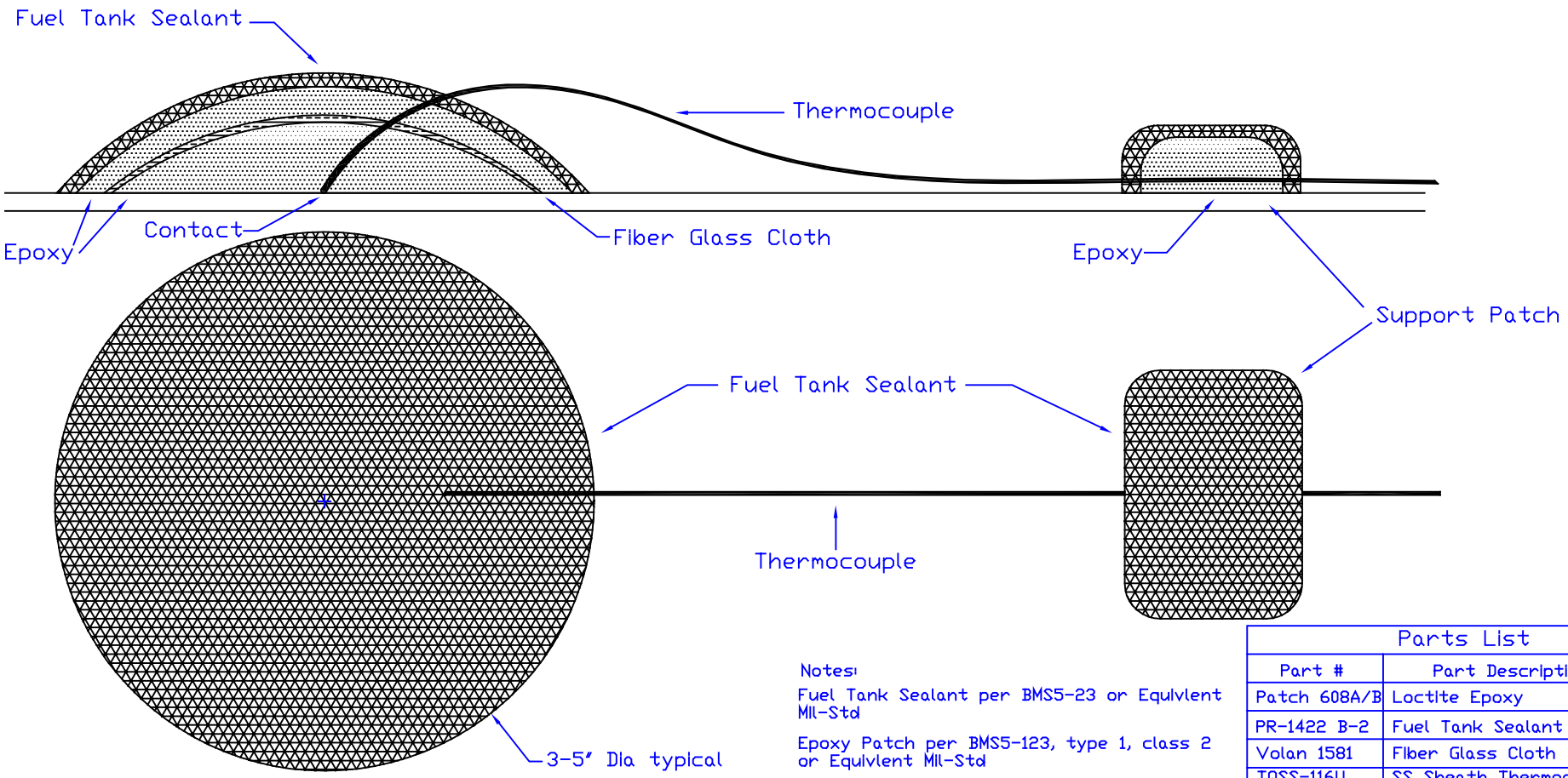

Notes:

Fuel Tank Sealant per BMS5-23 or Equivlent Mil-Std

Epoxy Patch per BMS5-123, type 1, class 2 or Equivlent Mil-Std

Fiber-Glass Cloth per BMS9-3 type h2, class 7 or Equivlent Standard

Use Support Patch or Wire Ties to Tank Structure Every 18 Inches

Parts List	
Part #	Part Description
Patch 608A/B	Loctite Epoxy
PR-1422 B-2	Fuel Tank Sealant
Volan 1581	Fiber Glass Cloth
TQSS-116U	SS Sheath Thermocouple

Federal Aviation Administration
Technical Center Atlantic City Airport, NJ

FAA □BIGGS Testing Surface Mounted Thermocouple Install

Dwg No. AAR440-029 rev B

Sheet 1 of 1

APPENDIX E—ONBOARD INERT GAS GENERATION SYSTEM MECHANICAL DRAWING WITH INTERFACE ILLUSTRATION

Attachment 1: FAA OBIGGS Engineering Drawing

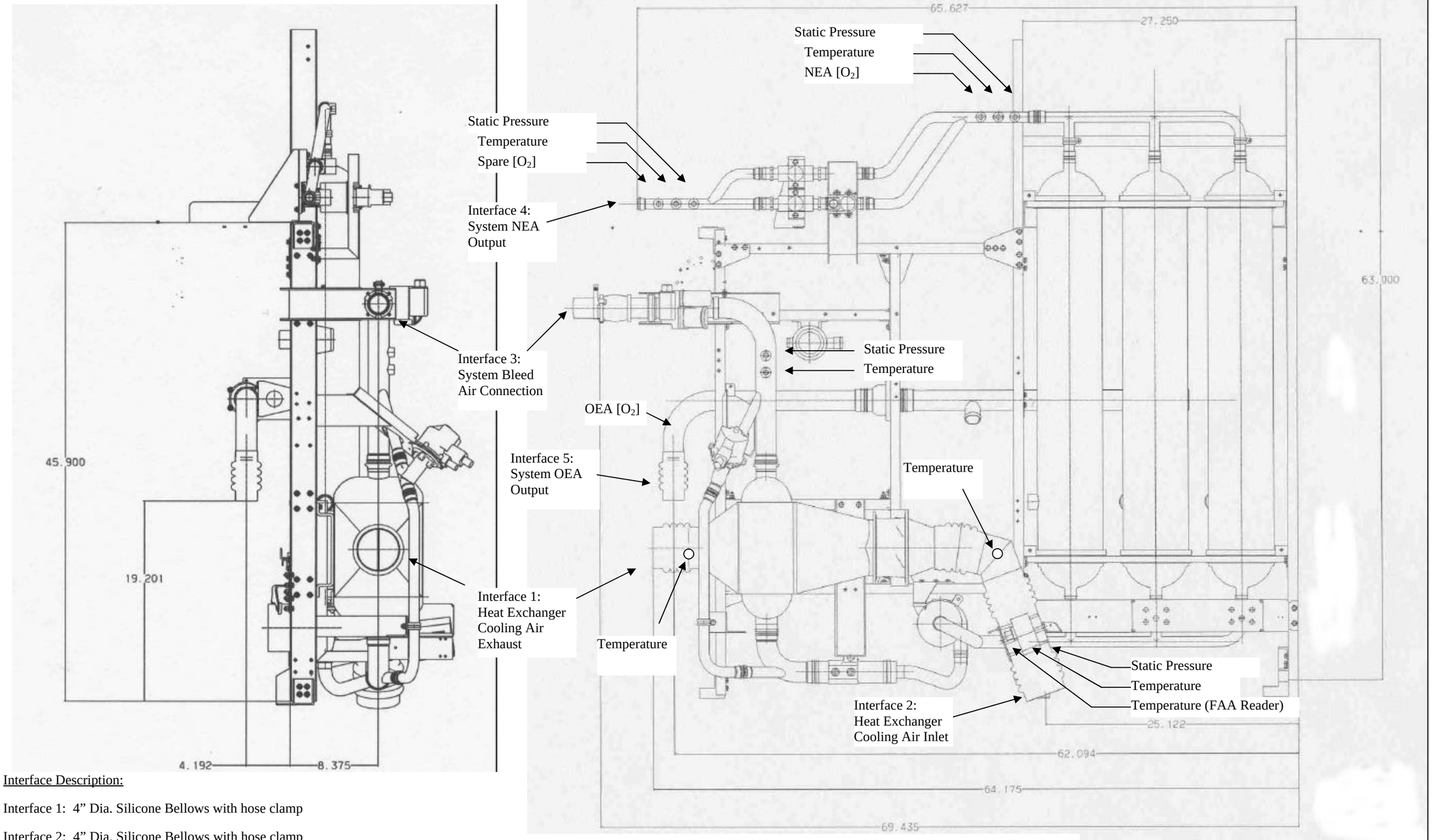

Interface Description:

Interface 1: 4” Dia. Silicone Bellows with hose clamp

Interface 2: 4” Dia. Silicone Bellows with hose clamp

Interface 3: 2” Dia SS Pipe with captive tubing mate and Perry Seal

Interface 4: 1” Dia Al tube with Hydraflow 14J02 Sleve, Coupling, Seal, and Clamp Assy

Interface 5: 2” Dia. Silicone Bellows with hose clamp

Notes:

All Instrumentation Ports ¼-Inch SwageLok with 1/8th-Inch Tubing Adaptors

All Thermocouples T-type 1/8th-Inch Probe through SwageLok Fitting

Federal Aviation Administration
Technical Center Atlantic City Airport, NJ

747 SCA OBIGGS
Flight Test
System Diagram

Dwg No. AAR440-022 rev A

Sheet 1 of 1

APPENDIX F—ONBOARD INERT GAS GENERATION SYSTEM INERT/DIVERT TUBING ASSEMBLY TOP DRAWING

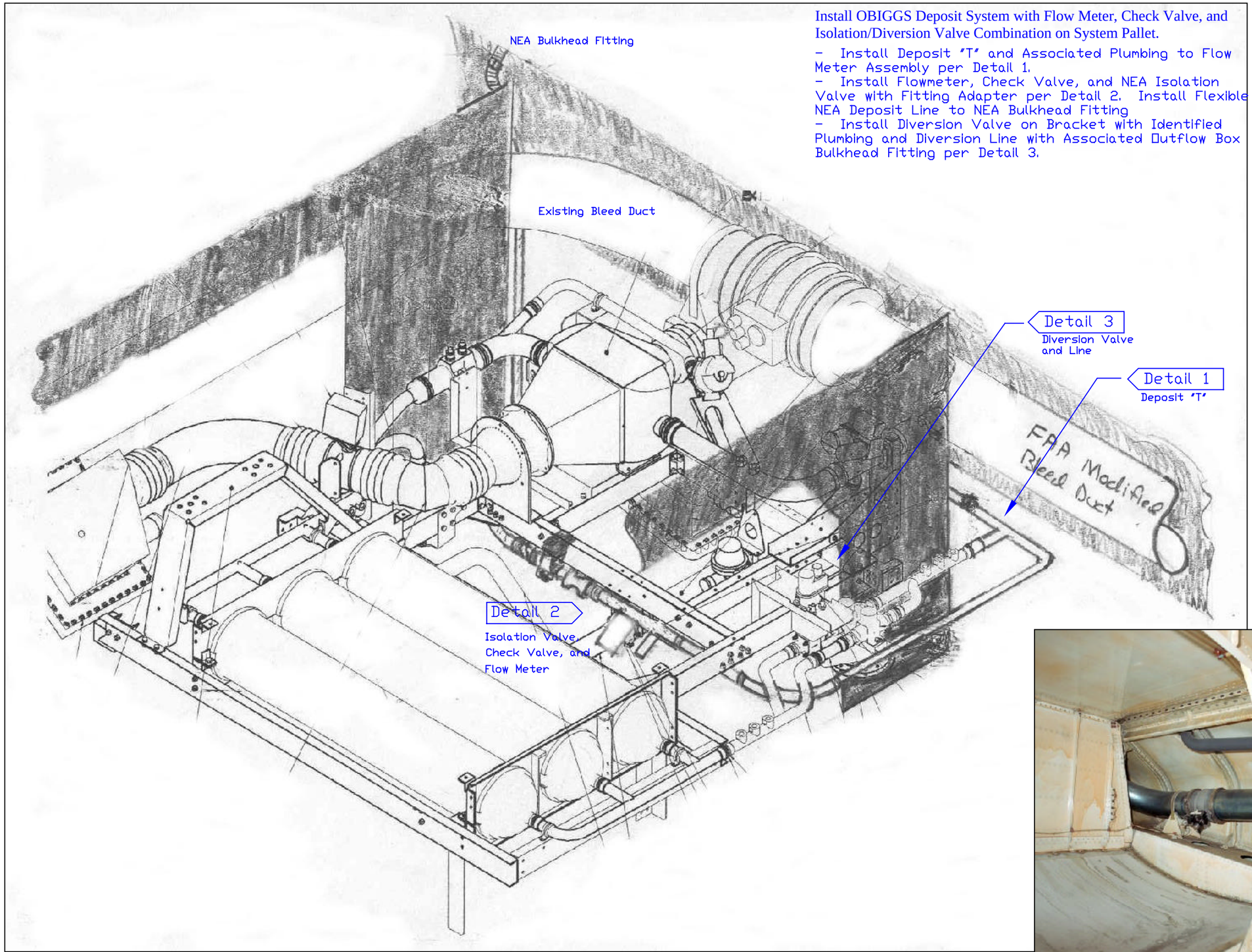

Install OBIGGS Deposit System with Flow Meter, Check Valve, and Isolation/Diversion Valve Combination on System Pallet.

- Install Deposit 'T' and Associated Plumbing to Flow Meter Assembly per Detail 1.
- Install Flowmeter, Check Valve, and NEA Isolation Valve with Fitting Adapter per Detail 2. Install Flexible NEA Deposit Line to NEA Bulkhead Fitting
- Install Diversion Valve on Bracket with Identified Plumbing and Diversion Line with Associated Outflow Box Bulkhead Fitting per Detail 3.

Notes:

Secure All Tubing and Wiring with Wire Tires and Cable Clamps as Needed

Federal Aviation Administration
Technical Center Atlantic City Airport, NJ

FAA OBIGGS Flight Test NEA Deposit Routing

Dwg No. AAR440-024 rev C

Sheet 1 of 4

APPENDIX G—NITROGEN-ENRICHED AIR DEPOSIT NOZZLE INSTALLATION DRAWING

Detail 4:

Instructions:
Install Bracket with NEA Deposit Nozzle and Associated Hardware on Stiffener in Aft Bay (6)

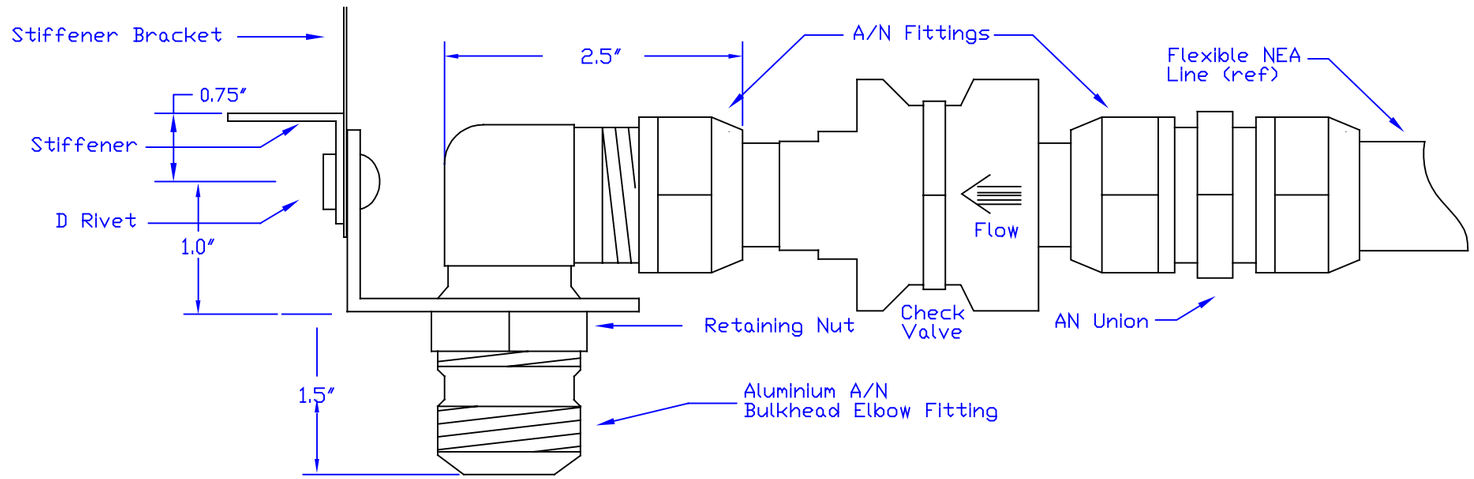

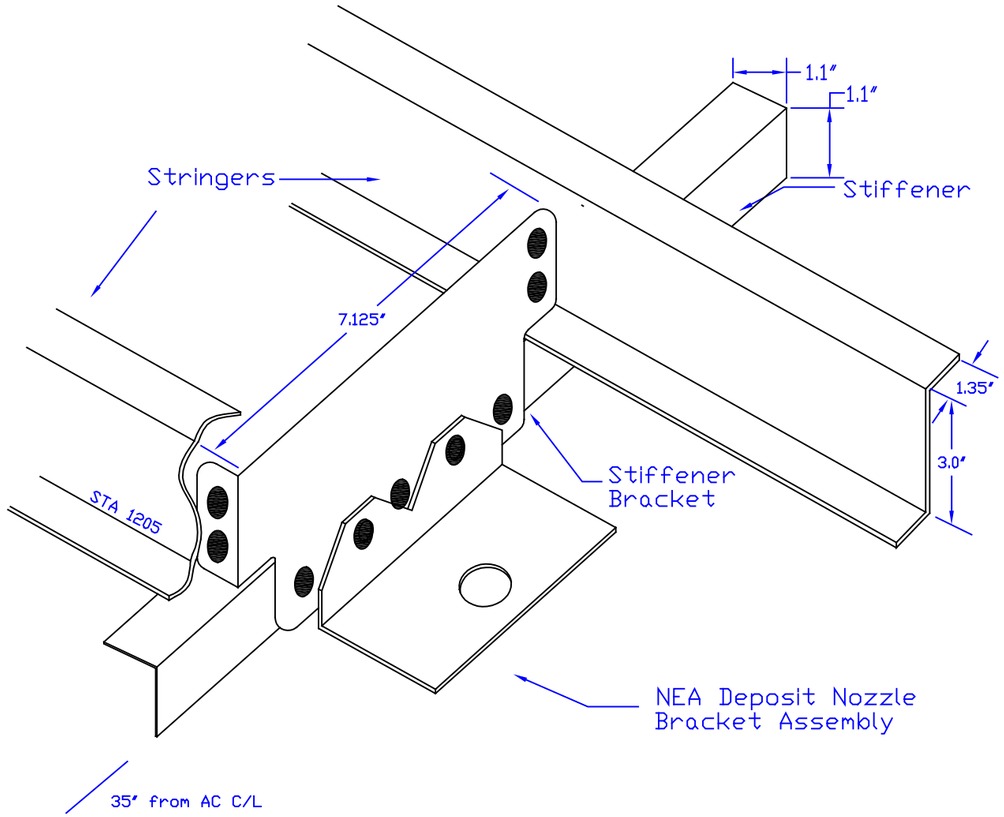

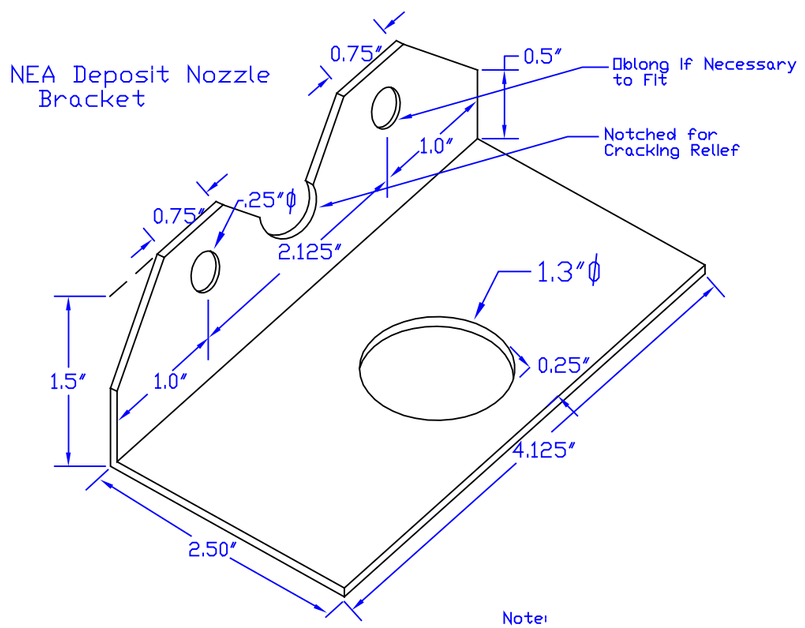

Note:
Remove 2 Stiffener Bracket "D" Rivets to Install Bracket and Replace Same
Bracket Mat'l - Al 5052-H32, 1/8th Inch
Secure Flexible NEA Line with Fuel Compatible Wire Ties
Stringer Mat'l - Aircraft Grade Al 0.25" thick
Stiffener Mat'l - Aircraft Grade Al 0.1" thick
Stiffener Bracket Mat'l - Aircraft Grade Al 0.05" thick

Parts List	
Part #	Part Description
AAR1-01	NEA Nozzle Mounting Bracket
AN 833-16D	1" A/N Bulkhead Elbow Fitting
390-0108-02	Check Valve
AN 815-16D	1" A/N Union
AAR1-11	1" NEA Line

Federal Aviation Administration
Technical Center Atlantic City Airport, NJ

FAA BIGGS Flight Test Instrumentation Installation

Dwg No. AAR440-023 rev G

APPENDIX H—ONBOARD INERT GAS GENERATION SYSTEM WIRING DIAGRAM

BIGGS Control Rack

System Shut-Off Valve — J5

Solenoid No 1	1
Solenoid No 1	2
Ground	3
No	4
Switch 1 NC	5
Com	6
No	7
Switch 2 NC	8
Com	9
Chassis Ground	10

Heat Xchg Bypass — J6

Bypass+	1
Bypass-	2

Modulating Valve — J1

Pot (CW) Wiper	A
Pot (CCW)	B
Case Ground	C
Close (CCW)	D
Open (CW)	E
Common	M
Dynamic Brake	K
	L
	J

Fan Motor — J10

Leg A	A
Leg B	B
Leg C	C
Neutral	D

NEA Divert Valve — J14

+28 VDC (Pwr to Open)	A
+28 VDC (Pwr to Close)	B
- 28 VDC	C
Case Ground	D
Open Contact	E
+28 VDC (For Indication)	G
Closed Contact	H

NEA Inert Valve — J15

+28 VDC (Pwr to Open)	A
+28 VDC (Pwr to Close)	B
- 28 VDC	C
Case Ground	D
Open Contact	E
+28 VDC (For Indication)	G
Closed Contact	H

Clamp Heater — TS1

A B

Purity Control Valve — J9

+28 VDC (Pwr to Open)	A
+28 VDC (Pwr to Close)	B
- 28 VDC	C
Case Ground	D
Open Contact	E
+28 VDC (For Indication)	G
Closed Contact	H

Thermocouple

BIGG System Pallet

Empty Pack Bay

Modified Waste Shoot STA 1240 (approx.) / Modified Waste Shoot Access Hole STA 1235 (approx.)

J4 — J X U V M I T e h W B C Y d k n p q s m t 1 N S R P G C F K J H b G a E F A D Z

J11 — J X U V M I T e h W B C Y d k n p q s m t 1 N S R P G C F K J H b G a E F A D Z

Pressurized Cabin

To NASA Aircraft Power Bus (M9) — J12

A	
B	
C	Neutral
D	GND
E	28V
F	

FAA BIGGS Box

Modulating Valve Position Controller — TS2

28V
Bypass+
Bypass-
COM+
COM-
28V
Brake+
Brake-
DVM+
DVM-

1 2 9 10 5 6 7 8 3 4

J13 — A B I J E F G H

System Switch

System On/Off Indicator

Fan Switch

Clamp Heater Switch

Inert/Divert Switch

High Flow Indicator

Purity Control Switch

Temperature Controller — J3

C B A E F J L K M

15V Rtn
Valve Out
+15V
Valve In
Com
Open Cmd
Open Ind
Close Cmd
28V Rtn

Thermo-copule Reader — TS3 TS4

A B C

To 115 VAC 60Hz Bus

Des	Connector Type
J1	MS3112E14-12P
J3	MS3112E14-12P
J4	MS3476W20-41S
J5	M83723/83R1814N
J6	M83723/72R1005N
J9	D38999/20WC98PN
J10	MS27473T10B98P
J11	MS3472W20-41S
J12	MS3120F16-8P
J13	MS3120F14-19P
J14	D38999/20WC98PN
J15	D38999/20WC98PN
TS1	Terminal Strip
TS2	Terminal Strip
TS3	Terminal Strip
TS4	Terminal Strip

Federal Aviation Administration
Technical Center Atlantic City Airport, NJ

747 SCA BIGGS Flight Test Wiring Diagram

Dwg No. AAR440-021 REV C

Sheet 1 of 1

APPENDIX I—TEST FUEL FLASHPOINT AND DISTILLATION DATA

747 Flight Test Flashpoint Data

Fuel From Flight Test No.	Flashpoint Sample 1 (°C)	Flashpoint Sample 1 (°F)	Flashpoint Sample 2 (°C)	Flashpoint Sample 2 (°F)
1	55.0	131.0	52.8	127.0
2, 4, 5	59.5	139.1	57.3	135.1
3	57.5	135.5	55.8	132.44
6	55.0	131.0	53.3	127.9

ASTM D 2887 Simulated Distillation for Fuel From Flight Test 1

% Off	BP°F	BP°C	% Off	BP°F	BP°C	% Off	BP°F	BP°C
IBP	235.4	113.0	34	380.8	193.8	68	431.1	221.7
1	262.0	127.8	35	382.0	194.5	69	433.0	222.8
2	274.7	134.8	36	382.9	194.9	70	435.3	224.1
3	284.0	140.0	37	383.7	195.4	71	437.1	225.1
4	295.6	146.5	38	384.8	196.0	72	438.7	225.9
5	301.9	149.9	39	386.4	196.9	73	440.4	226.9
6	310.9	155.0	40	388.2	197.9	74	442.2	227.9
7	315.2	157.3	41	389.8	198.8	75	443.8	228.8
8	318.5	159.2	42	391.2	199.6	76	446.0	230.0
9	323.2	161.8	43	392.4	200.2	77	448.5	231.4
10	326.1	163.4	44	393.6	200.9	78	451.1	232.8
11	329.0	165.0	45	394.9	201.6	79	452.6	233.7
12	331.0	166.1	46	396.3	202.4	80	453.7	234.3
13	334.5	168.1	47	397.8	203.2	81	455.1	235.1
14	339.6	170.9	48	399.5	204.2	82	457.7	236.5
15	341.5	171.9	49	401.5	205.3	83	460.4	238.0
16	342.8	172.6	50	403.5	206.4	84	464.0	240.0
17	344.8	173.8	51	404.9	207.1	85	467.8	242.1
18	348.5	175.9	52	406.2	207.9	86	471.2	244.0
19	351.3	177.4	53	407.6	208.7	87	474.1	245.6
20	353.3	178.5	54	409.1	209.5	88	477.5	247.5
21	355.1	179.5	55	411.0	210.6	89	480.7	249.3
22	356.7	180.4	56	413.0	211.6	90	484.8	251.6
23	358.2	181.2	57	414.8	212.7	91	486.8	252.7
24	360.6	182.5	58	417.1	214.0	92	490.2	254.6
25	363.7	184.3	59	418.5	214.7	93	496.3	257.9
26	365.7	185.4	60	419.6	215.3	94	502.4	261.3
27	367.0	186.1	61	420.3	215.7	95	507.6	264.2
28	368.4	186.9	62	421.4	216.3	96	515.8	268.8
29	370.2	187.9	63	423.3	217.4	97	521.7	272.0
30	372.3	189.0	64	424.9	218.3	98	533.8	278.8
31	374.6	190.3	65	426.3	219.1	99	551.5	288.6
32	376.7	191.5	66	428.1	220.1	FBP	573.8	301.0
33	379.0	192.8	67	429.8	221.0			

ASTM D 2887 Simulated Distillation for Fuel From Flight Tests 2, 4, and 5

% Off	BP°F	BP°C	% Off	BP°F	BP°C	% Off	BP°F	BP°C
IBP	264.2	129.0	34	382.9	195.0	68	431.5	222.0
1	273.9	134.4	35	383.7	195.4	69	433.4	223.0
2	285.7	140.9	36	384.5	195.8	70	435.6	224.2
3	298.0	147.8	37	385.6	196.5	71	437.4	225.2
4	308.6	153.7	38	387.4	197.5	72	438.8	226.0
5	314.5	156.9	39	389.1	198.4	73	440.4	226.9
6	318.2	159.0	40	390.5	199.2	74	442.1	227.8
7	323.3	161.8	41	391.7	199.8	75	443.8	228.8
8	326.4	163.6	42	392.9	200.5	76	445.7	229.9
9	329.3	165.2	43	394.1	201.1	77	448.4	231.3
10	331.5	166.4	44	395.3	201.8	78	450.9	232.7
11	336.1	168.9	45	396.5	202.5	79	452.4	233.6
12	340.4	171.3	46	398.0	203.3	80	453.4	234.1
13	342.0	172.2	47	399.5	204.2	81	454.5	234.7
14	343.3	172.9	48	401.6	205.3	82	456.7	235.9
15	345.8	174.3	49	403.4	206.4	83	459.0	237.2
16	349.7	176.5	50	404.9	207.2	84	462.3	239.0
17	352.0	177.8	51	406.1	207.8	85	465.6	240.9
18	354.0	178.9	52	407.3	208.5	86	469.4	243.0
19	355.8	179.9	53	408.8	209.3	87	472.3	244.6
20	357.2	180.7	54	410.6	210.3	88	475.1	246.2
21	358.9	181.6	55	412.7	211.5	89	478.5	248.1
22	361.6	183.1	56	414.5	212.5	90	482.3	250.2
23	364.5	184.7	57	416.7	213.7	91	485.7	252.1
24	366.1	185.6	58	418.4	214.7	92	487.6	253.1
25	367.4	186.3	59	419.3	215.2	93	491.8	255.4
26	368.8	187.1	60	420.1	215.6	94	498.4	259.1
27	370.3	188.0	61	420.9	216.0	95	504.7	262.6
28	372.4	189.1	62	422.2	216.8	96	511.6	266.4
29	374.5	190.3	63	424.0	217.8	97	518.1	270.1
30	376.7	191.5	64	425.5	218.6	98	529.8	276.5
31	378.8	192.7	65	426.9	219.4	99	546.0	285.6
32	380.8	193.8	66	428.7	220.4	FBP	569.7	298.7
33	382.0	194.5	67	430.1	221.2			

ASTM D 2887 Simulated Distillation for Fuel From Flight Test 3

% Off	BP°F	BP°C	% Off	BP°F	BP°C	% Off	BP°F	BP°C
IBP	249.9	121.0	34	381.7	194.3	68	435.3	224.1
1	268.8	131.6	35	382.5	194.7	69	437.0	225.0
2	282.3	139.1	36	383.3	195.2	70	438.4	225.8
3	295.1	146.2	37	384.5	195.8	71	440.1	226.7
4	301.6	149.8	38	386.3	196.8	72	441.8	227.7
5	310.7	154.9	39	388.2	197.9	73	443.5	228.6
6	314.7	157.1	40	389.7	198.7	74	445.4	229.6
7	318.0	158.9	41	391.2	199.6	75	447.9	231.1
8	322.6	161.4	42	392.5	200.3	76	450.4	232.4
9	325.7	163.2	43	393.7	200.9	77	452.0	233.3
10	328.4	164.7	44	395.0	201.7	78	452.9	233.9
11	330.5	165.8	45	396.5	202.5	79	454.2	234.6
12	333.8	167.7	46	398.2	203.5	80	456.4	235.8
13	338.9	170.5	47	400.3	204.6	81	458.9	237.2
14	340.8	171.6	48	402.3	205.7	82	462.2	239.0
15	341.8	172.1	49	404.1	206.7	83	465.3	240.7
16	343.6	173.1	50	405.4	207.5	84	469.0	242.8
17	347.2	175.1	51	406.8	208.2	85	471.8	244.4
18	350.4	176.9	52	408.4	209.1	86	474.4	245.8
19	352.3	177.9	53	410.5	210.3	87	477.4	247.5
20	354.1	179.0	54	412.5	211.4	88	480.3	249.1
21	355.9	179.9	55	414.5	212.5	89	484.2	251.2
22	357.4	180.8	56	416.9	213.8	90	486.1	252.3
23	359.6	182.0	57	418.2	214.5	91	488.5	253.6
24	363.1	183.9	58	419.1	215.1	92	493.4	256.3
25	365.1	185.1	59	419.9	215.5	93	499.2	259.5
26	366.5	185.8	60	421.0	216.1	94	504.5	262.5
27	367.9	186.6	61	423.0	217.2	95	509.6	265.4
28	369.6	187.5	62	424.6	218.1	96	516.3	269.1
29	371.9	188.8	63	426.1	219.0	97	522.4	272.5
30	374.2	190.1	64	428.0	220.0	98	534.2	279.0
31	376.4	191.3	65	429.4	220.8	99	552.2	289.0
32	378.7	192.6	66	430.9	221.6	FBP	576.2	302.3
33	380.5	193.6	67	433.0	222.8			

ASTM D 2887 Simulated Distillation for Fuel From Flight Test 6

% Off	BP°F	BP°C	% Off	BP°F	BP°C	% Off	BP°F	BP°C
IBP	236.8	113.8	34	380.9	193.8	68	439.8	226.6
1	264.0	128.9	35	382.2	194.6	69	441.5	227.5
2	277.4	136.3	36	383.1	195.1	70	443.1	228.4
3	287.7	142.0	37	384.0	195.6	71	444.8	229.4
4	297.7	147.6	38	385.2	196.2	72	446.9	230.5
5	304.9	151.6	39	387.4	197.5	73	449.5	231.9
6	311.3	155.2	40	389.6	198.7	74	451.7	233.2
7	314.8	157.1	41	391.3	199.6	75	453.0	233.9
8	317.6	158.7	42	392.6	200.3	76	454.0	234.4
9	321.3	160.7	43	394.1	201.2	77	455.6	235.3
10	324.9	162.7	44	395.9	202.1	78	458.2	236.8
11	327.3	164.1	45	397.9	203.3	79	461.0	238.4
12	329.8	165.4	46	400.0	204.4	80	464.3	240.2
13	331.6	166.4	47	402.2	205.7	81	467.8	242.1
14	335.0	168.3	48	404.3	206.8	82	470.8	243.8
15	339.6	170.9	49	405.9	207.7	83	473.2	245.1
16	341.4	171.9	50	407.5	208.6	84	475.8	246.5
17	342.5	172.5	51	409.4	209.7	85	478.4	248.0
18	343.7	173.2	52	411.7	210.9	86	480.6	249.2
19	347.1	175.1	53	413.8	212.1	87	484.1	251.2
20	350.2	176.8	54	416.1	213.4	88	486.2	252.4
21	352.2	177.9	55	418.1	214.5	89	487.8	253.2
22	354.2	179.0	56	419.2	215.1	90	491.1	255.1
23	356.1	180.1	57	420.1	215.6	91	496.1	257.9
24	357.7	181.0	58	421.2	216.2	92	500.8	260.4
25	360.0	182.2	59	423.1	217.3	93	505.4	263.0
26	363.8	184.3	60	424.9	218.3	94	509.0	265.0
27	365.8	185.5	61	426.6	219.2	95	515.3	268.5
28	367.5	186.4	62	428.5	220.3	96	518.6	270.4
29	369.1	187.3	63	430.3	221.3	97	526.5	274.7
30	371.2	188.4	64	432.2	222.3	98	536.6	280.3
31	373.9	190.0	65	434.6	223.7	99	551.6	288.7
32	376.2	191.2	66	436.8	224.9	FBP	570.9	299.4
33	378.8	192.6	67	438.2	225.7			